

**SYNTHESIS OF ZEOLITES FROM PERLITE AND  
STUDY OF THEIR ION EXCHANGE PROPERTIES**

**Miss Sudaporn Tangkawanit**

**A Thesis Submitted in Partial Fulfillment of the Requirements for the**

**Degree of Doctor of Philosophy in Chemistry**

**Suranaree University of Technology**

**Academic Year 2004**

**ISBN 974-533-343-3**

การสังเคราะห์ซีโอไลต์จากเพอร์ไลต์และการศึกษาสมบัติ  
การแลกเปลี่ยนไอออนของซีโอไลต์

นางสาวสุดาพร ตั้งกวนิช

วิทยานิพนธ์นี้เป็นส่วนหนึ่งของการศึกษาตามหลักสูตรปริญญาวิทยาศาสตรดุษฎีบัณฑิต

สาขาวิชาเคมี

มหาวิทยาลัยเทคโนโลยีสุรนารี

ปีการศึกษา 2547

ISBN 974-533-343-3

# SYNTHESIS OF ZEOLITES FROM PERLITE AND STUDY OF THEIR ION EXCHANGE PROPERTIES

Suranaree University of Technology has approved this thesis submitted in partial fulfillment of the requirements for the Degree of Doctor of Philosophy.

Thesis Examining Committee

*Malee Tangsathitkulchai*

(Asst. Prof. Dr. Malee Tangsathitkulchai)

Chairperson

*K. Rangriwatananon*

(Asst. Prof. Dr. Kunwadee Rangriwatananon)

Member (Thesis Advisor)

*Tongraar A.*

(Asst. Prof. Dr. Anan Tongraar)

Member

*P. Wathanakul*

(Asst. Prof. Dr. Pornsawat Wathanakul)

Member

*Jatuporn Wittayakun*

(Asst. Prof. Dr. Jatuporn Wittayakun)

Member

*Sarawut Sujitjorn* *Prasart Suebka*

(Assoc. Prof. Dr. Sarawut Sujitjorn)

(Assoc. Prof. Dr. Prasart Suebka)

Vice Rector for Academic Affairs

Dean of Institute of Science

สุภาพร ตั้งควนิช : การสังเคราะห์ซีโอไลต์จากเพอร์ไลต์และการศึกษาสมบัติการแลกเปลี่ยนไอออนของซีโอไลต์ (SYNTHESIS OF ZEOLITES FROM PERLITE AND STUDY OF THEIR ION EXCHANGE PROPERTIES) อาจารย์ที่ปรึกษา : ผู้ช่วยศาสตราจารย์ ดร.กฤษดา รังษีวัฒนานนท์, 188 หน้า. ISBN 974-533-343-3

งานนี้เป็นการศึกษาการสังเคราะห์ซีโอไลต์จากเพอร์ไลต์ซึ่งใช้เป็นแหล่งของซิลิกาและอะลูมินาที่นำมาจากจังหวัดลพบุรี และศึกษาจลนพลศาสตร์ในการเกิดผลึกของอะนอลซิม (analcime) นอกจากนี้ยังได้ศึกษาสมบัติการแพร่และการแลกเปลี่ยนไอออนของทองแดง นิกเกิล ตะกั่วและสังกะสีในอะนอลซิมที่สังเคราะห์ได้

การสังเคราะห์ซีโอไลต์เพื่อหาการเกิดผลึกใช้การแปรค่าความเข้มข้นของค่า อุณหภูมิ ความดัน และสัดส่วนของสารตั้งต้น การศึกษาพบว่าที่อุณหภูมิ 100 องศาเซลเซียสและความดันบรรยากาศผลึกชนิดที่ได้ออกคือซีโอไลต์โซเดียมพีวัน (zeolite Na-P1) ที่อุณหภูมิ 100 องศาเซลเซียสและความดัน 20-50 psi ซีโอไลต์ที่เกิดขึ้นคืออะนอลซิม (analcime) เมื่อใช้โซเดียมไฮดรอกไซด์ความเข้มข้น 3 โมลาร์ และอัตราส่วนของของแข็งต่อของเหลว 1:5 ที่อุณหภูมิ 140 องศาเซลเซียส เป็นเวลา 24 ชั่วโมง พบว่าเพอร์ไลต์เปลี่ยนไปเป็นผลึกอะนอลซิมเพียงอย่างเดียว เมื่อใช้อัตราส่วนของของแข็งต่อของเหลวเท่ากับ 1:20 ผลึกชนิดที่ได้ออกคือแคนครินต์ (cancrinite) เนื่องจากอะนอลซิมเป็นซีโอไลต์ที่เกิดดีที่สุดในแง่ของพื้นที่ศึกษา จึงใช้ศึกษาจลนพลศาสตร์ในการเกิดผลึก สมบัติการแพร่และการแลกเปลี่ยนไอออน

การศึกษาจลนพลศาสตร์ในการเกิดผลึกของอะนอลซิมพบว่าค่าพลังงานก่อกัมมันต์ ( $E_a$ ) จากสมการอาร์เรเนียส (Arrhenius) มีค่าเท่ากับ 11.2 กิโลแคลอรีต่อโมล ซึ่งสอดคล้องกับการสูญเสีย น้ำของไอออนของซิลิเกต (silicate) และอะลูมินา (aluminate) ค่าเอ็กซ์โพเนนต์ของอฟรามิ (Avrami, n) มีค่าอยู่ในช่วง 3.4 ถึง 6.4 สะท้อนให้เห็นว่าการเกิดผลึกจากอสังฐานเกิดในขั้นการเร่งปฏิกิริยาเอง (autocatalytic) ของกระบวนการเกิดผลึก

จากการแพร่ของไอออนบวกของทองแดง นิกเกิล ตะกั่วและสังกะสี เข้าสู่โซเดียมอะนอลซิม ที่อุณหภูมิช่วง 25-60 องศาเซลเซียส สามารถคำนวณค่าสัมประสิทธิ์ของการแพร่โดยใช้สมการ BBK (Barrer, Barri and Klinowski) ผลการคำนวณทางเทอร์โมไดนามิกส์ได้แก่ พลังงานก่อกัมมันต์ ( $E_a$ ) เอนโทรปี ( $\Delta S^*$ ) และพลังงานอิสระ ( $\Delta G^*$ ) ซึ่งว่าตำแหน่งในช่องว่างภายในโครงสร้างของอะนอลซิมเกี่ยวข้องกับกระบวนการแพร่

จากการแลกเปลี่ยนไอออนของทองแดง นิกเกิล ตะกั่วและสังกะสี ในโซเดียมอะนอลซิม ทำที่อุณหภูมิ 25-60 องศาเซลเซียส พบว่าลำดับในการเลือกเข้าไปของไอออนในอะนอลซิมคือ ตะกั่ว > ทองแดง > สังกะสี > นิกเกิล ซึ่งบ่งชี้ได้โดยค่าพลังงานอิสระมาตรฐาน ( $\Delta G^0$ ) ผลการศึกษาแสดง

ให้เห็นว่าค่าเอนทัลปีของการเกิดไฮเดรต (enthalpy of hydration,  $\Delta H_{\text{hyd}}$ ) เป็นตัวกำหนดการเลือกไอออนของซิลิเกต ค่าเอนโทรปีมาตรฐาน ( $\Delta S^\circ$ ) สัมพันธ์กับปริมาณน้ำที่เปลี่ยนไปในซิลิเกต และกระบวนการแลกเปลี่ยนไอออนเป็นกระบวนการดูดความร้อน

สาขาวิชาเคมี

ปีการศึกษา 2547

ลายมือชื่อนักศึกษา.....

ลายมือชื่ออาจารย์ที่ปรึกษา.....

ลายมือชื่ออาจารย์ที่ปรึกษาร่วม.....

ลายมือชื่ออาจารย์ที่ปรึกษาร่วม.....

SUDAPORN TANGKAWANIT : SYNTHESIS OF ZEOLITES FROM  
PERLITE AND STUDY OF THEIR ION EXCHANGE PROPERTIES. THESIS  
ADVISOR : ASST. PROF. KUNWADEE RANGSRIWATANANON,  
Ph.D. 188 PP. ISBN 974-533-343-3

This work was an intensive study on zeolite synthesis from perlite, an economic silica/alumina source in Lopburi, and crystallization kinetics of synthetic analcime. In addition, diffusion and ion exchange properties of analcime with  $\text{Cu}^{2+}$ ,  $\text{Ni}^{2+}$ ,  $\text{Pb}^{2+}$  and  $\text{Zn}^{2+}$  were studied.

The zeolite syntheses were carried out to determine zeolite crystallization under various conditions including concentrations of alkalinity, temperatures, pressures and ratios of the reactants. At 100 °C and 20 psi the product was zeolite Na-P1. At 100-140 °C and 20-50 psi the major product obtained was analcime. Under the influence of 3 M NaOH and 1:5 solid/liquid ratio at 140 °C for 24 hrs, perlite was mainly converted to analcime. When the solid/liquid ratio was changed to 1:20, cancrinite was formed. As the major product of this study, analcime was used for studying the crystallization kinetics, exchange diffusion and ion exchange properties.

The activation energy of analcime crystallization determined by kinetic study was 11.2 kcal mol<sup>-1</sup> corresponding to the dehydration of the silicate and aluminate ions in solution. The Avrami exponent (n) ranged from 3.4 to 6.4 indicating crystallization of the amorphous phase took place in the autocatalytic stage of the crystallization process.

The diffusion exchange of  $\text{Cu}^{2+}$ ,  $\text{Ni}^{2+}$ ,  $\text{Pb}^{2+}$  and  $\text{Zn}^{2+}$  with  $\text{Na}^+$  in the synthetic analcime was investigated in the temperature range 25-60 °C. The diffusion coefficients (D) were calculated from the BBK (Barrer, Barri and Klinowski)

equation. Thermodynamic results indicating activation energy ( $E_a$ ), entropy ( $\Delta S^*$ ) and free energy ( $\Delta G^*$ ) showed that all the channel sites were involved in the diffusion processes.

Finally the ion exchange of  $\text{Cu}^{2+}$ ,  $\text{Ni}^{2+}$ ,  $\text{Pb}^{2+}$  and  $\text{Zn}^{2+}$  with  $\text{Na}^+$  in the synthetic analcime was studied at 25-60 °C. The selectivity sequence for those ions entering analcime, indicated by the values of free energy ( $\Delta G^0$ ) was  $\text{Pb}^{2+} > \text{Cu}^{2+} > \text{Zn}^{2+} > \text{Ni}^{2+}$ . The results also indicated that the selectivity could be determined by enthalpy of hydration of cation. Standard entropy ( $\Delta S^0$ ) values were related to changes in water content and the exchange processes were endothermic.

School of Chemistry

Academic Year 2004

Student's Signature.....

Advisor's Signature.....

Co-advisor's Signature.....

Co-advisor's Signature.....

## Acknowledgements

I wish to express my sincere thanks to Assistant Professor Dr.Kunwadee Rangriwatananon who has supervised this work for her unfailing and constant advice, guidance and encouragement throughout the duration of this study. I would also like to thank Assistant Professor Dr.Malee Tungsathitkulchai for serving as Committee Chairman of the committee. My sincere thanks are due to Assistant Professor Dr.Anan Tongraar and Assistant Professor Dr.Pornsawat Wathanakul for serving as the co-advisors on my thesis committee. I would like to thank Assistant Professor Dr.Jatuporn Wittayakun as my thesis committee. I would like to give a special mention to Professor Alan Dyer whose constant advice has been greatly appreciated throughout both the Diffusion and Isotherm parts of this study and for making it possible for me to work at the Chemical Science Division in the Science Research Institute at the University of Salford, UK. A special mention also goes to Dr.Lina Al\_Attar, Brian and Thai students at the University of Salford whose friendship and help during my time in Manchester, UK, was greatly appreciated. I would also like to thank Dr.David Apperley, University of Durham, UK, for his excellent  $^{29}\text{Si}$  MAS NMR service. Special thanks to <http://www.iza-structure.org/databases/>, for their very useful datas.

Thanks are also due to Miss Natthiya Deeying, Miss Supaporn Dokmaisrijan and Dr.Jon Newton for their assistance with the calculation program. I would like to

thanks all lecturers in the Department of Chemistry at Suranaree University of Technology for their useful recommendations, and all of the staffs at the Center of Scientific and Technological Equipment for their excellent service and helpful suggestions for the use of XRD, XRF, FT-IR, AAS, SEM, BET, TGA-DTA, Laser particle size analyzer, Kjeldahl and Microwave digestion. I am indebted to Ubon Ratchatani Rajabhat University for their financial support for my research overseas. Suranaree University of Technology is gratefully acknowledged for their Research Grant Funds. Also I would like to thank Peter Bint for taking the time to proof read my thesis.

I would like to thank Miss Chutima Thongasam, Zeolite's group and all my friends at the Department of Chemistry, Suranaree University of Technology, Mr. Suntorn Worahan, Mr. Supoj Gonthong and Mr. Kanang Jittaganon (Siam Zimmerman LTD) for their help. Finally, I also wish to thank my family for their understanding, encouragement and support during the whole period of my education.

Sudaporn Tangkawanit

## Contents

Abstract in Thai.....	I
Abstract in English.....	III
Acknowledgement.....	V
Contents.....	VII
List of Tables.....	XII
List of Figures.....	XX
List of Abbreviations.....	XXI

### Chapters

<b>I</b>	<b>Introduction.....</b>	<b>1</b>
	1.1 Zeolite.....	1
	1.2 Structure of zeolites.....	2
	1.3 Occurrence and formation.....	5
	1.4 Diffusion.....	7
	1.5 Ion exchange property.....	9
	1.6 Analcime.....	12
	1.7 Perlite.....	14
	1.8 Heavy metals.....	16
	1.9 Research objectives.....	17

## Contents (Continued)

1.10	Scope and limitations of the study.....	18
<b>II</b>	<b>Theory and literature reviews.....</b>	<b>20</b>
2.1	Theory.....	20
2.1.1	The theory of synthetic zeolites.....	20
2.1.2	The theory of kinetics crystallization.....	22
2.1.3	The theory of diffusion kinetics.....	24
2.1.4	The cation exchange capacity theory.....	29
2.1.5	Ion exchange theory.....	30
2.1.5.1	The selectivity factors of ion exchange.....	31
2.1.5.1.1	Framework topology, ion size and shape.....	31
2.1.5.1.2	Charge density.....	35
2.1.5.1.3	Electrolyte concentration.....	36
2.1.5.1.4	Zeolite stability.....	36
2.1.5.2	Theoretical treatment of ion exchange.....	37
2.1.6	X-ray powder diffraction (XRD).....	42
2.1.7	Brunauer-Emmett-Teller (BET).....	44
2.1.8	X-ray fluorescence spectrometry (XRF).....	45
2.1.9	Fourier transform infrared spectrophotometer (FT-IR).....	47
2.1.10	Simultaneous thermogravimetry-differential thermal analysis (TGA-DTA).....	49

## Contents (Continued)

2.1.11 $^{29}\text{Si}$ MAS NMR spectrometer.....	49
2.1.12 Scanning electron microscope (SEM).....	52
2.1.13 Liquid scintillation Spectrometer (LSC).....	53
2.2 Literature reviews.....	54
<b>III Materials and Experiments.....</b>	<b>60</b>
3.1 Materials.....	60
3.1.1 Chemicals.....	60
3.1.2 Apparatus.....	61
3.1.3 Instruments.....	61
3.2 Experiments.....	62
3.2.1 Chemical and physical properties of raw perlite.....	62
3.2.2 Synthesis of zeolite.....	64
3.2.3 Chemical, physical properties and pH tolerance of analcime .....	66
3.2.4 Crystallization kinetics of analcime.....	67
3.2.5 Diffusion.....	68
3.2.5.1 Experiment of self-diffusion.....	69
3.2.5.2 Diffusion experiments.....	69
3.2.6 Ion exchange isotherms.....	70
3.2.6.1 Construction of exchange isotherm.....	71
3.2.6.2 Reversibility of isotherms.....	73

## Contents (Continued)

3.2.7 Powder X-ray diffraction.....	74
3.2.8 Thermal analysis.....	74
3.2.9 X-ray fluorescence spectrometry.....	75
3.2.10 Scanning electron microscopy.....	76
3.2.11 Fourier transforms infrared spectrophotometer.....	77
3.2.12 Particle size analysis.....	77
3.2.13 Surface area analyzer .....	78
3.2.14 Liquid scintillation Spectrometer (LSC).....	78
3.2.15 <sup>29</sup> Si MAS NMR spectrometer.....	79
<b>IV Results and Discussion.....</b>	<b>80</b>
4.1 Chemical and physical properties of raw perlite.....	80
4.2 Synthesis of zeolite.....	84
4.3 Chemical, physical properties and pH tolerance of analcime.....	98
4.4 Crystallization kinetics of analcime.....	106
4.5 Diffusion.....	121
4.6 Ion exchange.....	131
<b>V Conclusion.....</b>	<b>145</b>
References.....	148

**Contents (Continued)**

Appendices.....	160
Appendix A Isotherm construction calculations.....	161
Appendix B Atlas of zeolite structure types.....	174
Appendix C Simulated XRD powder patterns for zeolites.....	181
Curriculum vitae.....	188

## List of Tables

Table	Page
1.1	Simple secondary building units and shorthand notation of zeolite..... 4
1.2	Occurrence and effects of heavy metals in natural water..... 17
2.1	Exponents of the Avrami equation for different nucleation and growth mechanisms..... 24
2.2	Exchange capacities of some zeolites..... 30
2.3	Ion exchange properties..... 33
2.4	Hydration enthalpies of metal cations..... 33
2.5	Effective ion diameters (Å) for inorganic complexes in aqueous solution..... 34
2.6	Comparisons of the Si/Al ratios and water content of synthetic analcime..... 35
2.7	Exchange limits in faujasite (zeolite X) at room temperature..... 36
2.8	Range of <sup>29</sup> Si MAS NMR chemical shifts in zeolite..... 51
3.1	Composition of solutions used to construct the isotherms $\text{Na}^+ \rightleftharpoons \text{M}^+$ ..... 72
3.2	Conditions used for reverse isotherms..... 73
4.1	Chemical composition of raw perlite..... 81
4.2	Physical properties of raw perlite..... 83
4.3	Zeolite formation from perlite under various conditions ..... 86

## List of Tables (Continued)

<b>Table</b>	<b>Page</b>
4.4 Zeolite formation from perlite at 12 hours period of time in various conditions .....	88
4.5 Infrared assignments of vibrational framework of three different zeolite products.....	93
4.6 Chemical composition of synthetic analcime in weight percentage.....	99
4.7 Physical properties of synthetic analcime.....	100
4.8 The kinetics of analcime crystallization from perlite at various reaction temperatures.....	106
4.9 Activation energy of analcime crystallization at reaction condition 3 M NaOH 140 °C 1:5 solid/liquid ratio.....	114
4.10 The Avrami exponent for analcime crystallization.....	115
4.11 Activity of filtrates for Cu <sup>2+</sup> diffusion into analcime at various temperatures.....	121
4.12 Activity of filtrates for Ni <sup>2+</sup> diffusion into analcime at various temperatures.....	122
4.13 Activity of filtrates for Pb <sup>2+</sup> diffusion into analcime at various temperatures.....	122
4.14 Activity of filtrates for Zn <sup>2+</sup> diffusion into analcime at various temperatures.....	123
4.15 Thermodynamic parameters for the diffusion of cations into Na-analcime.....	128

## List of Tables (Continued)

<b>Table</b>		<b>Page</b>
4.16	Activity of filtrates for $\text{Cu}^{2+}$ exchanged by Na analcime.....	131
4.17	Activity of filtrates for $\text{Pb}^{2+}$ exchanged by Na analcime.....	132
4.18	Activity of filtrates for $\text{Ni}^{2+}$ exchanged by Na analcime.....	132
4.19	Activity of filtrates for $\text{Zn}^{2+}$ exchanged by Na analcime .....	133
4.20	Thermodynamic parameters for $\text{Na}^+$ /heavy metal ions exchange in analcime at various temperatures.....	139
4.21	Comparison selectivity series for ion exchange of heavy metals .....	140

## List of Figures

Figure	Page
1.1	Representations of primary tetrahedral units of $\text{AlO}_4$ and $\text{SiO}_4$ .....2
1.2	Representations of a primary tetrahedral unit of $\text{AlO}_4$ and $\text{SiO}_4$ linked together to create a three-dimensional structure.....2
1.3	Representations of secondary building units of zeolite.....3
1.4	Formation of three common zeolites from primary $\text{AlO}_4$ and $\text{SiO}_4$ tetrahedral units through a combination of secondary ring units, and different mixes of tertiary polyhedra.....5
1.5	Adsorption on a porous adsorbent particle.....8
1.6	Tube representation of analcime showing the lack of intersecting channels in the structure.....14
1.7	Characteristics of perlite and expanded perlite.....15
2.1	Illustration of the thermodynamic driving force for zeolite crystallization.....21
2.2	Representation of ion-sieving effect for $\text{Cs}^+$ and $\text{Rb}^+$ into analcime.....32
2.3	Derivation of the selectivity coefficient.....39
2.4	Diffraction of X-rays by a crystal.....43
2.5	Simplification of photoelectric effect leads to internal ionization and to emission of photoelectrons.....46
2.6	Diagram of Fourier transform infrared spectrophotometer.....48

## List of Figures (Continued)

Figure	Page
2.7 Schematic representation of a SEM.....	53
3.1 High Temperature/High Pressure Reactor .....	65
3.2 Stainless steel bomb vessel 500 ml for Parr instrument model 4575.....	65
4.1 X-ray diffraction pattern of raw perlite.....	81
4.2 TGA thermogram of a raw perlite.....	82
4.3 FT-IR spectra of a perlite.....	83
4.4 X-ray diffractogram of zeolite Na-P1 obtained from perlite.....	89
4.5 X-ray diffractogram of cancrinite obtained from perlite.....	90
4.6 X-ray diffraction pattern of analcime prepared from perlite.....	91
4.7 FT-IR spectra of raw perlite and zeolite products of zeolite Na-P1, cancrinite and analcime.....	92
4.8 Plot percent crystallinity of analcime against different crystallization periods of time at 140 °C .....	93
4.9 SEM photographs of kinetics of crystallization of analcime obtained by varying crystallization periods at 140 °C.....	94
4.10 Plot describing of analcime crystals obtained by varying crystallization periods at 140 °C.....	96
4.11 Particle size distribution of analcime crystallites synthesized at different crystallization periods at 140 °C.....	96

## List of Figures (Continued)

Figure	Page
4.12	Plot of particle size distribution trend of analcime crystallites synthesized at different crystallization periods at 140 °C .....97
4.13	TGA-DTA thermograms of a synthetic analcime sample .....99
4.14	SEM photographs of analcime crystals prepared from perlite .....100
4.15	<sup>29</sup> Si MAS NMR spectra of synthetic analcime prepared from perlite .....101
4.16	Particle size distributions of analcime crystallites.....102
4.17	Plot of percentage crystallinity of analcime samples at different pH treatments.....103
4.18	X-ray diffractrogram of analcime samples at different pH treatments.....104
4.19	FT-IR spectra of analcime samples calcined at different temperatures.....105
4.20	X-ray diffraction patterns of raw perlite and analcime samples obtained at different crystallization periods at 130 °C.....107
4.21	X-ray diffraction patterns of raw perlite and analcime samples obtained at different crystallization periods at 135 °C.....108
4.22	X-ray diffraction patterns of raw perlite and analcime samples obtained at different crystallization periods at 140 °C.....109
4.23	X-ray diffraction patterns of raw perlite and analcime samples obtained at different crystallization periods at 145 °C.....110
4.24	Kinetics of analcime crystallization at different temperatures.....111
4.25	Crystallinity as a function of time.....111

## List of Figures (Continued)

Figure	Page
4.26 Arrhenius plot for analcime crystallization.....	112
4.27 The Avrami plot for $\ln(-\ln(1-\alpha))$ against $\ln t$ of analcime crystallization.....	115
4.28 SEM photographs of raw perlite and kinetics of crystallization of analcime obtained by varying crystallization periods at 140 °C.....	116
4.29 FT-IR spectra of raw perlite and analcime samples obtained at different crystallization periods at 140 °C.....	118
4.30 Particle size distribution of solid products at different crystallization periods at 140 °C.....	119
4.31 Plot of particle size distribution describing solid products at different crystallization periods at 140 °C.....	120
4.32 Plots of $W_t/W_\infty$ against time (t) for $^{22}\text{Na}/\frac{1}{2}\text{Cu}^{2+}$ exchange in analcime in the range of 298-333 K.....	124
4.33 Plots of $W_t/W_\infty$ against time (t) for $^{22}\text{Na}/\frac{1}{2}\text{Ni}^{2+}$ exchange in analcime in the range of 298-333 K.....	124
4.34 Plots of $W_t/W_\infty$ against time (t) for $^{22}\text{Na}/\frac{1}{2}\text{Pb}^{2+}$ exchange in analcime in the range of 298-333 K.....	125
4.35 Plots of $W_t/W_\infty$ against time (t) for $^{22}\text{Na}/\frac{1}{2}\text{Zn}^{2+}$ exchange in analcime in the range of 298-333 K.....	125

## List of Figures (Continued)

Figure	Page
4.36 Arrhenius plots for exchange diffusion of $\text{Ni}^{2+}$ and $\text{Pb}^{2+}$ in analcime in the range of 298-333 K.....	126
4.37 Arrhenius plots for exchange diffusion of $\text{Cu}^{2+}$ and $\text{Zn}^{2+}$ in analcime in the range of 298-333 K.....	126
4.38 Plot of percentage of crystallinity against cation radii for cation exchanged analcime.....	127
4.39 Plot of the activation energy ( $E_a$ ) against cation radii for diffusion processes.....	129
4.40 Ion exchange isotherm for $\text{Na}^+ \leftrightarrow 1/2\text{Cu}^{2+}$ exchange in analcime at $T_N = 0.01\text{N}$ (a) and their Kielland plots (b).....	134
4.41 Ion exchange isotherm for $\text{Na}^+ \leftrightarrow 1/2\text{Pb}^{2+}$ exchange in analcime at $T_N = 0.01\text{N}$ (a) and their Kielland plots (b).....	135
4.42 Ion exchange isotherm for $\text{Na}^+ \leftrightarrow 1/2\text{Ni}^{2+}$ exchange in analcime at $T_N = 0.01\text{N}$ (a) and their Kielland plots (b).....	136
4.43 Ion exchange isotherm for $\text{Na}^+ \leftrightarrow 1/2\text{Zn}^{2+}$ exchange in analcime at $T_N = 0.01\text{N}$ (a) and their Kielland plots (b).....	137
4.44 Plots of $\Delta G^0$ ( $\text{kJ mol}^{-1}$ ) against $\Delta H_{\text{hyd}}$ ( $\text{kJ mol}^{-1}$ ) for $\text{Na}^+$ with $\text{Cu}^{2+}$ , $\text{Ni}^{2+}$ , $\text{Pb}^{2+}$ and $\text{Zn}^{2+}$ exchange in analcime at 298 K.....	141
4.45 XRD diffractrogram of the parent analcime and the solid products of ion exchange.....	142

## List of Figures (Continued)

<b>Figure</b>	<b>Page</b>
4.46 TGA curves for the parent analcime and the solid products of ion exchange.....	143
4.47 Differential thermal analysis curves for the parent analcime and the solid products of ion exchange.....	144

## List of Abbreviations

LSC	Liquid scintillation counter
BET	Brunauer-Emmett-Teller
FT-IR	Fourier transforms infrared spectrophotometer
SEM	Scanning electron microscope
XRD	X-ray diffractometer
XRF	X-ray fluorescence spectrometry
DTA	Differential Thermal analysis
TGA	Thermogravimetric analysis
MAS NMR	Magic-angle spin nuclear magnetic resonances
CEC	Cation exchange capacity
N	Normal
M	Molar
M	Minute
K	Degree Kelvin
Meqg <sup>-1</sup>	Milli equivalent per gram
cpm	Count per minute
LOI	Loss On Ignition
Å	Angstrom
m <sup>2</sup> s <sup>-1</sup>	Cubicmeters per second
kJ	Kilojoule

**List of Abbreviations (Continued)**

kcal	Kilocalorie
% T	Percent transmittance
t	time
$E_a$	Activation energy
$\Delta S^*$	Entropy of activation
$\Delta H^*$	Enthalpy of activation
$\Delta G^*$	Free energy of activation
$\Delta S^\circ$	Standard entropy change
$\Delta H^\circ$	Standard enthalpy change
$\Delta G^\circ$	Standard free energy change
A	pre-exponential
w/v	Weight by volume
BBK	Barrer, Barri and Klinowski equation
kV	Kilovolt
mA	Milliampere

# Chapter I

## Introduction

### 1.1 Zeolite

Zeolite is derived from two Greek words (Zeo, to boil and lithos, stone) meaning “boiling stones” and it was coined by a Swedish mineralogist Cronstedt in 1756, who had observed that stilbite loses water very easily when heated (Dyer, 1988).

By definition, zeolites are crystalline, hydrated aluminosilicate compounds that have three-dimensional structures arising from a framework of tetrahedral units  $\text{SiO}_4$  and  $\text{AlO}_4$ , each tetrahedral unit being linked by an oxygen atom. The three-dimensional structure is constructed from pores of molecules dimension. The framework is generally open and contains channels and cavities in which are located cations, water molecules (Breck, 1974, Dyer, 1988, Szostak, 1989 and Farrauto, 1997) and it is accessible for the adsorption of small molecules. The cations are quite mobile and may usually be exchanged, to varying degrees, with other cations (Breck, 1974). Thus, zeolite differs from porous amorphous adsorbents (Zhdanov, Khvoshchev and Feoktistova, 1990).

Zeolite has the general formula:  $\text{M}_{x/n} [(\text{AlO}_2)_x (\text{SiO}_2)_y] \cdot w\text{H}_2\text{O}$ ; where  $\text{M}_{x/n}$  is a non-framework, exchangeable cation, and  $(\text{AlO}_2)_x (\text{SiO}_2)_y$  is the framework component, and  $w\text{H}_2\text{O}$  is sorbed water,  $n$  is the valence of cation  $M$ ,  $w$  is the number of water molecules per unit cell, and  $x$  and  $y$  are the total numbers of tetrahedra per

unit cell (Breck, 1974, Szostak, 1989 and Farrauto, 1997). Zeolite contains amounts of water bound in their crystal grid, which will evaporate when heated so it has a unique ability for the adsorption of small molecules and ions (Marcus and Cormier, 2002).

## 1.2 Structure of zeolites

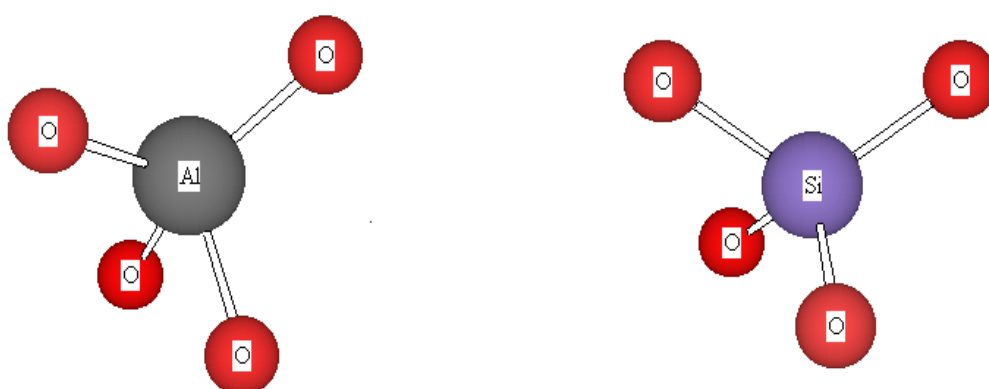


**Figure 1.1** Representation of primary tetrahedral units of  $\text{AlO}_4$  and  $\text{SiO}_4$ .

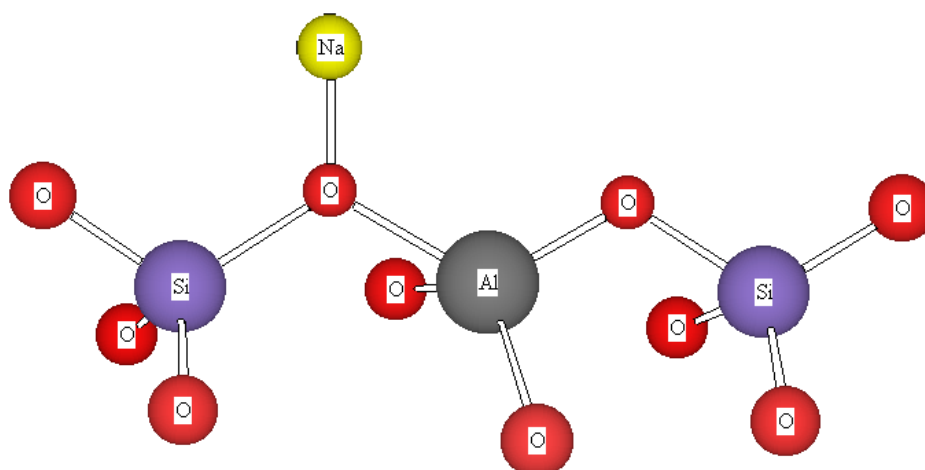


**Figure 1.2** Representation of a primary tetrahedral unit of  $\text{AlO}_4$  and  $\text{SiO}_4$  linked together to create a three-dimensional structure.

Zeolite framework structure types are commonly classified on the basis of constituent units (Meier, 1988). The primary building unit of a zeolite structure is the individual tetrahedral  $TO_4$  units, where T is either Si or Al as shown in figure 1.1. Primary tetrahedral unit of  $AlO_4$  and  $SiO_4$  are linked together by sharing oxygen as represented in figure 1.2.

There are sixteen secondary building units, consisting of geometric groupings of those tetrahedra which can be used to describe all of the known zeolite structures.

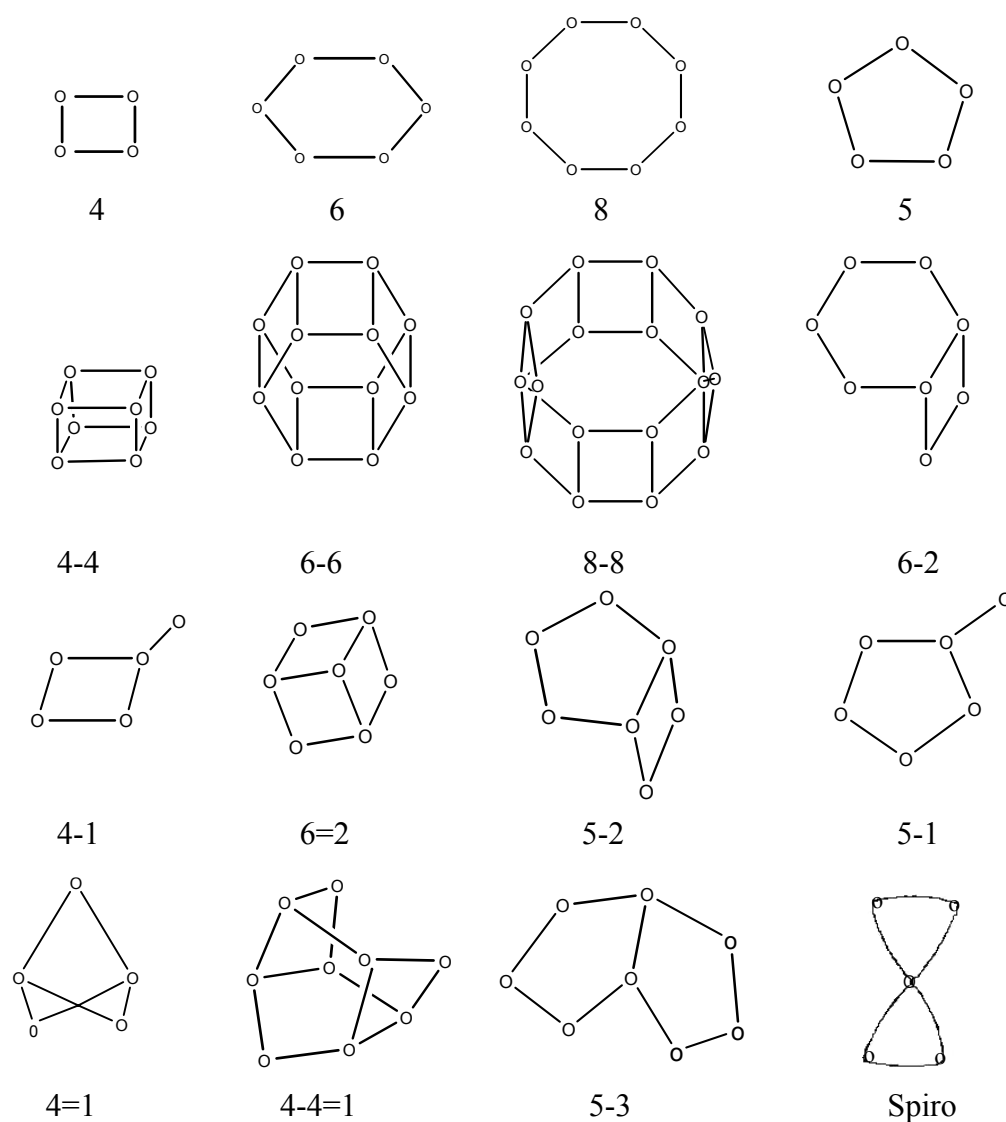


**Figure 1.3** Representations of secondary building units of zeolite (Szostak, 1998).

These secondary building units are composed of 4, 5, 6, and 8-member single rings, 4-4, 6-6, and 8-8 member double rings, and 4-1, 4=1, 5-1, 5-2, 5-3 6-1, 6-2 and 4-4=1 branch rings and spiro-5, as represented in figure 1.3 (Szostak, 1998).

Table 1.1 shows a description of secondary building units and the shorthand notation for zeolite (Bruce, 1994). Examples of synthetic zeolite, which is composed of basic building blocks, is illustrated in figure 1.4 (Farrauto and Bartholomew, 1997)

**Table 1.1** Simple secondary building units and shorthand notation for zeolite.

Number of linked tetrahedra	SUB created	Shorthand description <sup>a</sup>
4	4 oxygen ring	S4R
5	5 oxygen ring	S5R
6	6 oxygen ring	S6R
8	8 oxygen ring	S8R
8	4-4 oxygen rings	D4R
12	6-6 oxygen rings	D6R
16	8-8 oxygen rings	D8R

<sup>a</sup>S = single, D = double

A typical aluminosilicate is formed by polymerization of  $\text{SiO}_4$  and  $\text{AlO}_4$  tetrahedra to form sheet-like polyhedra (squares and hexagons) which in turn form cubes, hexagonal prisms and truncated octahedra (Farrauto and Bartholomew, 1997).

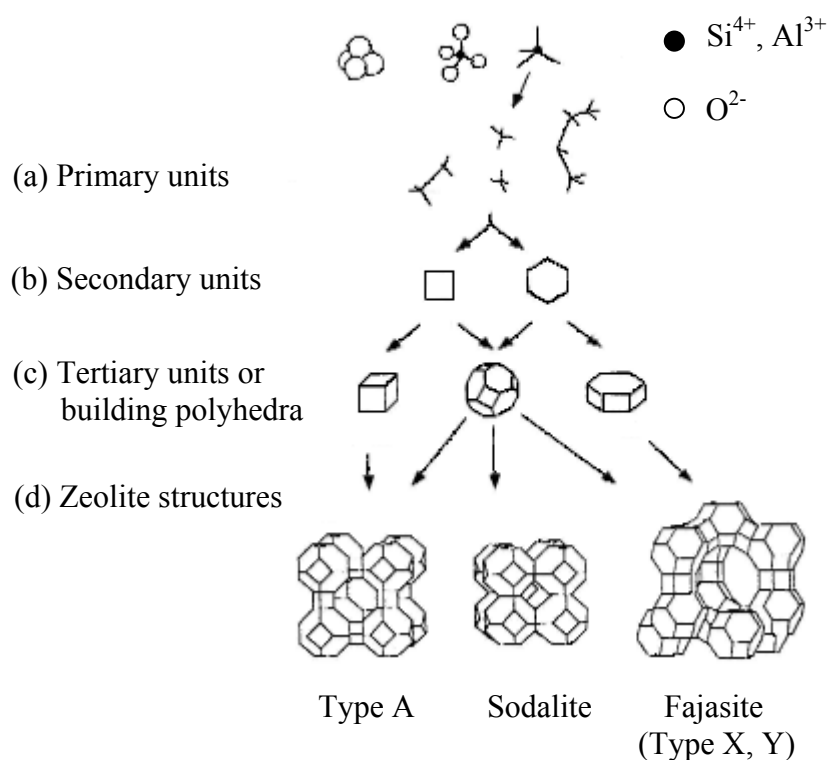


**Figure 1.4** Formation of three common zeolites from primary  $\text{AlO}_4$  and  $\text{SiO}_4$  tetrahedral units through a combination of secondary ring units, and different mixes of tertiary polyhedra.

### 1.3 Occurrence and formation

There are 40 known naturally occurring zeolites and more than 150 synthetic ones (Marcus and Cormier, 2002). Zeolite arises naturally by broadly two routes, one predominantly at low temperatures (below  $40^\circ\text{C}$ ) and associated with sedimentary processes, with the second being at higher temperatures and linked to volcanic and associated hydrothermal processes. Hydrologically closed systems also create zeolites when glassy ash falls into a saline lake under arid or semiarid conditions. Conditions

of high pH and salt concentration arise from evaporation, producing ideal conditions for zeolite to form (Bruce, 1994). The nature of zeolites crystallized in aqueous alkaline aluminosilicate systems under hydrothermal conditions at a given temperature depends largely on the ratios and concentrations of the components. However, the conditions of their production, nature and state of reagents, stirring, seeding, and other factors are often difficult to control, and affect the results of crystallization for the same composition of the system (Zhdanov, Khvoshchev, and Feoktistova, 1990).

Zeolite can be synthesized hydrothermally by using aqueous alkali. Synthetic zeolite is obtained by heating aqueous alkali aluminosilicate mixtures containing water, alkali,  $\text{SiO}_2$  and  $\text{Al}_2\text{O}_3$  as essential components similar to the formation of zeolite in nature (Zhdanov *et al.*, 1990). The final product can take hours or days depending on the raw material and synthesis conditions (temperature, pressure). Some of the parameters that control the type of zeolite formed are the composition and pH of the solution, as well as the temperature, pressure and time formation. Some zeolite properties, including structure, silicas to alumina ratio, pore size and framework densities are determined during synthesis (Marcus and Cormier, 2002).

A very wide range of silica sources have been used in zeolite synthesis for example natural materials such as kaolinite, volcanic glasses (perlite, pumice), rice husks, diatomite and chemical materials as silicates (Bruce, 1994). Synthetic and natural zeolites have been used in numerous applications including water treatment, radioactive waste storage, gas separation and purification, liquid phase separation, molecular sieves, detergents, fertilizers, ion exchanges, catalysts, desiccation, soil improvers and animal feed supplements (Dyer, 1984).

Synthetic zeolites are better for research and industrial applications because of their greater uniformity in composition and purity. This is particularly necessary where a high degree of reproducibility is required in an industrial separation process (Breck, 1974).

## **1.4 Diffusion**

Diffusion is the process by which matter is transported from one part of a system to another, as a result of random molecular motions, leading to an equalization of concentration in a single phase (Crank, 1956). The diffusion process in zeolite depends on a number of combined effects (Ali, 1987).

1. External diffusion or film diffusion, diffusion through the boundary layer of fluid surrounding the adsorbent particle.
2. Pore diffusion, diffusion through the pores of the particles.
3. Pore surface diffusion, diffusion along the surface of the pore.
4. Adsorption, adsorption on the internal pore surfaces.

The diffusion processes on a porous adsorbent particle are shown in figure 1.5 (Keinath and Wanielista, 1975).

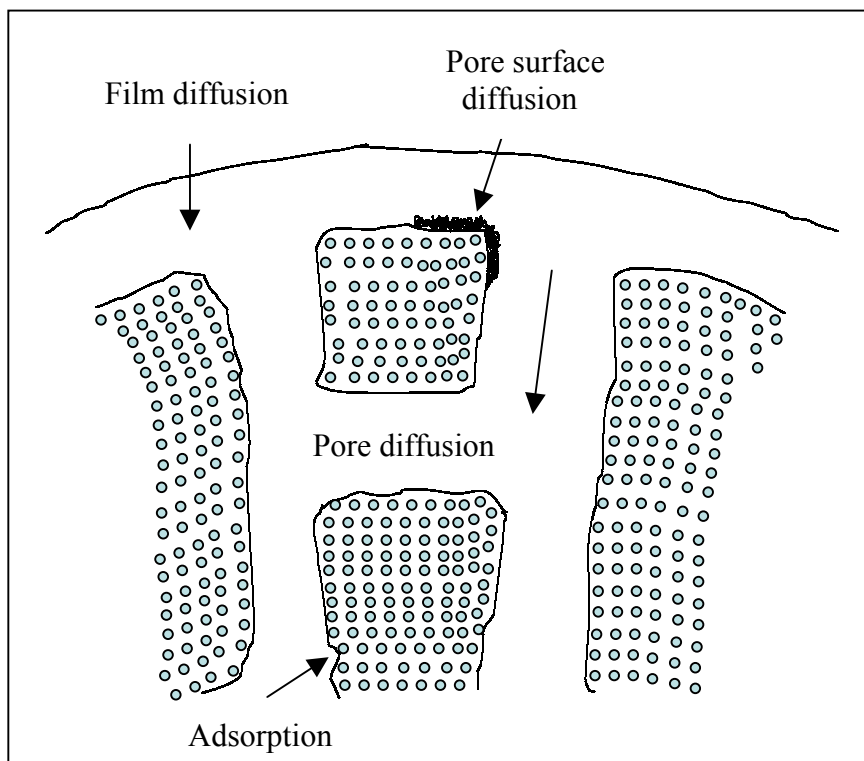


**Figure 1.5** Adsorption on a porous adsorbent particle.

Understanding the diffusion of cations, water molecules or cation-water complexes through zeolite frameworks is important because most industrial uses of ion exchange depend critically on kinetics (Dyer, 1988), as dyeing agents, selective sorbents and catalysts. Diffusion constants and activation energies have been determined for the adsorption of gases, natural zeolites and synthetic zeolites (Breck, 1984). The activation energy value represents the energy barrier to ion movement and can be used to suggest which route the ion may take through a zeolite. It can also indicate when movement is likely to be that of a hydrated or unhydrated species (Dyer, 1988).

## 1.5 Ion exchange property

Several commercial applications of zeolites exploit their ion exchange characteristics. Most of their ion exchange applications are nuclear waste containment, wastewater treatment, water purification, desiccation, carrier pesticides, odour control, oil and grease absorbent, agriculture and horticulture (Giordano, Recupero, Pino, and Bart, 1987). Ion exchange is a process in which cations or anions in a liquid are exchanged with cations or anions in a solid sorbent. Cations are exchanged with other cations, anions with other anions and electroneutrality is maintained in both the liquid and solid phase (Ruthven, 1997). Ion exchange is referred to as both an adsorption process and sorption process. However, ion exchange is most often defined as a reversible exchange of ions between a solid and liquid in which there is no substantial change in the structure of solids (Wachinski, 1997).

Zeolite has very attractive features to encourage their use as models for ion exchange which can be summarized (Qureshi and Varshney, 1991):

- 1) Unlike organic resins, zeolites do not swell appreciably when placed in water.
- 2) Zeolite unit cell dimensions do not significantly alter as a function of the size or charge of the ion present in the exchange.
- 3) Zeolite structures are the best characterized of all exchange materials (including cation and water sites), so interpretations of the mechanisms of ion replacements can be formulated.

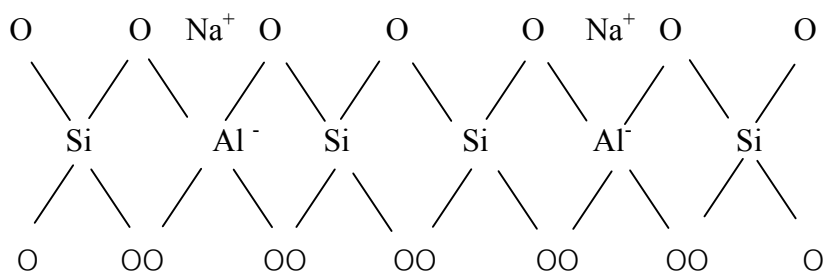
- 4) Some zeolites offer an isostructural series, so the effect of framework charge can be considered, which is in the relative proportion of Si/Al substituted in the framework (and the consequent change in total cation content).
- 5) The assemblage of SBU's into a framework creates a number of well-defined constraints to the passage of ions through the structure (ions enter the large cage in zeolite A through an eight-oxygen ring (S8R), while to gain entry to the sodalite cage, an ion must pass through a S6R. This gives rise to an ion sieve effect in some instances).
- 6) Zeolites also lend themselves well to the study of ion exchange in nonaqueous and mixed-solvent systems.

Because the silicon ion has a charge of +4, ( $\text{Si}^{4+}/4\text{O}^-$ ) and aluminium +3, ( $\text{Al}^{3+}/4\text{O}^-$ ) therefore a negative charge is in the aluminium atom, the number of  $\text{Na}^+$  ions required for charge equalization is equal to the number of aluminium ions (Farrauto, 1997). The  $\text{AlO}_4^-$  tetrahedral in the structure determines the framework charge. This is balanced by cations (for instance,  $\text{K}^+$ ,  $\text{Ca}^{2+}$  or  $\text{NH}_4^+$ ) that occupy nonframework positions (Szostak, 1989). The regularity and openness of zeolitic structures confers properties that have become of considerable industrial and fundamental research interest (Dyer, 1995).

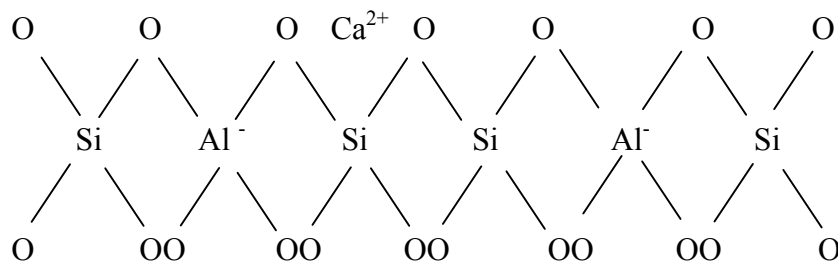
Zeolite also has the ability to exchange cations, which are positively charged ions. This substitution of ions enables zeolites to selectively adsorb certain harmful or unwanted elements from soil, water and air, for example, zeolite exchanges sodium ions for calcium ions, which results in soft water. Zeolite also has a strong affinity for certain harmful heavy metals such as mercury, lead and chromium (Amazorb, 2000).

The maximum ion exchange capacity is determined by the framework Si/Al ratio, although the actual capacity may be lower if a proportion of the cations are sited within small, inaccessible cages (Cheetham and Day, 1992).

To represent the structure of ion exchange simply, the exchangeable cations are placed near  $\text{AlO}_4^-$  tetrahedra, because the negative charges are predominantly located there. A segment of a zeolite in the sodium form is represented as follows:



when the  $\text{Na}^+$  is exchanged for  $\text{Ca}^{2+}$ , the structure is written as follows:



The single  $\text{Ca}^{2+}$  ion balances the charge of two  $\text{AlO}_4^-$  tetrahedra. In the actual zeolite, the negative charge is not localized on one or two tetrahedra but it is distributed over the framework of oxygen ions (Gates, 1992).

Most zeolites are synthesized in the alkali cation form (mostly  $\text{Na}^+$ ) in which the positively charged cations balance the negatively charged framework system. In

aluminosilicates, these cations are readily exchanged for other mono-, di and trivalent cations including  $\text{NH}_4^+$ ,  $\text{H}^+$ ,  $\text{Ca}^{2+}$  and  $\text{La}^{3+}$  (Farrauto, 1997).

The rate and degree of cation exchange in zeolites depends on:

1. The type of cation being exchanged; its diameter and charge
2. The nature of size and strength of cation coordination complexes
3. Ion exchange temperature; thermal treatment of the zeolite, before or after exchange
4. The structural properties of the zeolite and its Si:Al ratio
5. The location of cations in the zeolite
6. The concentration of the cation exchange solution and
7. Any previous treatment of the zeolite.

At the same time, Curkovic, Cerjan-Stefanovic and Filinpan (1996) reported that the metal uptake was increased with increasing temperature during the ion exchange process. Moreover, Akcay, Kilinc, and Karakas (1998) reported that a basic knowledge of the surface is of great help in understanding the adsorption behavior.

## **1.6 Analcime**

Analcime is found in deposits of various ages and types, in alter tuffs, sedimentary deposits, and in basic magmas. Whether analcime has preserved the isotopic composition from the time of formation depends on the age of the deposit, post-formation thermal history, and water/rock ratios (Faiia and Feng, 2000).

Analcime ( $\text{NaAlSi}_2\text{O}_6 \cdot \text{H}_2\text{O}$ ) is the smallest-pore zeolite and occurs widely in hydrothermal and diagenetic environments (Gottardi and Galli, 1985). The crystal

structure of analcime was one of the first zeolites to be determined (Taylor, 1930). Analcime is consistent with secondary building units based on 4-ring, 6-rings and 6-2 rings (Szostak, 1998). Its ideal crystal structure is composed of 16 formula units in a cubic unit cell (space group  $Ia3d$ ), with a random distribution of 16 Al and 32 Si atoms on the 48 tetrahedral positions and a random distribution of 16 Na atoms on the 24 channel positions. Framework O atoms are in 96 general positions, and the O atoms of the H<sub>2</sub>O molecules are in 16 channel positions. Framework O atoms are shared between linked (Si, Al) tetrahedra to form an aluminosilicate framework composed of rings of six and four tetrahedra. Sodium is coordinated inside these channels by 4 framework oxygen atoms and two water molecules. Water is found in the centre of the largest pore cages. Upon dehydration, the sodium cations become less stable due to a lower coordination number and begin to move into the position that were initially occupied by the water molecules. It is possible that the sodium migration coupled with changing unit cell dimension blocks the external water vapor from reaching some of the framework oxygen sites. This prevents the bulk isotopic composition of analcime from reaching the expected equilibrium value. As the silica content increases, the sodium content decreases, and there is a concurrent linear increase in the number of H<sub>2</sub>O molecules (Breck, 1984). This structure is similar to that of leucite (KAlSi<sub>2</sub>O<sub>6</sub>), which is tetragonal. The only difference is that the larger K atoms in leucite occupy the H<sub>2</sub>O 16 positions of analcime, instead of the Na 24 position (Kim and Kirkpatrick, 1998). Barrer (1971) reported diffusion coefficients for heulandite, chabazite, melinite and various sieve zeolites of the order of 100 thousand to 100 million times greater than that for analcime. Other zeolites can be expected to be greater in water content

and internal surface area. Analcime has the densest structure of any zeolite as shown in figure 1.6 (Szostak, 1998).

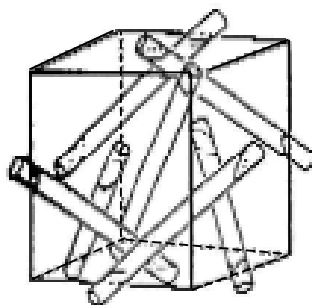


**Figure 1.6** Tube representation of analcime showing the lack of intersecting channels in the structure.

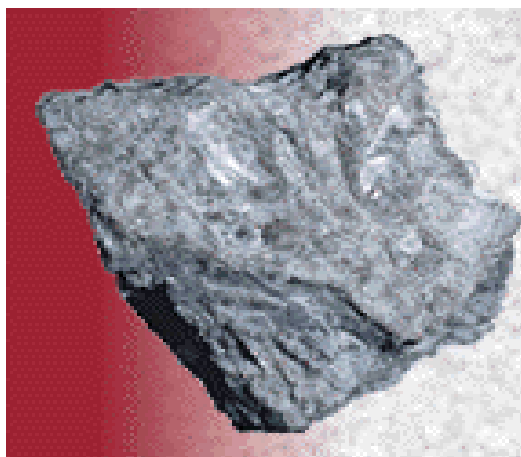
The water content of analcime varies linearly with the silica content. As the silica content increases, the cation population decreases and there is a concurrent increase in the number of water molecules. The  $\text{Na}^+$  ions can be exchanged by alkali metal cations ( $\text{Li}^+$ ,  $\text{K}^+$ ),  $\text{NH}_4^+$ ,  $\text{Ag}^+$  and divalent ions ( $\text{Ca}^{2+}$ ,  $\text{Mg}^{2+}$ ) at high temperatures (225 °C). If the ions are too large, they occupy the water positions. For example, replacement of the  $\text{Na}^+$  in analcime by  $\text{K}^+$  or  $\text{Cs}^+$  removes  $\text{H}_2\text{O}$  molecules due to occupancy of the water sites by the alkali metal ion. Therefore, the degree of hydration varies with the degree of ion exchange (Breck, 1974).

## 1.7 Perlite

Perlite is a volcanic glassy rock with a characteristic texture and an amorphous structure, usually gray, white and almost black in color, but contains two to six percent combined water. Therefore, when heated to a suitable point in its softening range, it

expands from four to twenty times its original volume. This expansion is due to the presence of two to six percent combined water in the crude perlite rock. The temperature at which expansion takes place ranges from 760 °C-1100 °C, the crude rock pops in a manner similar to popcorn as the combined water vaporizes (Bous *et al.*, 1993, Incon coporation, 2000 and Schundler, 2000). It becomes light weight perlite which is called expanded perlite. The characteristics of perlite and expanded perlite are shown in figure 1.7 (<http://www.worldminerals.com/perliteindex.asp>, 2001).

(a)



(b)



**Figure 1.7** Characteristics of perlite (a) and expanded perlite (b).

Perlite has many benefits and applications. When perlite is expanded it has a high porosity so it can be used to hold water and to provide air for roots of plants. Perlite is an essential element for plant growing such as  $\text{Fe}_2\text{O}_3$ ,  $\text{MgO}$ ,  $\text{CaO}$ ,  $\text{Na}_2\text{O}$ ,  $\text{K}_2\text{O}$ ,  $\text{MnO}$  and  $\text{P}_2\text{O}_5$  so we can use it in horticultural applications, for example, as fertilizer, to adjust the pH of soil and to adsorb chemicals in pesticides, in hydroponic growing and green houses. Because it is light in weight; has high heat resistance, and it reduces noise transmission, it is used in the construction industries in materials such as gypsum board, wall boards and swimming pool bases (Incon corporation, 2000 and Schundler, 2000).

## **1.8 Heavy metals**

During the past two decades, increasing attention has been focused on the pollution of the natural environment, especially the pollution of water. Now the threat of water pollution by heavy metals is well-known. Some heavy metals are among the most harmful of pollutants, such as toxic metals, like lead, nickel, zinc, copper and silver. Their occurrence and effects on natural water are shown in table 1 (Manahan, 1991).

World Health Organization (WHO) and European Community guidelines permitting maximum acceptable concentrations of metal pollutants in water for human consumption are copper 2.0 mg/l, nickel 0.05 mg/l and lead 0.01 mg/l (Alloyway and Ayres, 1997). The U.S. Public Health Service limits concentrations of metal pollutants in natural water to zinc 5.0 mg/l and silver 0.05 mg/l (Manahan, 1991).

**Table 1.2 Occurrence and effects of heavy metals in natural water.**

Metals	Sources	Effects
Lead	Industry, mining, coal, petrol, paint flakes	Toxicity (kidney disease, nervous system), wildlife destruction
Nickel	Ceramics, stainless steel, electronics,	Low toxicity than zinc, manganese and chromium , assumed that toxic symptoms in humans
Zinc	Industrial waste, metal plating, plumbing	Essential element in many metallo-enzymes, toxic to plants at higher levels; major component of sewage sludge, limiting land disposal of sludge
Copper	Metal plating, industrial and domestic waste, mining, mineral leaching	Essential trace element, not very toxic to animals, toxic to plants and algae at moderate levels
Silver	Natural geological sources, mining, electroplating, disinfectants of water, film-processing waste,	Causes blue-grey discoloration of skin, mucous membranes, eyes

As mentioned earlier, researchers have conducted extensive research on the conversion of zeolites from perlite collected from Lopburi province in Central Thailand and investigated their diffusion kinetic and ion exchange properties.

## 1.9 Research objectives

The objectives of this research can be summarized as follows:

1. To synthesize zeolites from perlite.

To study conditions affecting the synthesis of zeolites including:

- concentration of alkalinity (NaOH)
- reaction temperatures

- reaction times
  - solid/liquid ratios
2. To study properties of synthesized zeolite including:
    - chemical composition
    - surface area
    - particle size
    - cation exchange capacity
    - Si/Al ratio
  3. To study the kinetics of crystallization of synthetic analcime.
  4. To study the diffusion kinetics of synthetic analcime
  5. To study the ion exchange isotherm of synthesized analcime.
  6. To determine the free energy, entropy and enthalpy of ion exchange processes.

### **1.10 Scope and limitations of the study**

This research focuses on the synthesis of zeolites from perlite collected from Lopburi province in central Thailand. The factors affecting the synthesis of zeolites from perlite in various conditions, such as concentration of alkalinity (NaOH), a reaction temperatures, reaction times and solid/liquid ratios will be studied. The kinetics of zeolite crystallization, diffusion kinetics and ion exchange isotherms, as well as the physical properties of crystal products that are correlated with diffusion and ions exchange properties such as chemical composition, surface area, particle size and cation exchange capacity were determined. In addition, the thermodynamic quantities of diffusion ( $E_a$ ,  $\Delta G^*$ ,  $\Delta S^*$  and  $\Delta H^*$ ) and ion exchange ( $\Delta G^0$ ,  $\Delta S^0$  and

$\Delta H^\circ$ ) in analcime were determined. The solid products obtained from synthesis were characterized by XRD, SEM and FT-IR. All cation concentrations in the liquid phase were investigated by LSC. Chemical composition, Si/Al ratio, surface area, particle size and cation exchange capacity were determined by XRF,  $^{29}\text{Si}$  MAS NMR, BET, laser particle size analyzer and LSC method respectively.

## **Chapter II**

### **Theory and literature reviews**

#### **2.1 Theory**

##### **2.1.1 Synthetic zeolites**

At present, synthetic zeolites are used commercially more often than mined natural zeolites due to the purity of crystalline products and the uniformity of particle sizes, which can usually be produced in industry. Moreover, syntheses can be carried out using inexpensive starting materials. The synthesis of most molecular sieve zeolites is carried out in batch systems in which a caustic aluminate solution and a caustic silicate solution are mixed together. The temperature is held at some level above ambient (60 °C -180 °C) at autogenous pressures for some period of time (hours-days). Then it is quite common for the original mixture to become somewhat viscous shortly after mixing because of the formation of an amorphous phase, an amorphous alumino-silicate gel suspended in the basic medium. The viscous amorphous gel phase normally becomes less viscous as the temperature is increased. However, this is not universally true as in the case of some NH<sub>4</sub>OH-based systems which remain viscous throughout the synthesis. The amorphous gel can be filtered from the solution and dehydrated by conventional drying methods.

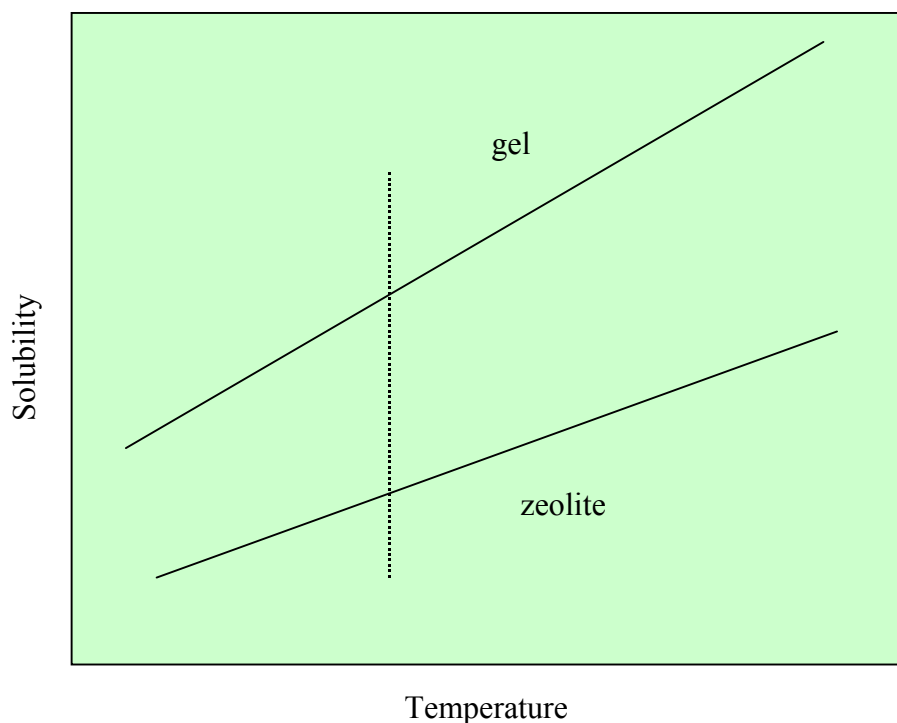


**Figure 2.1** Illustration of the thermodynamic driving force for zeolite crystallization.

As the synthesis proceeds at evaluated temperatures, zeolite crystals are formed by nucleation step, and these zeolite nuclei then grow larger by assimilation of aluminosilicate material from the solution phase. Thus during a zeolite synthesis, one might imagine that the aluminosilicate concentration in solution lies somewhere between the solubility levels of the gel and crystal phases as shown along the vertical dashed line in figure 2.1. During the synthesis, the amorphous gel has a thermodynamic tendency to dissolve, while the thermodynamic driving force is toward the formation of the crystalline zeolite phase. As crystallization occurs, the solution composition falls between the gel solubility and the crystal solubility. Zeolite crystal growth stops when sufficient material has been deposited to reduce the solution

concentration to the zeolite “equilibrium” level, which is represented in figure 2.1 (Karge and Weitkamp, 1998).

### 2.1.2 The theory of kinetics crystallization

To understand the formation mechanism of zeolite is important because of its huge industrial and commercial value. The determination of reaction kinetics is often the first step in determining the mechanism of any reaction (Walton *et al.*, 2001). This work has used XRD technique for recording the kinetic crystallization spectra of analcime. The percentage of crystallinity of synthetic analcime is defined as follows (Ghosh *et al.*, 1994):

$$\% \text{ Crystallinity} = \frac{\text{total area 12 strong peaks of sample}}{\text{total area 12 strong peaks of standard}} \times 100 \quad (2.1)$$

The optimum value of percent crystallinity of analcime was taken as the standard for the calculation of the percentage of crystallinity.

In the kinetics of crystallization of analcime, the rate of crystallization will vary proportionally to the temperature. So a study of a particular kinetic of crystallization of analcime at a temperature range of 130 °C to 145 °C will yield a rate constant for each temperature. The rate of reaction (k) dependence on temperature can be fitted to the Arrhenius equation (Laidler and Meiser, 1999).

$$\ln k = \ln A - \frac{E_a}{RT} \quad (2.2)$$

Where:

$E_a$  is the energy of activation

R is the gas constant, equal to  $8.314 \text{ JK}^{-1}\text{mol}^{-1}$

T is the temperature in Kelvin unit

To extract A and  $E_a$  from kinetic data, plot  $\ln k$  against reciprocal temperature ( $\text{K}^{-1}$ ) will be a straight line of slope  $-E_a/R$ . In order to extract the exponent n and rate constant about the kinetics crystallization of this work were determined from the Avrami equation (Walton *et al.*, 2001).

$$-\ln(1-\alpha) = kt^n \quad (2.3)$$

$$\alpha = 1 - \exp(-kt^n) \quad (2.4)$$

$$\ln(-\ln(1-\alpha)) = \ln k + n \ln t \quad (2.5)$$

Where:

$\alpha$  is the conversion factor ranging from 0 to 1

k is the rate constant( $k = d\alpha/dt$ )

n is the exponent parameter which describes reaction mechanism

Thus the plot of  $\ln(-\ln(1-\alpha))$  against  $\ln t$  will obtain a straight line of gradient n and intercept  $\ln k$ .

The Avrami exponent value depends on the dimensionality of the growth process and on the kinetic order of nucleation. In general, three-dimensional growths is combined with the first order nucleation, the Avrami exponent  $n = 3+1 = 4$ . The

Avrami exponent for different nucleation and growth mechanisms represented in table 2.1.

**Table 2.1** Exponents of the Avrami equation for different nucleation and growth mechanisms.

N	
3+1=4	Spherulitic growth + random nucleation
3+0=3	Spherulitic growth + instantaneous nucleation
2+1=3	Disc-like growth + random nucleation
2+0=2	Disc-like growth + instantaneous nucleation
1+1=2	Rod-like growth + random nucleation
1+0=1	Rod-like growth + instantaneous nucleation

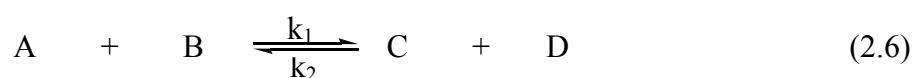
After Sharples, 1966.

### 2.1.3 The theory of diffusion kinetics

In a zeolite ion exchange, the rate of the exchange depends upon the diffusion process, cations, water molecules or cation-water complexes through the zeolite framework (Dyer, 1988). An ionic diffusion process is comparable to the movements of particle displacement in a chemical reaction. The process is initiated when molecules or atoms react to the approach of one another with collisions between them being unavoidable. Then, there is a transfer of energy and the free energy barrier is overcome (Eying, 1935). As mentioned earlier, the phenomenon of diffusion has been described assuming a random forward and backward displacement process which has to overcome a series of energy barriers, which can be obtained by a sequence of

activating and deactivating collisions with the neighboring species (Yusof, 1984). The evaluation of thermodynamic parameters in the diffusion process can be investigated using the following equations respectively.

Firstly, the Arrhenius equation can be derived by considering a simple second order Reaction (Latham and Burgess, 1977):



An Arrhenius equation can explain the rate of certain processes which is controlled by the ability to overcome a critical energy barrier known as activation energy. If  $k_1$  and  $k_2$  are the rates of forward and backward reaction respectively, then at equilibrium:

$$\begin{aligned} k_1 ab &= k_2 cd && \text{or} \\ \frac{cd}{ab} &= \frac{k_1}{k_2} \end{aligned} \quad (2.7)$$

Where a, b, c and d are the concentrations of species A, B, C and D, respectively.

When a collision occurs between two molecules, they pass into a transition state with the formation of an activation complex. If there is a difference in energy between the transition state and the reactants, the activation energy of the forward reaction is represented by  $E_1^*$  and for the reverse reaction is  $E_2^*$ . Then the total energy change,  $\Delta E$  would be given by:

$$\Delta E = E_1^* - E_2^* \quad (2.8)$$

At constant temperature and pressure where there is no change in volume:

$$\Delta E = \Delta H$$

Where  $\Delta H$  is the change in enthalpy. Therefore the relation is represented as:

$$\Delta H = E_1^* - E_2^* \quad (2.9)$$

Van't Hoff proposed an equation relating the equilibrium constant  $K$  and the absolute temperature  $T$  to the enthalpy change  $\Delta H$  and it is given by:

$$\frac{d \ln K}{dT} = \frac{\Delta H}{RT^2} \quad (2.10)$$

Since  $k_1/k_2 = K$  and  $\Delta H = E_1^* - E_2^*$ , so equation 2.10 becomes:

$$\frac{d}{dT} \ln \frac{k_1}{k_2} = \frac{E_1^* - E_2^*}{RT^2} \quad (2.11)$$

then rearranging the relationship to obtain:

$$\frac{d \ln k_1}{dT} - \frac{d \ln k_2}{dT} = \frac{E_1^*}{RT^2} - \frac{E_2^*}{RT^2} \quad (2.12)$$

As suggested by Arrhenius, the kinetics of the forward and reverse process of the reaction is independent, so equation 2.12 can be written as:

$$\frac{d \ln k_1}{dT} = \frac{E_1^*}{RT^2} + I \quad (2.13)$$

$$\frac{d \ln k_2}{dT} = \frac{E_2^*}{RT^2} + I \quad (2.14)$$

Where I is a constant.

Prior to chemical reaction, Arrhenius (1988) proposed that an activated complex should be formed and then the activated energy represents the amount of energy that the reactant molecules must attain before the formation of this activated complex. The value of I is assumed to be zero. Thus, the variation of the rate constant K with temperature T and activation  $E_a$  can be represented by the relationship:

$$\frac{d \ln K}{dT} = \frac{E_a}{RT^2} \quad (2.15)$$

where R is the gas constant.

If  $E_a$  is constant, then integrating equation 2.15 with respect to T will give the Arrhenius equation:

$$d \ln K = \frac{E_a}{RT} + \text{constant} \quad (2.16)$$

When  $E_a$  is assumed to be independent of  $T$ , then equation 2.16 can be expressed as:

$$K = A \exp^{-E_a/RT} \quad (2.17)$$

where  $A$  is a constant known as the pre-exponential factor.

Arrhenius gave the diffusion coefficient,  $D$ , an analog form of equation 2.17 incorporating.

$$D_i = D_o \exp^{-E_a/RT} \quad (2.18)$$

where:

$E_a$  is the activation energy

A plot of  $\ln D_i$  against reciprocal temperature ( $K^{-1}$ ) could yield a straight line of slope  $-E_a/R$ . The entropy of activation ( $\Delta S^*$ ) can be calculated from:

$$D_o = 2.72(kTd^2/h) \exp\left(\frac{\Delta S^*}{R}\right) \quad (2.19)$$

where  $k$  is the Boltzmann constant ( $1.3806 \times 10^{-23} \text{ JK}^{-1}$ )

$d$  is the interionic jump distance between adjacent sites (0.75 nm)

$h$  is the Planck's constant ( $6.6260 \times 10^{-34} \text{ Js}$ )

$D_o$  is a pre-exponential factor presenting the hypothetical self-diffusion coefficient at absolute zero.

In 1979, Barrer, Barri and Klinowski developed the BBK equation to evaluate the diffusion coefficient ( $D_i$ ). The equation can be represented as:

$$I_0 = \int_0^{\infty} \left(1 - \frac{w_t}{w_{\infty}}\right) dt = \frac{r_0^2}{15D_i} \quad (2.20)$$

where  $I_0$  is the area between asymptotes

$W_t$  is the extent of exchange at time  $T = t$

$W_{\infty}$  is the extent of exchange at time  $T_{\infty}$  (amount of diffusion at equilibrium)

$r$  is the radius of the particle size

$D_i$  is the diffusion coefficient

The enthalpy of activation ( $\Delta H^*$ ) was calculated from:

$$\Delta H^* = E_a - RT \quad (2.21)$$

The free energy of activation ( $\Delta G^*$ ) was estimated by using the equation:

$$\Delta G^* = \Delta H^* - T\Delta S^* \quad (2.22)$$

#### 2.1.4 The cation exchange capacity (CEC)

The cation exchange process occurs when ions from a solution replace cations in the zeolite crystal structure. The cation exchange capacity (CEC) is a measure of the number of cations per unit weight or volume available for exchange, and is a very important property of zeolite species. It is usually expressed as milliequivalents per

100 g of sample. The exchangeable ions commonly are  $\text{Ca}^{2+}$ ,  $\text{Mg}^{2+}$ ,  $\text{K}^+$ ,  $\text{Na}^+$  and  $\text{NH}_4^+$ . When studying natural zeolites, the ammonium ion is most usually used for the CEC test (Holmes, 1987). The exchange medium solution should be of high concentration such as 1 M and the sample should be saturated until exchange no longer occurs. For zeolite minerals, it could take as long as 7 days. The cation exchange capacities of some zeolites show high selectivity as shown in table 2.2.

**Table 2.2** Exchange capacities of some zeolites (Vaughan, 1978).

Zeolites	Exchange capacities(meq/100g)
Edigtonite $\text{Ba}[\text{Al}_2\text{Si}_3\text{O}_{10}]\cdot 4\text{H}_2\text{O}$	390
Natrolite $\text{Na}_2[\text{Al}_2\text{Si}_3\text{O}_{10}]\cdot 2\text{H}_2\text{O}$	530
Thomsonite $\text{NaCa}_2[\text{Al}_5\text{Si}_5\text{O}_{20}]\cdot 6\text{H}_2\text{O}$	620
Heulandite $\text{Ca}[\text{Al}_2\text{Si}_6\text{O}_{16}]\cdot 5\text{H}_2\text{O}$	330
Analcime $\text{Na}[\text{AlSi}_2\text{O}_6]\cdot \text{H}_2\text{O}$	450
Mordenite $1/2\text{Ca}, \text{Na}[\text{AlSi}_5\text{O}_{12}]\cdot 3.3\text{H}_2\text{O}$	230
Chabazite $1/2\text{Ca}, \text{Na}[\text{AlSi}_2\text{O}_6]\cdot 3\text{H}_2\text{O}$	400
Faujasite $\text{Ca}, \text{Na}_2[\text{Al}_2\text{Si}_5\text{O}_{14}]\cdot 6.6\text{H}_2\text{O}$	390

### 2.1.5 Ion exchange

Heavy metal is well-known as a toxic substance and therefore their removal from wastewater is required prior to discharge into receiving waters. Among several methods available, ion exchange is an attractive one. Ion exchange is the exchange of ions between a liquid phase and a porous solid, which may be synthetic analcime, especially when an economically exchanger is used. Moreover, the synthetic zeolite is

better for research and industrial applications because of its greater uniformity in composition and purity (Breck, 1974). Other physico-chemical systems for ion exchange can be studied from the viewpoint of equilibrium (selectivity), energy and kinetics (exchange and tracer diffusion).

### **2.1.5.1 The selectivity factors of ion exchange**

The selectivity factors of ion exchange may be summarized:

- a) framework topology
- b) ion size and shape
- c) charge density on anionic framework
- d) ion valency
- e) electrolyte concentration in the aqueous phase.

#### **2.1.5.1.1 Framework topology, ion size and shape**

Framework topology, ion size and shape often determine whether a given ion can fit readily into the framework and stability of the product. The more open zeolite structures are regularly observed in the thermodynamic affinity sequences (Vaughan, 1978). Most common ions will exchange readily into most zeolites. However, the ion-sieving effect is observed with the zeolites having the smallest pore openings and with the largest cations. For example,  $\text{Rb}^+$  (3.0 Å diameter) will slowly enter analcime but  $\text{Cs}^+$  (3.4 Å diameter) will not, suggesting that analcime has an effective pore size of

$\sim 3.2 \text{ \AA}$  which contrasts with the pore opening for analcime of  $2.6 \text{ \AA}$  calculated from crystallography data represented in figure 2.2 (Sherman, 1978).

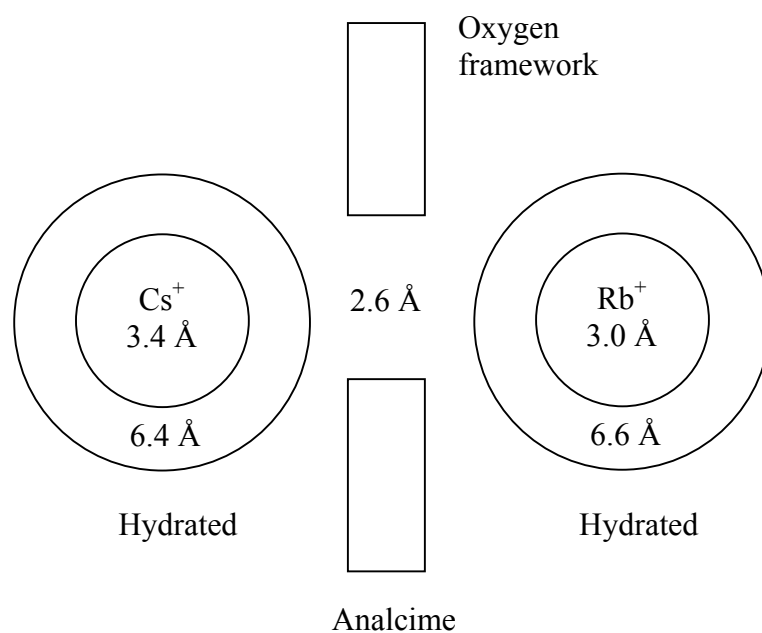


**Figure 2.2** Representation of ion-sieving effect for  $\text{Cs}^+$  and  $\text{Rb}^+$  into analcime (Dyer, 1988).

Examples of ion exchange properties of zeolites are represented in table 2.3. The data in table 2.4 shows that the hydration energy of a cation depends on the charge, the radius of the cation and the electronegativity of the element. The list of effective diameter values for various ions in aqueous solution is shown in table 2.5.

**Table 2.3** Ion exchange properties.

zeolites	Si/Al ratio	Original Cations	Exchange selectivity
Analcime	2	Na	$K^+ < Li^+ < Na^+ \leq Ag^+$ (Barrer, 1950)
Chabazite	1.4-2.8	Ca, K	$Tl^+ > Cs^+ > K^+ > Ag^+ > Rb^+ > NH_4^+ > Pb^{2+} > Na^+ = Ba^{2+} > Sr^{2+} > Ca^{2+} > Li^{2+}$
Clinoptilolite	3-4	Ca, Na, K	$Cs^+ > K^+ > Sr^{2+} > = Ba^{2+} > Ca^{2+} > >> Na^+ > Li^+$ $Pb^{2+} > Ag^+ > Cd^{2+} \sim Zn^{2+} > Cu^{2+} > Na^+$
Erionite	3.2-6.2	Na, K	$Cs^+ > Sr^{2+} > K^+ > Na^+$
Mordenite	4.4-5.5	Ca, Na	$Cs^+ > K^+ > NH_4^+ > Na^+ > Ba^{2+} > Li^+$ $NH_4^+ > Na^+ > Mn^{2+} > Cu^{2+} > Co^{2+} \sim Zn^{2+} > Ni^{2+}$
Phillipsite	1.3-2.9	K, Ca, Na	$Ba^{2+} > Rb^+ \sim Cs^+ \sim K^+ > Na^+ >> Li^+$

**Table 2.4** Hydration enthalpies of metal cations.

Electronegativity < 1.5			Electronegativity > 1.5		
Ion	Radius (Å) (shannon, 1976)	$\Delta H_{hyd}$ (kJ mol <sup>-1</sup> ) (Burgess, 1978)	Ion	Radius (Å) (shannon, 1976)	$\Delta H_{hyd}$ (kJ mol <sup>-1</sup> ) (Burgess, 1978)
Li <sup>+</sup>	0.59	-515	Tl <sup>+</sup>	1.50	-326
Na <sup>+</sup>	0.99	-405	Ag <sup>+</sup>	0.67	-475
K <sup>+</sup>	1.37	-321	Pb <sup>2+</sup>	0.98	-1480
Rb <sup>+</sup>	1.52	-296	Co <sup>2+</sup>	0.58	-2054
Cs <sup>+</sup>	1.67	-263	Ni <sup>2+</sup>	0.55	-2106
Ca <sup>2+</sup>	1.00	-1592	Cu <sup>2+</sup>	0.57	-2100
Mg <sup>2+</sup>	0.57	-1922	Zn <sup>2+</sup>	0.60	-2044

**Table 2.5** Effective ion diameters (Å) for an inorganic complexes in aqueous solution (after Kielland, 1937)<sup>a</sup>.

(Å)	
2.5	Rb <sup>+</sup> , Cs <sup>+</sup> , Tl <sup>+</sup> , NH <sub>4</sub> <sup>+</sup> , Ag <sup>+</sup>
3	K <sup>+</sup> , Cl <sup>-</sup> , Br <sup>-</sup> , I <sup>-</sup> , CN <sup>-</sup> , NO <sub>2</sub> <sup>-</sup> , NO <sub>3</sub> <sup>-</sup>
3.5	OH <sup>-</sup> , F <sup>-</sup> , NCS <sup>-</sup> , NCO <sup>-</sup> , HS <sup>-</sup> , ClO <sub>3</sub> <sup>-</sup> , ClO <sub>4</sub> <sup>-</sup> , BrO <sub>3</sub> <sup>-</sup> , IO <sub>4</sub> <sup>-</sup> , MnO <sub>4</sub> <sup>-</sup>
4	Hg <sub>2</sub> <sup>2+</sup> , SO <sub>4</sub> <sup>2-</sup> , S <sub>2</sub> O <sub>3</sub> <sup>2-</sup> , S <sub>2</sub> O <sub>8</sub> <sup>2-</sup> , SeO <sub>4</sub> <sup>2-</sup> , CrO <sub>4</sub> <sup>2-</sup> , HPO <sub>4</sub> <sup>2-</sup> , S <sub>2</sub> O <sub>6</sub> <sup>2-</sup> , PO <sub>4</sub> <sup>3-</sup> , Fe(CN) <sub>6</sub> <sup>3-</sup> , Cr(NH <sub>4</sub> ) <sub>6</sub> <sup>3+</sup> , Co(NH <sub>3</sub> ) <sub>5</sub> H <sub>2</sub> O <sup>3+</sup>
4-4.5	Na <sup>+</sup> , CdCl <sup>+</sup> , ClO <sub>2</sub> <sup>-</sup> , IO <sub>3</sub> <sup>-</sup> , HCO <sub>3</sub> <sup>-</sup> , H <sub>2</sub> PO <sub>4</sub> <sup>-</sup> , HSO <sub>3</sub> <sup>-</sup> , H <sub>2</sub> AsO <sub>4</sub> <sup>-</sup> , Co(NH <sub>3</sub> ) <sub>4</sub> (NO <sub>2</sub> ) <sub>2</sub> <sup>+</sup>
4.5	Pb <sup>2+</sup> , CO <sub>3</sub> <sup>2-</sup> , SO <sub>3</sub> <sup>2-</sup> , MO <sub>4</sub> <sup>2-</sup> , Co(NH <sub>3</sub> ) <sub>5</sub> Cl <sup>2+</sup> , Fe(CN) <sub>5</sub> NO <sup>2-</sup>
5	Sr <sup>2+</sup> , Ba <sup>2+</sup> , Ra <sup>2+</sup> , Cd <sup>2+</sup> , Hg <sup>2+</sup> , S <sup>2-</sup> , S <sub>2</sub> O <sub>4</sub> <sup>2-</sup> , WO <sub>4</sub> <sup>2-</sup> , Fe(CN) <sub>6</sub> <sup>4-</sup>
6	Li <sup>+</sup> , Ca <sup>2+</sup> , Cu <sup>2+</sup> , Zn <sup>2+</sup> , Sn <sup>2+</sup> , Mn <sup>2+</sup> , Fe <sup>2+</sup> , Ni <sup>2+</sup> , Co <sup>2+</sup> , Co(S <sub>2</sub> O <sub>3</sub> )(CN) <sub>5</sub> <sup>4-</sup>
8	Mg <sup>2+</sup> , Be <sup>2+</sup>
9	H <sup>+</sup> , Al <sup>3+</sup> , Fe <sup>3+</sup> , Cr <sup>3+</sup> , Sc <sup>3+</sup> , Y <sup>3+</sup> , La <sup>3+</sup> , Ce <sup>3+</sup> , Pr <sup>3+</sup> , Nd <sup>3+</sup> , Sm <sup>3+</sup> , In <sup>3+</sup> , Co(SO <sub>3</sub> ) <sub>2</sub> (CN) <sub>4</sub> <sup>5-</sup>
11	Th <sup>4+</sup> , Zr <sup>4+</sup> , Ce <sup>4+</sup> , Sn <sup>4+</sup>

<sup>a</sup>Ottonello, 1997

### 2.1.5.1.2 Charge density

For both of synthetic and natural zeolites it is possible to vary the  $\text{SiO}_2/\text{Al}_2\text{O}_3$  ratio of a given framework, for example for, synthetic and natural chabazite it was found that the above ratio varies between 2.1 (Barrer and Baynham, 1956) to 7.8. (Gude and Sheppard, 1966). The higher  $\text{SiO}_2/\text{Al}_2\text{O}_3$  ratio represents a large charge density which could affect the selectivity of the ion pair. For the exchange of a pair of ions between the alumina (high charge) and silica (low charge) forms of the given zeolite, the larger ion was preferred by the low charge form and the smaller by the high charge one (Vaughan, 1978). The Si/Al ratios and water content of synthetic analcime in this work and others is shown in table 2.6.

**Table 2.6** Comparison of the Si/Al ratios and water content of synthetic analcime in this work and other studies.

Si/Al ratios	Water content (%)	References
1.97	8.5	This work
1.81	8.9	Dyer and Yusof, 1964
2.0	7.3	Dyer and Molyneux, 1968
4	8.5	Barrer and Hinds, 1953
-	8.4	Todorovic <i>et al.</i> , 1987

### 2.1.5.1.3 Electrolyte concentration

The exchange process for the univalent ions, concentration of electrolyte has no large effect upon its selectivity. However, when the ions have different charges, the situation becomes more complex. Selectivity is greater for the ion of higher valence in the dilute exchanging solution (table 2.7).

**Table 2.7** Exchange limits in faujasite (zeolite X) at room temperature

(Barrer, Buser, and Grutter, 1956).

Ion	Exchange solution	% Exchange
$\text{NH}_4^+$	2 N	92
$\text{CH}_3 \text{NH}_3^+$	2 N	58
$(\text{CH}_3)_2 \text{NH}_2^+$	1 N	37
$(\text{CH}_3)_3 \text{NH}^+$	2 N	28
$(\text{CH}_3)_4 \text{N}^+$	2 N	23

### 2.1.5.1.4 Zeolite stability

Zeolites have rigid, strong frameworks, stable at high temperatures, oxidation/reduction and ionizing radiation, not subject to physical attrition due to osmotic shock. The ion exchange properties of the zeolites are more constant and predictable over wide ranges of temperature and ionic strength than other ion exchangers. Zeolites are also stable at evaluated pH levels (for example 7 to 12) at

which other inorganic ion exchangers (Zirconium phosphates, etc) tend to lose functional group due to slow hydrolysis (Larsen and Vissers, 1960).

### 2.1.5.2 Theoretical treatment of ion exchange

The ion exchange process can be represented by the following equation (Breck, 1974):



where  $Z_A$  and  $Z_B$  are the charge of the exchange of cations A and B and the subscripts z and s refer to the zeolite and solution.  $A^{Z_A+}$  is the ionic species in the solution phase and is called the in-going cation and species  $B^{Z_B+}$  is in the zeolite.

The ion exchange isotherm is plotted by expressing the equilibrium values of a component of the solid phase against the same component in the solution phase. Graphical representation of the equivalent fractions of exchanging cation in the solution and zeolite are defined by:

$$A_s = \frac{z_A m_A}{\sum_1^i z_i m_i}, \quad (2.24)$$

$$A_z = \frac{z_A \bar{m}_A}{\sum_1^i z_i \bar{m}_i}, \quad (2.25)$$

where;

$A_s, A_z$  = equivalent fraction of  $A^{Z_A+}$  ion in solution and zeolite, respectively

$m_A, m_B$  = Molality of ions  $A^{Z_A+}$  and  $B^{Z_B+}$  in the solution phase, respectively

$\bar{m}_A, \bar{m}_B$  = Molality of ions  $A^{Z_A+}$  and  $B^{Z_B+}$  in the exchanger phase, respectively

$\sum_1^i z_i m_i$  = Total normality of the solution

$\sum_1^i z_i \bar{m}_i$  = Total cation exchange capacity of the exchanger (Q)

The equilibrium can be described in one of three ways;

- i) As the separation factor ( $\alpha_B^A$ )
- ii) As the selectivity coefficient (mass action quotient  ${}^A K_m$ ) and as the corrected selectivity coefficient ( ${}^A K_C$ )
- iii) As the thermodynamic equilibrium constant ( ${}^A K_a$ )

### The separation factor, $\alpha_B^A$

The preference of zeolite for one of two ions is expressed by the separation factor,  $\alpha_B^A$ , defined by

$$\alpha_B^A = \frac{A_Z B_S}{B_Z A_S} = \frac{\text{Area I}}{\text{Area II}}, \quad (2.26)$$

where  $A_Z$  and  $B_S$  are the equivalent fractions of the exchanging cation A in zeolite and B in solution. If the value of the separation factor is greater than unity, the exchanger reflects preference for the in-going cation,  $A^{Z_A+}$ . It follows that if the value is unity

there is no preference for either ion and if less than unity then the exchanger prefers the counter ion. The separation factor is the ratio of the two areas depicted in the figure below.

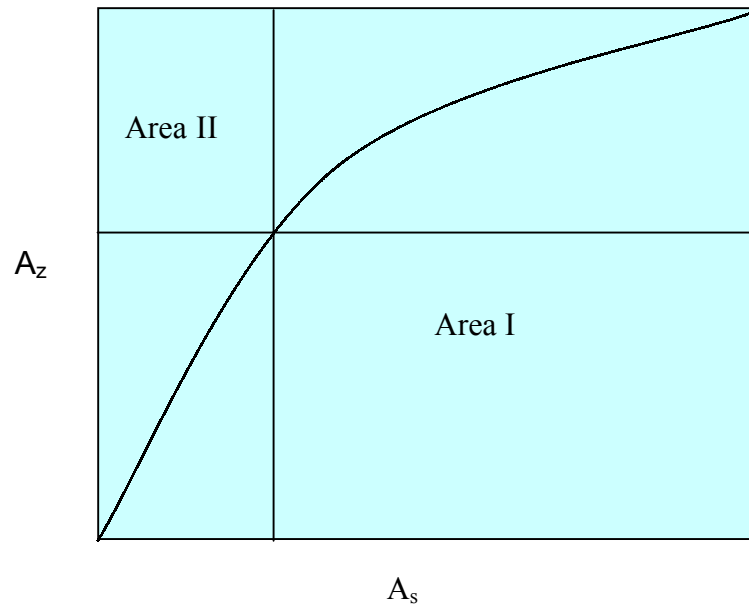


**Figure 2.3** Derivation of the selectivity coefficient.

The rational selectivity coefficient ( $\overset{A}{B}K_m$ ) can be defined by

$$\overset{A}{B}K_m = \frac{m_B^{z_A} A_z^{z_B}}{m_A^{z_B} B_z^{z_A}}, \quad (2.27)$$

where  $\overset{A}{B}K_m$  includes the charge of ion  $Z_A$  and  $Z_B$ .  $m_A$ ,  $m_B$  = Molality of the  $A^{z_A+}$  and  $B^{z_B+}$  in the solution phase ( $\text{mole kg}^{-1}$ ), respectively.  $z_A$ ,  $z_B$  = Modulus of the charge of the ions  $A^{z_A+}$  and  $B^{z_B+}$ , respectively.

In terms of the dissolved electrolytes, the corrected selectivity coefficient ( ${}^A K_c$ ) is defined by

$${}^A K_c = {}^A K_m \Gamma \quad (2.28)$$

$$\Gamma = \frac{\gamma_B^{z_A}}{\gamma_A^{z_B}} = \left[ \frac{\left( \gamma_{\pm BX}^{AX} \right)^{z_A(z_B + z_X)}}{\left( \gamma_{\pm AX}^{BX} \right)^{z_B(z_A + z_X)}} \right]^{\frac{1}{z_X}} \quad (2.29)$$

$\Gamma$  = Ratio of the mean molal stoichiometric activity coefficients.

$\gamma_B^{z_A}$ ,  $\gamma_A^{z_B}$  = Activity of ion  $B^{z_B+}$  and  $A^{z_A+}$  raised to the power of the modulus of the valency of the counter ion.

Therefore, the thermodynamic equilibrium constant  ${}^A K_a$  is defined by

$${}^A K_a = {}^A K_c \frac{f_A^{z_B}(z)}{f_B^{z_A}(z)}, \quad (2.30)$$

where  $f_A(z)$  and  $f_B(z)$  are the activity coefficients of ion  $A^{z_A+}$  and  $B^{z_B+}$  in the zeolite.

The thermodynamics equilibrium constant is evaluated by using the reaction:

$$\ln {}^A K_a = (z_B - z_A) + \int_0^1 \ln {}^A K_c dA_Z \quad (2.31)$$

${}^A K_a$  can be determined from the graphical integration of a plot of Kielland plot,

$\ln {}^A K_c$  against  $A_Z$ . The free energy of ions exchange ( $\Delta G^\circ$ ) are determined by the equation (2.32).

$$\Delta G^\circ = \frac{-RT}{Z_A Z_B} \ln {}^A_B K_a \quad (2.32)$$

and the standard entropy, ( $\Delta S^\circ$ ) by

$$\Delta S^\circ = \frac{\Delta H^\circ - \Delta G^\circ}{T} \quad (2.33)$$

The standard enthalpy is obtained from the variation of  ${}^A_B K_a$  with temperature:

$$\frac{d \ln {}^A_B K_a}{dT} = \frac{\Delta H^\circ}{RT^2} \quad (2.34)$$

### 2.1.6 X-ray powder diffraction

A very powerful method for the characterization of inorganic solids is powder X-ray diffraction. In this technique, a beam of X-rays is directed at a powdered sample of the compound to be studied. The X-ray beam is scattered by the atoms in the sample and is detected. If the sample is crystalline, constructive and destructive interference cause the X-rays to be scattered only in certain directions. The intensities of the scattered X-rays are determined as a function of the angle between the incident beam and the scattered ray (Girolami *et al.*, 1999). The relationship between the wavelength of the X radiation, the angle of diffraction, and the distance between each set of atomic planes of the crystal lattice is given by the Bragg condition. From the Bragg condition one can calculate the interplanar distances of the crystalline material. The interplanar spacing depends solely on the geometry of the crystal's unit cell while the intensities of the diffracted X-ray depend on the type of atoms in the crystal and the location of the atoms in the fundamental repetitive unit cell (Dean, 1995). As for zeolites, it reflects the framework and nonframework symmetry of the constituents of each zeolite to produce a diagnostic fingerprint of  $2\theta$  (or  $d$ ) spacing according to Bragg's equation:

$$n \lambda = 2d \sin \theta, \quad 2.35$$

where  $n$  = an integer,  $\lambda$  is the wavelength of the incident X-ray,  $d$  is the value of the interlayer spacing of the component atoms and ions and  $\theta$  is the scattering angle (Dyer, 1988). Diffraction of X-rays by a crystal lattice is shown in figure 2.3 (Skoog, 1998).

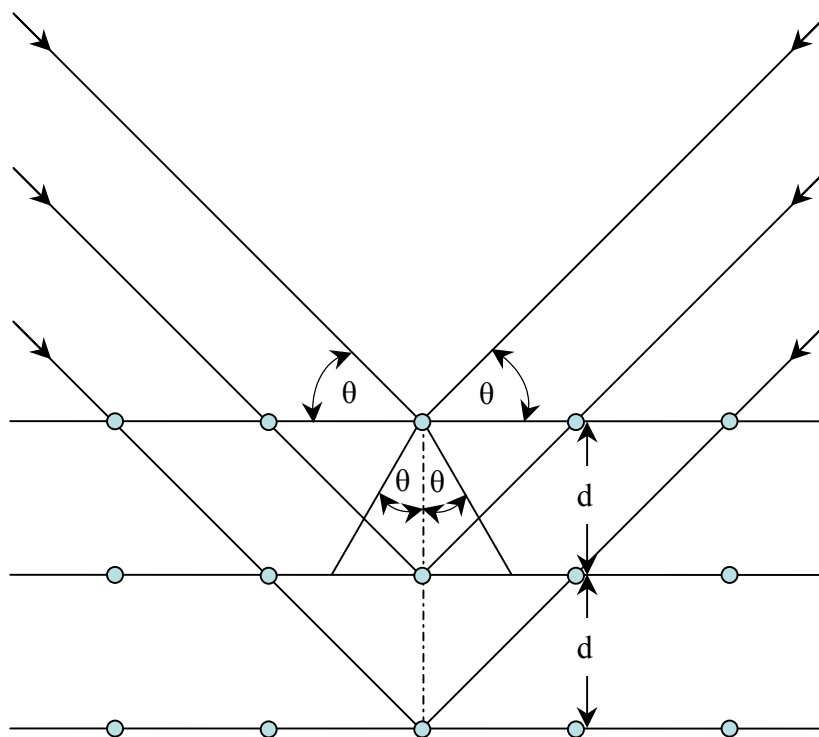


**Figure 2.4** Diffraction of X-rays by a crystal.

The plot of the intensity of the scattered X-ray against angle is called a diffraction pattern, which is different for different substances. One can often match the observed diffraction pattern with that of a known compound and in this way one can often quickly identify what the solid sample is made of. Powder X-ray diffraction patterns can also be used to determine the structures of new compounds. Crystalline solids give X-ray diffraction patterns that contain sharp peaks. In contrast, amorphous or noncrystalline substances (such as glass or liquid water) scatter X-rays in all directions and give X-ray diffraction that contains no sharp peaks.

### 2.1.7 Brunauer-Emmett-Teller (BET)

In 1938, Brunauer *et al.* first developed the BET theory for a flat surface and there is no limit in the number of layers that can be accommodated on the surface. The surface is energetically homogeneous (adsorption energy does not change with the progress of adsorption in the same layer) and there is no interaction among adsorbed molecules.

$$\frac{V}{V_m} = \frac{1}{(1-P/P_o)} \quad 2.36$$

Equation 2.36 is the famous BET equation, and it is used extensively for the determination of area because once the monolayer coverage  $V_m$  is known and if the area occupied by one molecule is known the surface area of the solid can be calculated. To conveniently determine  $V_m$ , the BET equation can be cast into the form, which is amenable for a linear plot as follows:

$$\frac{P}{V(P_o - P)} = \frac{1}{V_m C} + \left( \frac{C-1}{V_m C} \right) \frac{P}{P_o} \quad 2.37$$

The pressure range of validity of the BET equation is  $P/P_o = 0.05-0.3$ . For relative pressures above 0.3, there exists capillary condensation, which is not amenable to multilayer analysis. A plot of  $(P/(V(P_o-P)))$  versus  $P/P_o$  would yield a straight line with a slope  $((C-1)/CV_m)$  and an intercept  $(1/CV_m)$ . Usually the value of  $C$

is very large because the adsorption energy of the first layer is larger than the heat of liquid faction, the slope is then simply the inverse of the monolayer coverage, and the intercept is effectively the origin of such plot. Therefore, very often only one point is sufficient for the first estimate of the surface area.

Once  $V_m$  (mole/g) is obtained from the slope, the surface area is calculated from:

$$A = V_m N_A a_m, \quad 2.38$$

Where  $N_A$  is the Avogadro number and  $a_m$  is the molecular project area (nitrogen = 16  $\text{Å}^2$ /molecule at 77 K) (Do, 1998).

### 2.1.8 X-ray fluorescence spectrometry (XRF)

X-ray fluorescence is a spectroscopic technique of analysis based on the fluorescence of atoms in the x-ray domain, to provide qualitative or quantitative information on the elemental composition of a sample. Excitation of the atoms is achieved by an x-ray beam or by bombardment with particles such as electrons. The universality of this phenomenon, the speed with which the measurements can be obtained and the potential to examine most materials without preparation all contribute to the success of this analytical method, which does not destroy the sample. However, the calibration procedure for x-ray fluorescence is a delicate operation.

In general, when a sample is irradiated by a source that emits photons of very high energy (from 5 to 60 keV). X-ray photoluminescence is observed and it is characteristic of the elements present in the sample. The fluorescence spectrum is

made up of radiation with frequencies and intensities which are characteristic of the composition of the sample, allowing a qualitative or quantitative analysis. In practice, this non-destructive mode of analysis can be used for all elements starting from Boron ( $Z = 5$ ) in solids or liquid homogeneous samples without, in theory, any particular preparation. The emission spectrum varies slightly on the chemical combination or chemical state of the elements in the sample. X-ray fluorescence of an element is a two step process. The first step is excitation during which the interaction of the photon, given sufficient energy, leads to the stippling off of a lower shell electron such as a K electron. This photoelectric effect leads to internal ionization and to emission of photoelectrons as shown in figure 2.4.

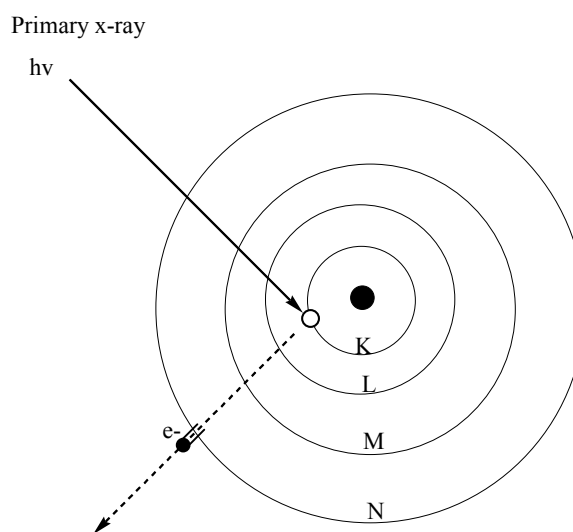


**Figure 2.5** Simplified of photoelectric effect leads to internal ionization and to emission of photoelectrons.

The second step corresponds to the stabilization of the reemission of part or all of its energy-required excitation. The energy gap caused by the preceding step is

immediately followed by electron reorganization that takes the atom back to its ground state (in  $10^{-16}$  s). For all the elements, fluorescence appears in the energy range of 40 eV to more than 100 keV (Rouessac, 2000).

### **2.1.9 Fourier transform infrared spectrophotometer (FT-IR)**

Infrared spectroscopy (IR) includes several methods that are based on the absorption (or reflection) of electromagnetic radiation with wavelengths in the range of 1  $\mu\text{m}$  to 1000  $\mu\text{m}$ . This spectral range can be divided into three groups, near IR (1 to 2.5  $\mu\text{m}$ ), mid IR (2.5  $\mu\text{m}$  to 25  $\mu\text{m}$ ) and far IR (beyond 25  $\mu\text{m}$ ). The frequency range that is the most accessible and the richest in providing structural information is the middle range. Molecules have specific frequencies that are directly associated with their rotation and vibration motions. Infrared absorption results from changes in the vibration and rotation state of a molecular bond. The absorption bands present in this frequency domain form a molecular fingerprint, thus allowing the detection of compounds and the destruction of structural details. The mid-infrared region is divided into the group frequency region,  $4000\text{ cm}^{-1}$  to  $1300\text{ cm}^{-1}$  (2.5  $\mu\text{m}$  to 7.69  $\mu\text{m}$ ), and the fingerprint region,  $1300\text{ cm}^{-1}$  to  $650\text{ cm}^{-1}$  (7.69  $\mu\text{m}$  to 15.38  $\mu\text{m}$ ). In the group-frequency region the principal absorption bands are more or less dependent on the only the functional group from which the absorption arises and not on the complete molecular structure. The fingerprint region involves motion of bonds linking a substituent group to the remainder of the molecule. These are single bond stretching frequencies and bending vibrations of a polyatomic system (Dean, 1995 and Rouessac, 2000).

Fourier transform infrared spectrophotometers first appeared in the 1970s. These single beam instruments differ from scanning spectrometers, which have an interferometer of the Michelson type placed between the source and the sample, replacing the monochromator as shown in figure 2.5. Fourier transforms spectrometers are capable of simultaneous analysis of the full spectral range using interferometry (Rouessac, 2000).

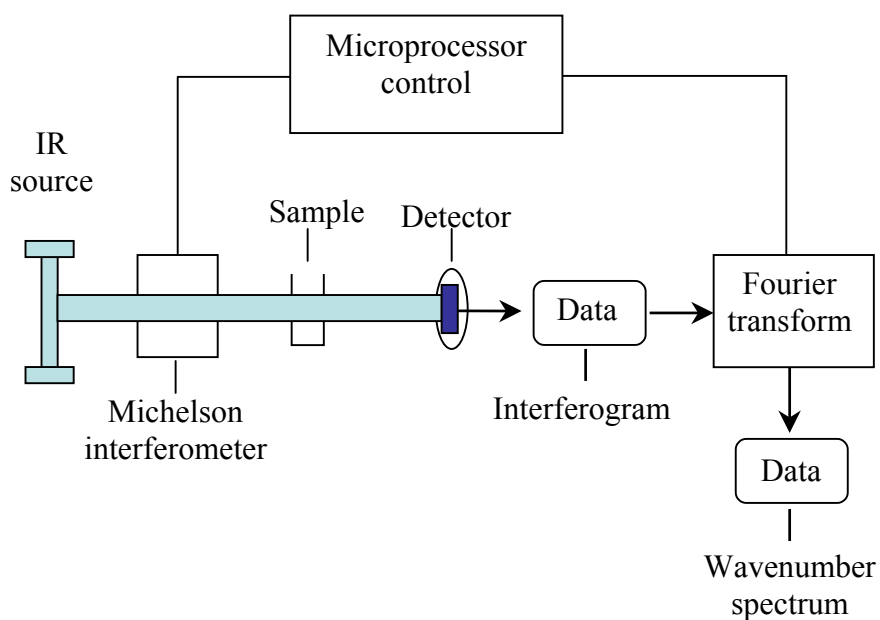


**Figure 2.6** Diagram of Fourier transform infrared spectrophotometer.

### **2.1.10 Simultaneous thermogravimetry-differential thermal analysis (TGA-DTA)**

TGA and DTA have been the two commonest techniques for thermal analysis for many years. TG is a technique in which a change in the weight of a substance is recorded as a function of temperature or time. DTA measures the temperature difference between a substance and a reference material as a function of temperature whilst the substance and reference are subjected to a controlled temperature program (Mendham *et al.*, 2000).

Simultaneous thermal analysis (STA) techniques are two or more types of measurement, which are made at the same time on a single sample. Modern TG-DTA instruments are capable in general of a TG resolution of around 1  $\mu\text{g}$ , using samples typically from 5 mg to 100 mg, which can give sensitive and quantitative DTA performance when the head is of the appropriate type i.e. there is a heat flow link between sample and reference (Haines, 2002).

### **2.1.11 $^{29}\text{Si}$ MAS NMR spectrometer**

The  $^{29}\text{Si}$  isotope is the best characterized nucleus of importance to zeolites. With spin  $I = \frac{1}{2}$  it produces relatively straightforward spectra with high resolution. The low natural abundance of the isotope (4.7%), means that many hours are usually required to record a spectrum of zeolite. Magic-angle spinning techniques are able to reduce linewidths to  $< 200$  Hz, except when a sample contains significant amounts of iron. In these cases there is loss of resolution and of spectra intensity because of the

large dipolar interactions and overall magnetic susceptibility of the sample. The  $^{29}\text{Si}$  isomer shift is strongly influenced by the chemical environment of the nucleus. For tetrahedral silicon there is a good correlation between the isomer shift and the degree of polymerization, and with the next-nearest-neighbor Al atoms. The shielding of the silicon nucleus is progressively decreased with decreasing polymerization and with increasing numbers of next-nearest-neighbor Al atoms for framework and layer silicates. There is a correlation with group electro-negativity, which is calculated by considering the total electro-negativity of the oxygen atoms of a tetrahedron, the other cations with which they are coordinated and for framework silicates. The isomer shift is also correlated with the mean Si-O-T (T = Si or Al) bond angle.

When an element occupies more than one type of site in a crystal structure, separate resonances are usually observed for each distinct coordination environment. Resonance position can also be influenced by the nature of next-nearest-neighbor ions. For example, in an alumino-silicate where the tetrahedral site occupancy is shared between  $\text{Si}^{4+}$  and  $\text{Al}^{3+}$  ions, the  $^{29}\text{Si}$  MAS spectrum will consist of a series of peaks corresponding to 0, 1, 2, 3, or 4  $\text{Al}^{3+}$  ions in the next-nearest-neighbor site (Wilson, 1994). Assuming that there are no Al-O-Al linkages in the framework, the Si/Al ratio can be calculated from the  $^{29}\text{Si}$  MAS spectra using the relationship:

$$\text{Si/Al} = \frac{\sum_{n=0}^4 I_{\text{Si}(n\text{Al})}}{\sum_{n=0}^4 (n/4) I_{\text{Si}(n\text{Al})}}, \quad 2.39$$

where I is the relative peak intensity and n is the number of Al tetrahedra linked to the Si tetrahedron (Kim and Kirkpatrick, 1998). Table 2.7 shows how each geometry creates ranges of chemical shifts.

**Table 2.7** Range of  $^{29}\text{Si}$  MAS NMR chemical shifts in zeolite.

Corrdination	Notation	Chemical shifts (ppm)
$\begin{array}{c} \text{Al} \\   \\ \text{O} \\   \\ \text{Al-O-Si-O-Al} \\   \\ \text{O} \\   \\ \text{Al} \end{array}$	Si(4Al)	-86 to -90.5
$\begin{array}{c} \text{Al} \\   \\ \text{O} \\   \\ \text{Al-O-Si-O-Al} \\   \\ \text{O} \end{array}$	Si(3Al)	-88 to -97
$\begin{array}{c} \text{Al} \\   \\ \text{O} \\   \\ \text{Al-O-Si-O} \\   \\ \text{O} \end{array}$	Si(2Al)	-93 to -102
$\begin{array}{c} \text{Al} \\   \\ \text{O} \\   \\ \text{O-Si-O} \\   \\ \text{O} \end{array}$	Si(1Al)	-97.5 to -107
$\begin{array}{c} \text{O} \\   \\ \text{O-Si-O} \\   \\ \text{O} \end{array}$	Si(0Al)	-101.5 to -116.5

### 2.1.12 Scanning electron microscope (SEM)

In many fields of chemistry, material science, geology and biology, detailed knowledge of the physical nature of the surfaces of solids is of great importance. SEM scans the surface of a sample in a raster pattern with a beam of energetic electrons. Several types of signals are produced from a surface in this process, including backscattered, secondary, and Auger electrons; X-ray fluorescence photon; and other photons of various energies. All of these signals have been used for surface studies, but the most common are backscattered and secondary electrons, which serve as the basis of scanning electron microscopy. In obtaining an image by each of these techniques, the surface of a solid sample is swept in a raster pattern with a finely focused beam of electrons or with a suitable probe. A raster is a scanning pattern similar to that used in a cathode-ray tube or in a television set in which an electron beam is, firstly, swept across a surface in a straight line (the x direction), second, returned to its starting position, and finally, shifted downward (the y direction) by a standard increment. This process is repeated until a desired area of the surface has been scanned. During this scanning process, a signal is received above the surface (the z direction) and stored in a computer system, where it is ultimately converted to an image (Mendham *et al.*, 2000). Figure 2.6 is a schematic representation of a combined instrument that is both a scanning electron microscope and a scanning electron microprobe. Note that a common electron source and electron focusing system is used but that the electron microscope employs an electron detector, whereas the microprobe uses an X-ray detector.

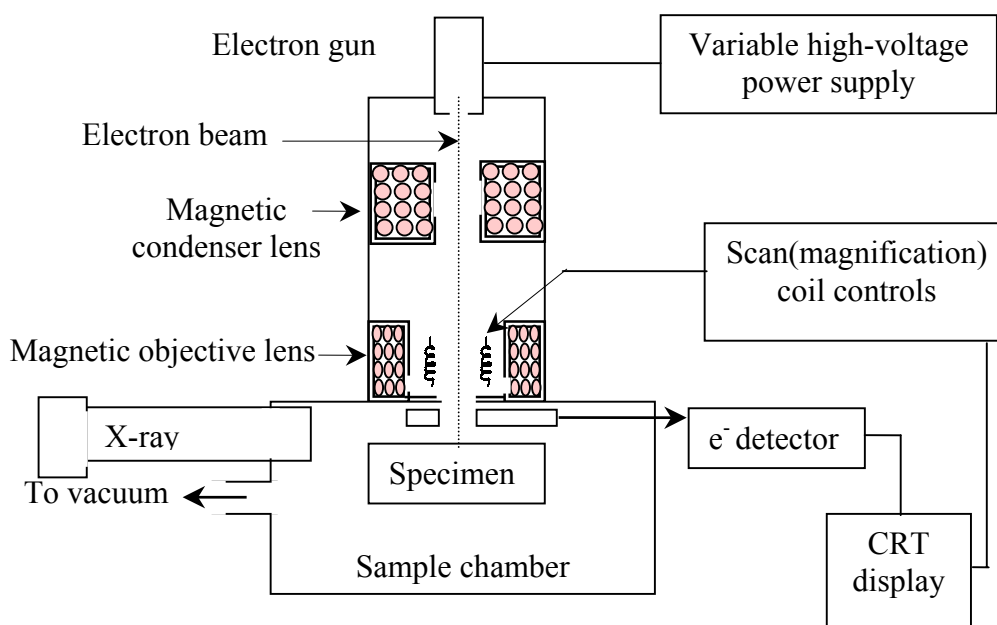


**Figure 2.7** Schematic representation of a SEM.

### 2.1.13 Liquid scintillation Spectrometer (LSC)

In 1950, liquid scintillation counting was first used as a tool in radioactivity measurement. Liquid scintillation counting is a commonly used method particularly for counting weak  $\beta$  emitters, for example,  $^{22}\text{Na}$ ,  $^{14}\text{C}$ ,  $^3\text{H}$ , and  $^{32}\text{S}$ . A scintillator material will emit a weak light flash (scintillation) when it interacts with a quantum of radiation. The intensity of this scintillation is proportional to the energy of the radiation deposited in the scintillator. The scintillation solution is composed of a solvent and a solute. The solvents have an important role in absorbing the energy of nuclear radiation and in dissolving samples. The solute acts as an efficient source of photons after accepting energy from the excited solvent molecules (Faghihian, 1990).

The mixture of solutes and solvents are often called cocktails. Some of the most favored solutes are PPO (2, 5-diphenyloxazole), PBD (2-phenyl-5-(d-biphenyl)-1,3,4 oxadiazole) and POPOP(1,4-di(2-(5-phenyloxazolyl)benzene). All primary solvents are aromatic with a  $\pi$  system of electrons (toluene, pseudocumene and p-xylene), which can be easily excited by  $\beta$  radiation, with the exception of 1,4 dioxane, which needs an addition of about 60 g/l of naphthalene to promote its participation in the energy transfer process (Dyer, 2001). In the interaction of ionizing radiation with a sample, the excited molecules will emit photon or efficiently transfer the energy to a solute, which in turn will emit the photons. Because each excited molecule can emit only one photon, the number of emitted photons depends on the number of excited molecules, which are produced by the ionizing particles. The photons can be measured by a photomultiplier tube, which will convert them into electrical pulses that are counted by a scaler (Faghihian, 1990).

## 2.2 Literature reviews

The properties and applications of perlite have been studied in many fields such as in 1997 Dogan *et al.* (1997) who conducted an experiment on the electrokinetic properties of expanded and unexpanded perlite. They found that perlite samples yield practically no isoelectric points in the pH range of 3 to 11. The expanded perlite has a more negatively charged surface than unexpanded perlite.

Sodeyama and others (1999) studied the preparation of fine expanded perlite. The results obtained in this study showed that using a fluidized sand-bed furnace produced fine expanded perlite products. Fine expanded perlite with a particle size of

less than 15  $\mu\text{m}$  and bulk density under 0.5  $\text{g}/\text{cm}^3$  was prepared successfully by using a rapid heat furnace.

Since 1987 perlite has been experimentally converted to zeolite. Giordano *et al.* (1987) conducted research on the zeolitization of perlite. The zeolitization process of perlite is attacked hydrothermally for 3–10 hours at 90 °C–130 °C in 8–20 % NaOH and 1:5 to 1:50 solid/liquid ratios. They reported that hydroxy sodalite and zeolite Pc were formed.

Barth-Wirsching *et al.* (1993) studied the formation of synthetic zeolites formed from expanded perlite: type, formation conditions and properties. They showed that in the experiment with KOH solutions phillipsite, merlionicite, chabazite and edingtonite were formed. Without the addition of aluminium, a high percentage of phillipsite and merlionicite were obtained. With addition of aluminium, chabazite and edingtonite were formed. In an experiment with NaOH solution using zeolite Na-Pc, sodalite hydrate and zeolite A were formed with a higher percentage and a higher percentage of zeolite A was obtained with the addition of aluminium.

Christidis and others (1999) researched the zeolitization of fine perlite: the mineralogical characteristics of the end products and the mobilization of chemical elements. Perlite fines were treated with 1 N and 5 N NaOH solution at 100 °C–140 °C for 2 and 4 hours. They found that perlite fines were converted to zeolite–Pc, zeolite V and hydroxysodalite. In 1996, they synthesized zeolite from perlite waste using environmental applications. They reported that zeolite P was formed at a low temperature and analcime and albite at a higher temperature range. Zeolite P is an efficient absorber of various heavy metal ions like  $\text{Pb}^{2+}$ ,  $\text{Zn}^{2+}$ ,  $\text{Ni}^{2+}$ ,  $\text{Cu}^{2+}$ ,  $\text{Mn}^{2+}$ ,  $\text{Cr}^{3+}$ ,  $\text{Cd}^{2+}$  and  $\text{Pb}^{2+}$  which are the most efficiently absorbed ions.

Khodabanden *et al.* (1997) conducted research on the alteration of perlite to calcium zeolites. Synthetic versions of the zeolites of gismondine, epistilbite and heulandite were synthesized from perlite using calcium-containing solutions. Their results were as follows: zeolites Na-P1 (GIS) were formed at high sodium activities and pH values between 11.0 and 11.5, higher alkalinity typically favors mordenite and analcime in sodium-rich systems as does a higher temperature. Epistilbite was formed from perlite glass at higher calcium activities at a pH value below 8. Heulandite was also formed from perlite glass at a higher pH value of 10.9.

Zeolites are synthesized at evaluated pH levels at 12 to 13 and temperatures at 100 °C to 300 °C. At high pH levels (pH>12), zeolites will slowly dissolve. The restriction in the use of zeolite ion exchanger is due to their limited acid resistance. Although some zeolites are stable at lower pH levels (pH 2), most zeolite ion exchanges should not be employed below about pH 4 to 5, except for very brief exposures operating at pH > 6 preferred (Sherman, 1978).

Dyer and Keir (1989) studied pH tolerance in zeolites, analcime treated with 0.1, 1.0, 5.0 and 0.8 M nitric solution. SEM images obtained of the treated sample show surprisingly little difference in crystal structure between any of the treatments. In addition, the peak intensities on the X-ray diffractograms showed that a significant reduction in crystallinity was effected only by nitric acid strength of 5.0 M and above.

Shevade (in press) reported that the  $\text{NH}_4^+$ /Y zeolite is very active in arsenic removal over the pH range 2-12. At a very high pH (13.2) the zeolite structure is not stable and it started dissolving in the highly alkaline solution which is reflected by a decrease in the arsenic removal capacity. The arsenic removal activity decreased at very low pH (0.76) while the zeolite structure remained constant.

Gates (1992) reported that the stability of the crystal framework also increases with increasing Si/Al ratios with decomposition temperatures of the different zeolites ranging from roughly 700 °C to 1300 °C. Zeolite with high Si/Al ratios are stable in the presence of concentrated acids, but those with low Si/Al ratios are not, which tend to reverse for basic solution.

Analcime can be synthesized from a variety of cation containing mixtures such as Na, K, Rb, Cs, Ca, Sr. Crystallization can occur at 100 °C under atmospheric pressure over a time span of 120 hours or less. Crystals form with the composition governed by the initial ratios of hydroxide, alumina and silica in the gel and appearing independent of the depletion of solution species with time (Szostak, 1998).

Zhdanov *et al.* (1990) reported that analcime appears only from starting glass with high SiO<sub>2</sub>/Al<sub>2</sub>O<sub>3</sub> ratio and at higher temperatures. Low temperatures favor the formation of zeolite A, as well as zeolite X, which is completely absent at 120 °C.

Balgord and Roy (1971) have synthesized analcime with Si/Al ratios in the range 1.5 to 3 and investigated their ion exchange properties. They found that ion exchange of Na<sup>+</sup> by Ca<sup>2+</sup> is very interesting, as they have similar ionic radii. The ion exchange capacities for Ca<sup>2+</sup> with Si/Al ratio 1.5 was completed exchange 100%, while 80% exchange was found with Si/Al ratio equal 2 or 3 (Balgord and Roy, 1971). Balgord and Roy (1973) found that the high-silica analcime contained a percentage of water of 8.70 %.

Analcime has a relatively compact structure compared with other zeolites and has an idealized unit cell of Na<sub>16</sub> [Al<sub>16</sub>Si<sub>32</sub>O<sub>96</sub>] 16H<sub>2</sub>O (Meier, 1996). However, Barrer (1950) reported that analcime can act as an ion sieve, and Dyer and Yusof (1987) carried out extensive studies on cation and water self-diffusion, concluding that

analcime has the potential for use in the storage and disposal of tritiated water (Dyer and Molyneux 1968). In previous work, little attention has been paid to cation exchange rates in other zeolites, apart from those for self-exchange (Dyer and Yusof, 1987). Barrer and Ree (1960) investigated self-diffusion of alkali metal ions in analcime by using radiotracers. They suggested that the movement of cations with the structural framework of analcime have no bearing on the presence of water molecules which contrast to the assumptions studied by Beaties and Dyer (1957) that the water molecules imposed some restrictions on the cationic movements.

Zeolites are well known and are used on a large scale as ion exchange (Dyer, 1988). Many researchers studied their ion exchange properties, for example, Curkovic *et al.* (1996) studied  $Pb^{2+}$  and  $Cd^{2+}$  removal from waste water by using natural zeolite and treated zeolite. They reported that treatment improved both the exchange capacity and the removal efficiency. Clinoptilolite was shown to have high selectivity for certain heavy metal ions such as  $Pb^{2+}$ ,  $Cd^{2+}$ ,  $Zn^{2+}$  and  $Cu^{2+}$  (1994).

In addition, in 2000 Moirou *et al.* studied an application of synthesized zeolite on ion exchange of zeolite Na-Pc with  $Pb^{2+}$ ,  $Zn^{2+}$  and  $Ni^{2+}$  ions. The results revealed that the Gibbs standard free energy,  $\Delta G^{\circ}$ , of the  $Na \rightarrow \frac{1}{2} Pb$  exchange is  $-3.11 \text{ kJeq}^{-1}$  and  $Na \rightarrow \frac{1}{2} Zn$  exchange is  $2.75 \text{ kJeq}^{-1}$ .

Faiia and Feng (2000) examined the kinetics of oxygen isotopic exchange between water vapor and analcime of two-size distribution. The results showed a small particle size fraction was faster than a larger particle size at  $400 \text{ }^{\circ}\text{C}$ . The difference in rate with grain size indicates that isotopic exchange is limited by diffusion. The equilibrium was not reached may be explained by structural changes upon dehydration which cause Na cations to migrate into former water sites. Karlsson and Clayton

(1990) suggested that the rate of isotopic exchange is controlled by sorption and desorption of water molecules onto surfaces in analcime.

As mentioned previously, many researchers have conducted research on the conversion of zeolites from perlite and some of them investigated the benefits and applications of synthesized zeolite as diffusion and ion exchange. Furthermore, the environmental problems must be significantly controlled and made safe from harmful heavy metals in the environment. As a result, the purpose of this work is to convert perlite to zeolites and to study their diffusion and ion exchange properties.

# Chapter III

## Materials and Experiments

### 3.1 Materials

#### 3.1.1 Chemicals

- (a) Perlite from Lopburi Province
- (b) Sodium hydroxide anhydrous pellets (NaOH), Analytical reagent, Merck
- (c) Lead (II) nitrate ( $\text{Pb}(\text{NO}_3)_2$ ), Nickel (II) chloride hexahydrate ( $\text{NiCl}_2 \cdot 6\text{H}_2\text{O}$ ),  
Copper (II) nitrate trihydrate ( $\text{Cu}(\text{NO}_3)_2 \cdot 3\text{H}_2\text{O}$ ) and Zinc chloride ( $\text{ZnCl}_2$ )  
Analytical reagent, Merck
- (d) Distilled and deionized water
- (e) Lithium bromide (LiBr), Analytical reagent, Claisse, Canada
- (f) Lithium tetraborate ( $\text{Li}_2\text{B}_4\text{O}_7$ ), Analytical reagent, Claisse, Canada
- (g) Standard powder of kaolin, MBH reference materials 1998-99, UK
- (h) Standard reference materials 98b (plastic clay) National Bureau of  
Standards, USA
- (g) Standards reference materials 679 (brick clay) National Bureau of  
Standard, USA
- (i) Standard reference materials 2709 (soil), National Institute of Standards  
and Technology, USA

### 3.1.2 Apparatus

- (a) Oven for drying, Memmert D06060, Model 400, Germany
- (b) Thermostatic shaker bath
- (c) Sieve shaker, Octagon digital, Germany
- (d) Sieve 230 mesh, Analysensieb, Retsch, USA
- (e) Fusion machine for sample preparation, XRF analysis, Claisse, Fluxer Bis
- (f) pH meter , HACH, Model 50215, USA
- (g) Glass microfiber filters, Whatman GF/C diameter 47 mm
- (h) Vacuum filtration apparatus, Büchi, B-169 vacuum system, Switzerland
- (i) Analytical balance, Precica, Model 250A, Switzerland
- (j) Porcelain and platinum crucible
- (k) Desiccator
- (l) Watch glass
- (m) Micropipette
- (n) Beaker
- (o) SpectroMill Ball Pestle Impact Grinder
- (p) Chasher disk crusher, Fritsch, Industriestr8 D-55743, Ldar-Oberstein,  
Germany
- (q) Muffle furnace (Carbolite, Model CWF12/23, UK)

### 3.1.3 Instruments

- (a) High Temperature/High Pressure Reactor, (Model 4575, 500 ml, Parr)

- (b) Powder X-Ray diffractometer (XRD), (Model D5005, Bruker)
- (c) Wavelength dispersive X-Ray fluorescence spectrophotometer (XRF), (Model Negative Magix Pro, Phillips)
- (d)  $^{29}\text{Si}$  MAS NMR, using a Varian Unity Inova spectrometer
- (e) Fourier transform infrared spectrophotometer (FT-IR), (Model spectrum GX, Perkin-Elmer)
- (f) Scanning electron microscope (SEM), (Model JSM6400, JEOL)
- (g) Brunauer-Emmett-Teller (BET), Surface area analyzer, (Model micromeritics, ASAP ASAP 2010)
- (h) Liquid scintillation Spectrometer (LSC), Mark II Scintillation system, Model 4643, Chicago
- (i) Thermal analyzer (TGA-DTA), SDT 2960
- (j) Lazer particle size analyzer, Malvern Instruments Mastersizer S

## **3.2 Experiments**

### **3.2.1 Chemical and physical properties of raw perlite**

A series of experiments was carried out to investigate the chemical and physical properties of raw perlite collected from Lopburi Province in Central Thailand, which was used as the starting material. The procedure was as follows:

1. Characteristic amorphous peaks of perlite were investigated by Powder X-Ray diffractometer (XRD), (Model D5005, Bruker).

2. The chemical composition of raw perlite was determined by the wavelength dispersive X-Ray fluorescence spectrophotometer (XRF), (Model Negative Magix Pro, Phillips).
3. Water contents of perlite was obtained by heating 10 mg samples at 10 Kmin<sup>-1</sup> in dry nitrogen using a thermal analyzer (TGA-DTA), SDT 2960.
4. The surface area of perlite was determined by BET (Bruauer-Emmett Teller), Surface area analyzer, Model micromeritics ASAP 2010.
5. Loss on ignition (LOI) of perlite
  - 5.1 In loss on ignition, platinum crucible was placed in the air oven at 105 °C for 2 hours.
  - 5.2 Cooled it down to room temperature in desiccator.
  - 5.3 Weighted the empty crucible (A) then put at least 2 g of sample into the crucible and weighted it again (B).
  - 5.4 Placed the crucible in the air oven at 105 °C for 24 hours.
  - 5.5 Transferred the crucible into desiccator and cooled it down to room temperature.
  - 5.6 Weighted the crucible again (C).
  - 5.7 The crucible in number 5.6 was calcined in a chamber furnace at 1000 °C for 6 hours and cooled at room temperature in a desiccator.
  - 5.8 Finally, weighted the crucible again.
  - 5.9 To calculate weight loss on ignition from equation 3.1 as follows:

$$\text{LOI} = \frac{(C-D)}{(C-A)} \times 100 \quad (3.1)$$

6. Infrared spectra of perlite was prepared using 5 g of sample in 300 mg KBr. The samples were scanned in the range of  $4000\text{ cm}^{-1}$  to  $370\text{ cm}^{-1}$ , by Fourier transform infrared spectrophotometer (FT-IR), (Model spectrum GX, Perkin-Elmer).
7. Particle size analysis of perlite was carried out using a Malvern Instruments Mastersizer S.

### 3.2.2 Synthesis of zeolite

Zeolite was synthesized from the perlite starting material. Synthesis experiments were carried out to inspect the zeolite crystallization under various NaOH concentrations, solid to liquid ratios, temperatures and times. The procedures were as follows:

1. Perlite was prepared by grinding with SpectroMill Ball Pestle Impact grinder and sieved with sieving size 230 mesh before using as starting material.
2. The starting material reacted with NaOH solution at various concentrations between 1 M and 3 M and with the ratio (w/v) of solid to liquid 1:5-1:20 and the temperature was used at  $100\text{ }^{\circ}\text{C}$  to  $140\text{ }^{\circ}\text{C}$ , at various times, in a 500 ml high pressure/high temperature stirred reactor (Parr Instrument).
3. After hydrothermal treatment, the reactor is cooled to room temperature; synthesized products were filtered, washed with distilled water and dried at  $120\text{ }^{\circ}\text{C}$  for 6 hours.
4. The solid products were characterized by XRD, FT-IR and SEM.

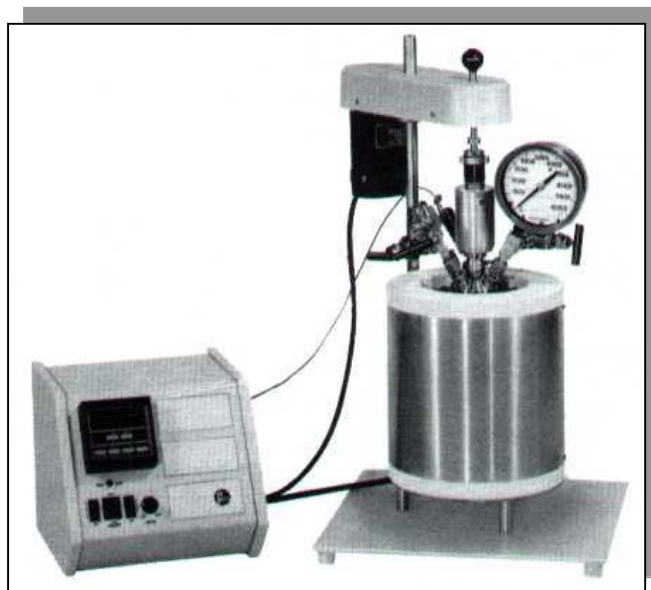


**Figure 3.1** High Temperature/High Pressure Reactor (Model 4575, Parr instrument).

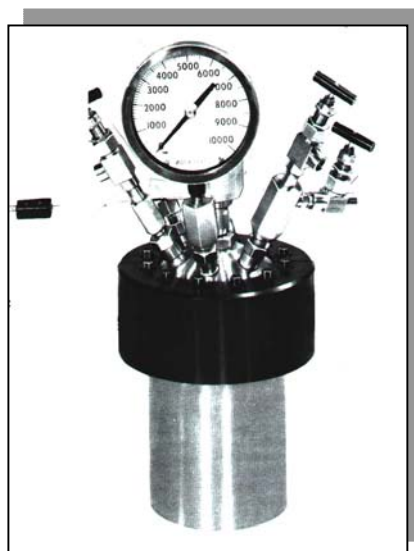


**Figure 3.2** Stainless steel bomb vessel 500 ml for Parr instrument model 4575.

### 3.2.3 The chemical, physical properties and pH tolerance of analcime

After producing analcime in the best condition, 3 M NaOH 1:5 solid/ liquid ratio at 140 °C for 24 hours. Analcime was then investigated for its chemical, physical properties and pH tolerance before being used for studies in diffusion and ion exchange properties with four heavy metals. A series of experiments was performed to demonstrate the chemical, physical properties and pH tolerance of analcime as follows:

1. The chemical composition of analcime was determined by the wavelength dispersive X-Ray fluorescence spectrophotometer (XRF), (Model Negative Magix Pro, Phillips).
2. Analcime silicon-aluminium ordering was characterized by  $^{29}\text{Si}$  MAS NMR, using a Varian Unity Inova spectrometer, at a frequency of 59.58 MHz.
3. The surface area of analcime was determined by BET (Bruauer-Emmett Teller), Surface area analyzer, Model Micromeritics ASAP 2010.
4. The water content of analcime was obtained by heating 10 mg samples at 10  $\text{Kmin}^{-1}$  in dry nitrogen using a thermal analyzer (TGA-DTA), SDT 2960.
5. Particle size analysis of analcime was carried out using a Malvern Instruments Mastersizer S.
6. Determination of the cation exchange capacity (CEC).
  - 6.1 Weighing of 0.1g of analcime was carried out cation exchange capacity into a plastic container.
  - 6.2 Equilibrating with 20 ml 0.01M  $^{22}\text{Na}$  in a thermostatically controlled air oven until it reached equilibrium (2 days). The concentration of the liquid

phase was measured by a liquid scintillation counter (LSC).

7. Infrared spectra analcime was prepared using 5 g of sample in 300 mg KBr. The samples were scanned in the range of  $4000\text{ cm}^{-1}$  to  $370\text{ cm}^{-1}$ , Fourier transform infrared spectrophotometer (FT-IR), (Model spectrum GX, Perkin-Elmer).
8. Loss on ignition (LOI) in analcime was carried out by same procedure as loss on ignition in perlite.
9. Scanning electron microscope (SEM), (Model JSM6400, JEOL) was used to investigate the morphology of the analcime product.
10. pH tolerance in analcime

To study the pH tolerance in the analcime structure, 1 g of dried analcime was treated with adjusted pH 1 to 12 solution in 125 ml polyethylene bottle for 3 hours. Then, solid phase was separated, dried at  $120\text{ }^{\circ}\text{C}$  for 6 hours and stored in desiccator. XRD spectrometry was used to investigate the crystalline effect and the percent of crystalline that remained.

### **3.2.4 Crystallization kinetics of analcime**

As analcime was the best product found under the conditions studied, so this work carried out extensive studies of crystallization kinetics of analcime at constant NaOH concentration and solid/liquid ratio with varying temperatures. The procedures were as follow:

1. The perlite starting material was reacted with 3 M NaOH solution and with the ratio (w/v) of solid to liquid 1:5 at various temperature reactions from 130 to

145 °C and reaction time from 1 to 24 hours, in a 500 ml high pressure/high temperature stirred reactor (Parr Instrument).

2. The percentage of crystallinity as a function of time was determined by XRD.

The percentage of crystallinity of synthetic analcime is defined as follows

(Ghosh *et al.*, 1994 ):

$$\% \text{ Crystallinity} = \frac{\text{total area 12 strong peaks of sample}}{\text{total area 12 strong peaks of standard}} \times 100 \quad (3.2)$$

3. The optimum value of percent crystallinity of analcime was taken as the standard for percent crystallinity calculation. The A and E<sub>a</sub> values from kinetic data were extracted from Arrhenius equation, the plot of ln k against reciprocal temperature (K<sup>-1</sup>).
4. The exponent n and rate constant for the kinetics crystallization of this work were determined from Avrami equation (Walton *et al.*, 2001).
5. XRD, FT-IR, particle size analyzer and SEM confirmed the analcime products.

### 3.2.5 Diffusion

The diffusion procedure was used to investigate the diffusion parameters of various forms of exchanged analcime such as Cu<sup>2+</sup>, Ni<sup>2+</sup>, Pb<sup>2+</sup> and Zn<sup>2+</sup>. Analcime sample was labeled with <sup>22</sup>Na, self-diffusion, and they were then placed in contact with a specific amount of the non-isotopic species of Cu<sup>2+</sup>, Ni<sup>2+</sup>, Pb<sup>2+</sup> and Zn<sup>2+</sup> solution. The diffusion experiment was carried out at a constant temperature over varying periods of time. The details of the procedure are given below:

### 3.2.5.1 Self-diffusion experiment

1. A stock solution of  $^{22}\text{Na}$  was prepared that had a specific activity of  $2.22 \times 10^4$  cpm/0.1 g.
2. 1 ml of  $^{22}\text{Na}$  stock solution was dispensed into 10 ml of water in a plastic container.
3. The plastic container was shaken and then 1 ml of solution was taken to measure the Activity ( $A_0$ ) count per minute (cpm) by LSC.
4. 1 g of Na-Analcime was placed into the remaining 9 ml and the container was sealed with parafilm.
5. The container was put on a roller and left for 2 hours. The mixed solution was allowed to settle.
6. 1 ml sample of the liquid phase was taken again to measure the Activity ( $A_t$ ) by LSC. The specific activity per gram of analcime was calculated:

$$\frac{A_0 - A_t}{\text{Weight of zeolite}} \quad (3.3)$$

### 3.2.5.2 Diffusion experiments

1. The analcime was pre-labeled with a known activity of  $^{22}\text{Na}$ , as supplied by Amersham International, UK.
2. The diffusion of heavy metal cations into analcime was studied by equilibrating 0.1 g of  $^{22}\text{Na}$  analcime with 5 ml of 0.01 M solution of the in-going

cation in plastic vials.

3. The vials were rotated about their horizontal axes, in a thermostatically controlled air oven, for various times from 5 mins to 24 hours.
4. At the end of the appropriate time periods the plastic containers were taken from the oven and immediately centrifuged.
5. The extent of heavy metal cation diffusion into the analcime was measured from the release of  $^{22}\text{Na}$  into solution, as determined by liquid scintillation counting.
6. The Barrer, Barri and Klinowski equation was used to estimation of the diffusion coefficients (D). The activation energy can be evaluated by using the Arrhenius equation. Kinetic plots were constructed at 298 K, 313 K and 333 K.
7. The solid phase after exchange was used to confirm the retention of crystallinity as below:
  - 7.1 Fully exchanged forms were prepared by using nitrate salt solutions of Cu, Ni, Pb and Zn divalent cations (all reagents were Merck analytical grade).
  - 7.2 Duplicate exchanges with 0.5 M salt solution were performed, twice a day, for 7 days, and X-ray powder diffraction was used to confirm the retention of crystallinity in the solid phase.

### 3.2.6 Ion exchange isotherm

Ion exchange isotherm experiments were carried out to demonstrate the content of exchange with the completion of equilibrium for various systems. A reversibility test of  $\text{Cu}^{2+}$ ,  $\text{Ni}^{2+}$ ,  $\text{Pb}^{2+}$  and  $\text{Zn}^{2+}$  on  $^{22}\text{Na}$ -analcime, respectively was carried out at 298 K with known volume and concentration of competing ion. The procedure was as follows:

#### 3.2.6.1 Construction of exchange isotherms

The equilibrium time of ion exchange isotherms were checked by a prior kinetic experiment.

1. The isotherms were constructed by equilibrating 0.1 g of  $^{22}\text{Na}$ -analcime with total 0.01N of solution that made up the volume to 20 ml of in-going cation (Cu, Ni, Pb and Zn) and  $\text{NaNO}_3$  was placed into a plastic container as shown in table 3.1, then it was sealed container with parafilm.
2. Plastic containers were put on rollers that and were rotated about their horizontal axis in a thermostatically controlled air oven until they reached equilibrium (2 days), then the mixed solution was allowed to settle by centrifuge.
3. The concentration of the liquid phase was measured by liquid scintillation counter (LSC). The isotherms were observed at 298 K, 313 K and 333 K.
4. Reverse exchanges were also checked for all systems studied.  $^{22}\text{Na}$  solution was obtained from Amersham International (UK).

**Table 3.1** Composition of solutions used to construct the isotherms  $\text{Na}^+ \rightleftharpoons \text{M}^+$ .

Plastic container number	$\text{NaNO}_3$ 0.01 N	$\text{MNO}_3$ 0.01 N
1	0	20
2	1	19
3	2	18
4	4	16
5	6	14
6	8	12
7	10	10
8	12	8
9	14	6
10	16	4
11	18	2
12	19	1
13	20	0

5. Ion exchange isotherms were plotted base on the measured equivalent fractions of cation in solution ( $A_S$ ) and solid ( $A_Z$ ) phases.
6. Free energy, enthalpy and entropy of the exchange process for each ion pair were produced from the plot of  $\log K'_B{}^A$  (selectivity coefficient) against  $A_Z$ . (cation A in zeolite). The  $\log K'_B{}^A$  against  $A_Z$  plots were constructed using the Kielland programme, which is based on the methodology described by Fletcher and Townsend (Fletcher, P. and Townsend, R.P, 1982).
7. XRD and TGA-DTA were used to confirm the solid phase.

### 3.2.6.2 Reversible isotherms

1. The isotherms was repeated only at room temperature, carried out the same procedure as for the construction of exchange isotherms number 1 to 2.
2. A sample 1 ml of the liquid phase was measured for the Activity by LSC.
3. The solution was added as shown in tables 3.2 into the remaining solution.  
Then the container was sealed with parafilm.
4. The plastic containers were put on rollers that rotated about their horizontal axis in a thermostatically controlled air oven until they reached equilibrium again, then the mixed solution was allowed to settle by centrifuge.
5. The concentration of the liquid phase was measured by liquid scintillation counter (LSC).

**Table 3.2** Conditions used for reverse isotherms.

Ratio of solutions		Number after equilibrium of forward	Added solutions number for reverse
Heavy metals	NaNO <sub>3</sub>		
20	0	1	12
16	4	3	12
12	8	5	12
8	12	7	1
4	16	9	1
1	19	11	1
0	20	12	-

### 3.2.7 Powder X-ray diffraction

X-ray diffraction methods are suitable for the examination of the crystalline materials. The information obtained from powder X-ray diffraction can be identified by a molecular sieve structure. X-ray techniques can indicate uniqueness in structure, as the diffraction pattern is a fingerprint of individual zeolite structure. In addition, it can also provide information about the solid phase from the diffraction pattern such as a successful or unsuccessful formation of a crystalline material, the presence of a single phase or a mixture of phases and the determination of a new structure. And if standards are available, the level of crystallinity can be obtained from that synthesis bath (Szostak, 1998). All raw perlite, synthesized products and solid phases confirm the diffusion and ion exchange processes were investigated by a powder x-ray diffractometer (XRD), (Model D5005, Bruker), with Ni-filtered Cu-K $\alpha$  radiation. All the spectra were recorded with 2 $\theta$  angle in the range of 5 to 50  $^{\circ}$ , Cu target, 35 kV, 35 mA and speed scan of 0.02 degree per 0.55 second.

### 3.2.8 Thermal analysis

TGA and DTA have often been used to characterize zeolite material for their thermal stability, quantity of zeolitic water by monitoring of weight loss or phase changes from a material versus temperature. Thermal analyzer (TGA-DTA), SDT 2960 was used for all samples throughout this work. The STD 2960 combines two thermal analysis measurements in a single instrument. This instrument was able to perform both TGA and DTA measurements at the same time, instrument and sample.

Calcium Oxalate Monohydrate is a standard material often used. The details of operating conditions used in the runs are as follows:

Temperature range	:	Ambient to 1200
Nitrogen flow rate	:	100 mlmin <sup>-1</sup>
Heating rate	:	10 °Cmin <sup>-1</sup>
Sample pan	:	Alumina 90 µl
Sample weight	:	10 mg
Atmosphere	:	Nitrogen

The sample holder is placed in the centre of a furnace. One holder is filled with the sample and the other with an inert reference material, such as alumina cup. When the sample holder is heated at the programmed rate, the temperature increases uniformly for both the sample and the reference material. The furnace temperature is recorded as a function of time. If the sample undergoes a phase change, energy is absorbed or emitted, and the temperature difference between the sample and the reference ( $\Delta T$ ) is detected (Hatakeyama and Quinn, 1999).

### **3.2.9 X-ray fluorescence spectrometry**

The x-ray fluorescence technique provides qualitative and quantitative information of the element composition of a sample. This technique is widely used in industry because it is fast and non-destructive to the sample. The nondestructive wavelength dispersive x-ray fluorescence spectrophotometer (XRF), (Model Negative Magix Pro, Phillips) was used to identify and determine the concentrations of elements present in the perlite and analcime samples. The tube high voltage was 40 kV with the

tube current of 30 mA. Raw perlite and analcime were for the measurement of their chemical compositions by using the Borate-fusion method as below:

1. 1 g of the sample was weighed and 7 g of  $\text{Li}_2\text{B}_4\text{O}_7$  (flux) was placed in a platinum crucible.
2. LiBr 0.03 g was added to the mixture in the platinum crucible then allowed to melt in the fusion machine. The fusion machine was preprogrammed for power and fusion time according to the instruction manual.
3. After cooling, the solidified disk was stored in a desiccator for XRF analysis. Prepared the disk of all the standard reference material with the same procedure as perlite and analcime sample.

### **3.2.10 Scanning electron microscopy (SEM)**

SEM is very useful in the field of material science and industrial research. A scanning electron microscope, Model JSM6400, JEOL, was used to investigate the morphology of raw perlite and analcime samples with an accelerating voltage of 15-40 kV. The JSM-6400 scanning microscope given high- resolution with modern digital image processing. The samples were prepared by the following procedures. The dried samples were placed onto a small piece of a double-side adhesive tape, which was placed on a brass stub used as a target. Then the stub was inserted into the holder in a vacuum system. The gold was heated to produce vapors, which would coat the sample particle on the target with a thin film of the metal. Then, the samples were recorded at 15 kV, 4500X modification.

### **3.2.11 Fourier transforms infrared spectrophotometer (FT-IR)**

Infrared spectroscopy is one of the main techniques normally used to investigate zeolites. The surface properties and reactivity of zeolites are of major importance for their applications. Infrared spectroscopy can provide useful information on the constitution, surface properties of zeolites and how they are modified by various treatments. In addition, changes in the spectra of zeolite and of molecules adsorbed on the surface can yield direct information about the surface, how adsorbed molecules interact, and where molecules are adsorbed because the major structural groups present in zeolites can be detected from their infrared patterns. A fourier transform infrared spectrophotometer (Model spectrum GX, Perkin-Elmer) was used to characterize all spectra. Infrared spectra of perlite and analcime were prepared using 5 ml of the sample in 300 mg KBr. The samples were scanned in mid IR ranging from  $4000\text{ cm}^{-1}$ - $370\text{ cm}^{-1}$  by the KBr pellet technique. The scan number was 10 at a resolution of  $4.0\text{ cm}^{-1}$ .

### **3.2.12 Particle size analysis**

Characterization of the size of component particles in industrial dispersion is often required for research purposes and is an essential part of the overall quality control procedures invariably applied to the products. Particle size analyses of perlite and analcime were carried out using a Malvern Instruments Mastersizer S. The average particle size was obtained by taking part in the diffusion process.

### **3.2.13 Surface area analyzer**

The surface areas of raw perlite and analcime were investigated using Brunauer-Emmett-Teller (BET), Surface area analyzer, (Model Micromeritics, ASAP 2010). The sample and a glass sample tube used were dried in an air oven at 120 °C for 6 hours and cooled down in a desiccator. A glass sample tube was weighed and, filled with approximately 25 mg of the sample into a sample tube and weighed, then degassed by connecting to port with a seal fit. The sample was degassed at 300 °C and 277 psi, and finally weighed again. The sample glass tube was connected to the BET analyzer port with the nitrogen adsorption processed at -78 °C from the range P/P<sub>0</sub> of 0.01 to 0.3.

### **3.2.14 Liquid scintillation Spectrometer (LSC)**

A scintillator is a material that emits a weak light flash (scintillation) when it interacts with a quantum of radiation. The intensity of this scintillation is proportional to the energy of the radiation deposited in the scintillator (Dyer, 2001). For liquid scintillation counting, a sample was dissolved in a liquid cocktail that contained a suitable solvent and additives to improve water miscibility and to permit counting at low temperatures. The characteristics essential to a solvent for use within LSC include a high flash point, low vapor pressure, biodegradability, low toxicity and irritancy, high counting efficiency, high quench resistance, no permeation through plastics, low photo- and chemiluminescence, and low viscosity (Dean, 1995). The instrument used for counting was a Liquid scintillation counter (LSC), Mark II Scintillation system,

Model 4643, Chicago. An automatic sample changer capable of holding 300 samples was found in this instrument. A polyethylene plastic container of 20 ml capacity was used.

### **3.2.15 $^{29}\text{Si}$ MAS NMR spectrometer**

The rotation of asymmetric nuclei required to produce nuclear magnetic resonances at specific (magic) angles gives information as to the nearest coordination neighbors of the assumption nucleus. So MAS NMR is important (with neutron diffraction) in defining the Si/Al ordering in aluminosilicate frameworks. The spectra observed can give information on the differences between Si coordinated to 1, 2 or 3 other Si atoms or to various Al atoms. Moreover, it quantitatively defines the number of Si atoms in each different environment and the difference between Al tetrahedrally and octahedrally coordinated to oxygen atoms (Dyer, 1988). To define Si/Al ratio in analcime  $^{29}\text{Si}$  MAS NMR was used, with a Varian Unity Inova spectrometer, at a frequency of 59.58 MHz. The spectra were recorded at a spinning rate of 6 kHz in a Varian 5.0 mm Magic-angle spinning (MAS) probe, at ambient temperature.

## **Chapter IV**

### **Results and Discussion**

In this chapter results and discussion were separated into main five parts as follow: the characterization of perlite, the characterization of analcime, the kinetics of analcime crystallization and the diffusion and ion exchange of analcime, respectively.

#### **4.1 Chemical and physical properties of raw perlite**

Raw perlite used as the starting material in this study was first characterized to overview its characteristics and properties. The characterization of amorphous glass were determined by using powder XRD. XRF and TGA-DTA were carried out to measure their chemical properties. The BET and laser particle size analyzer and FT-IR were also used to investigate the physical properties of raw perlite. The XRD pattern showed an amorphous broad band at 2-Theta 20 to 30 degrees of perlite (figure 4.1). Table 4.1 shows the chemical composition of the raw perlite which was determined by the wavelength dispersive XRF. Perlite has the following main compositions expressed as percent oxide by weight: SiO<sub>2</sub>, 70.63%; Al<sub>2</sub>O<sub>3</sub>, 32.36%; Na<sub>2</sub>O, 2.36% and 4.71% of K<sub>2</sub>O. The ignition loss was determined from the weight loss after heating at 1000 °C for 6 hours in a furnace. It was found to be of 3.97 %. This weight loss is mainly due to water desorption from the powder. Water content was found to be 3.5 %

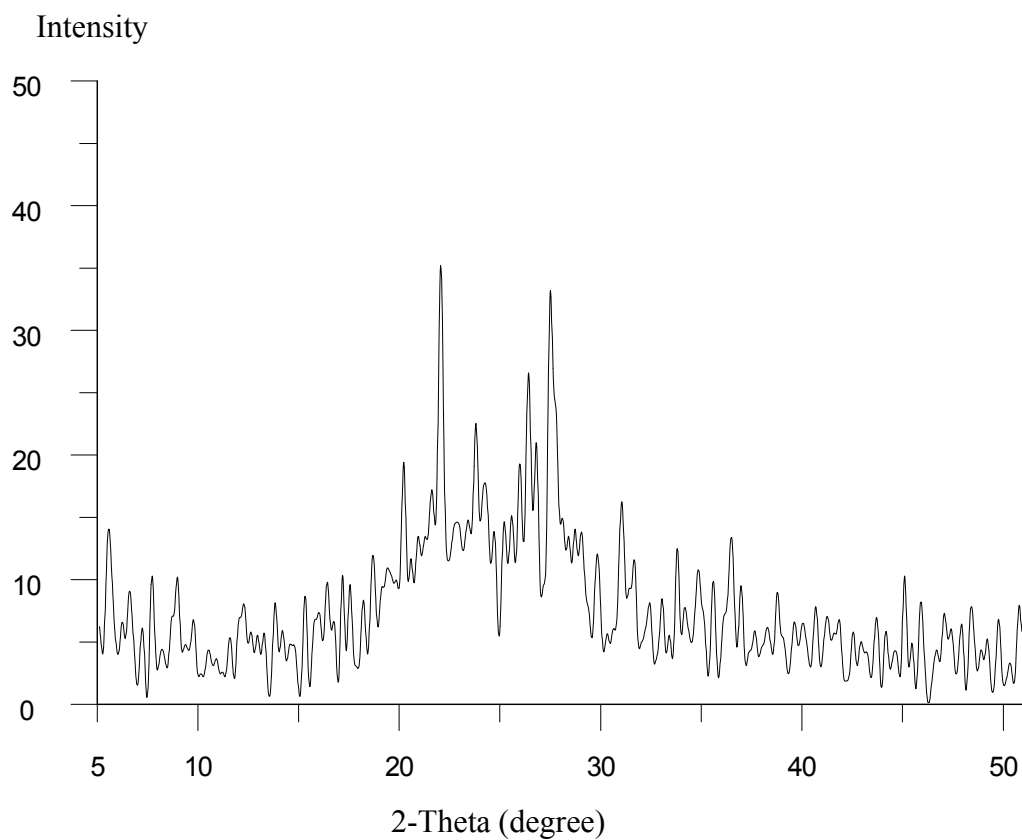


**Figure 4.1** X-ray diffraction pattern of raw perlite.

**Table 4.1** Chemical composition of raw perlite.

Oxides	Perlite (This work)	Perlite (Wathanakul <i>et al.</i> , 1995)	Perlite (Moirou <i>et al.</i> , 2000)	Perlite (Akçay <i>et al.</i> , 1998)
SiO <sub>2</sub>	70.63	71.56	72.52	73.31
Al <sub>2</sub> O <sub>3</sub>	13.10	12.98	13.39	12.23
K <sub>2</sub> O	4.71	4.37	3.41	4.52
Na <sub>2</sub> O	2.36	3.20	3.70	3.00
CaO	0.48	0.56	1.15	0.56
Fe <sub>2</sub> O <sub>3</sub>	1.49	1.35	1.41	1.14
MgO	0.90	0.21	0.57	0.09
TiO <sub>2</sub>	0.24	0.28	0.1	-
MnO	0.03	0.04	-	0.03
H <sub>2</sub> O	3.50	4.27	3.21	-
LOI	3.97	-	-	5.00

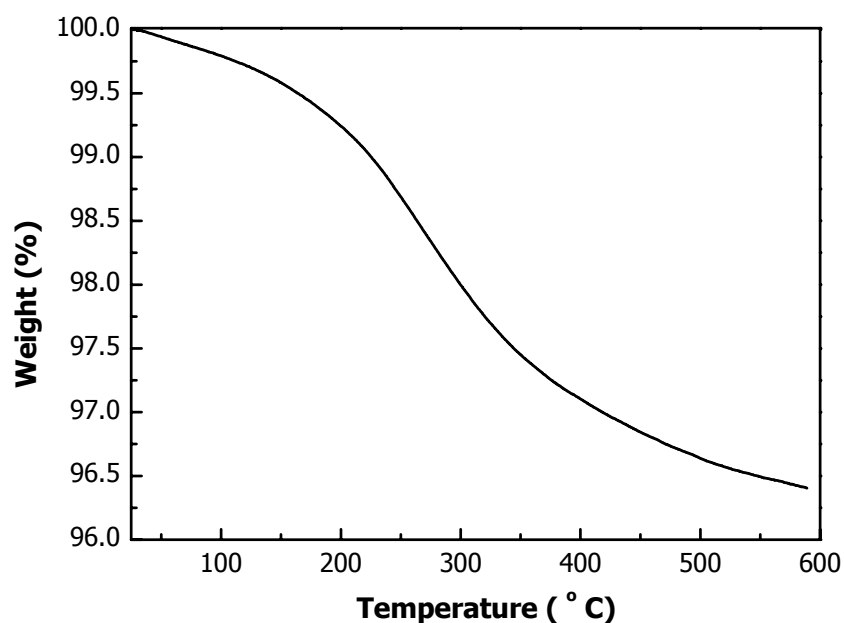


**Figure 4.2** TGA thermogram of a raw perlite.

by a thermal analyzer (TGA-DTA) recorded at ambient temperature to 600 °C (figure 4.2). This value corresponds to loss on ignition. Usually the chemical composition of perlite is suitable for synthesis of zeolite. Table 4.1 shows the chemical composition of the raw perlite compared to other studies.

Table 4.2 shows some physical properties of the perlite. The surface area and average pore size of perlite was determined by BET. Its surface area is 15.8582 m<sup>2</sup>/g with an average pore diameter of 9.27 nm. In addition, the particle size of perlite was found to be 3.20 μm, which was determined by laser particle size analyzer.

A Fourier transforms infrared spectrophotometer (FT-IR) was used to investigate the characteristics of raw perlite. The infrared spectra of perlite showed mainly 5 absorption bands observed around at 3442 cm<sup>-1</sup>, 1629 cm<sup>-1</sup>, 1054 cm<sup>-1</sup>, 788

$\text{cm}^{-1}$  and  $464 \text{ cm}^{-1}$ . The band at  $3442 \text{ cm}^{-1}$  is attributed to OH stretching of  $\text{H}_2\text{O}$  forming hydrogen bonds. The band at  $1629 \text{ cm}^{-1}$  is the deformation band of water molecules. The bands at  $1054 \text{ cm}^{-1}$  and  $788 \text{ cm}^{-1}$  are attributed to Si-O stretching vibrations of Si-O-Si and Si-O-Al, respectively (Sodeyama *et al.*, 1999). The band at  $464 \text{ cm}^{-1}$  is assigned to be O-Si-O bending.

**Table 4.2** Physical properties of raw perlite.

Physical properties	Raw perlite
Surface area ( by BET)	15.85 $\text{m}^2/\text{g}$
Average pore diameter	9.2757 nm
Particle size	3.20 $\mu\text{m}$

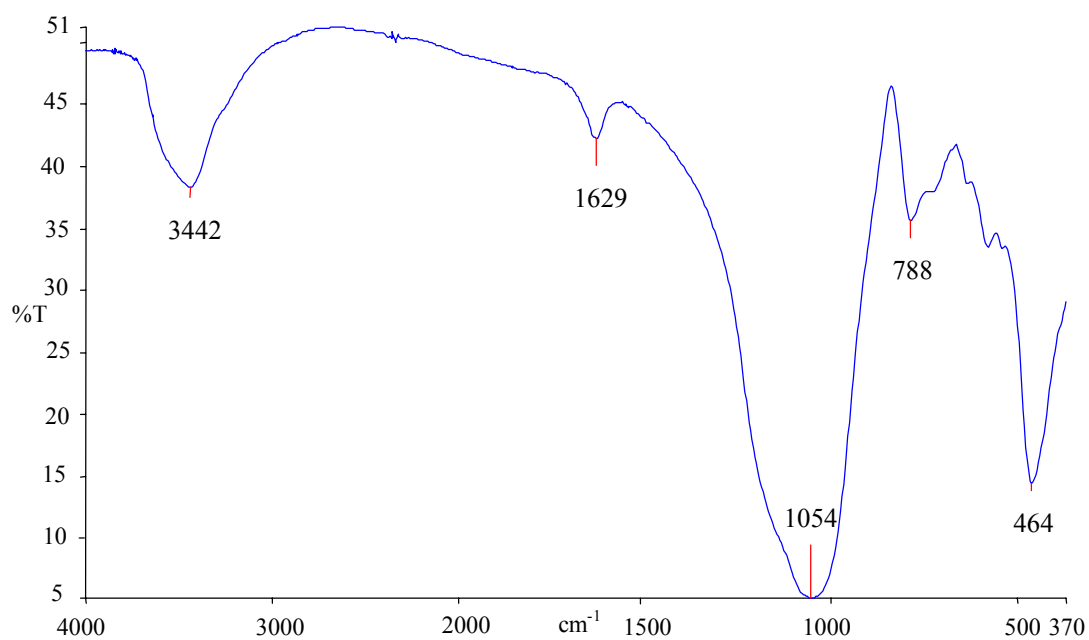


**Figure 4.3** FT-IR spectra of a perlite.

## 4.2 Synthesis of zeolite

Zeolite was synthesized from perlite collected from Lopburi Province. Synthesis inspections examined the zeolite crystallization under interesting conditions. The reaction and crystallization were carried out in a High Temperature/High Pressure stirred Reactor with a stainless steel, vessel of 500 ml capacity, at a pressure of 20 psi to 60 psi.

Conversion of inexpensive raw perlite into zeolites under various conditions is shown in table 4.3 and table 4.4. It shows that zeolite Na-P1, analcime and cancrinite can be synthesized from perlite under the conditions studied. At atmospheric pressure and low temperature, the results show that the product was only zeolite Na-P1 at a concentration of 1 M to 3 M NaOH and transformation to Na-P1 takes place over a period of 1 to 4 days. This result corresponds to Khodabandeh and David (1997). Yang *et al.* (1997) was reported that at a crystallization temperature of 100 °C the most stable structure is gismondine (Na-P1). Zeolite Na-P1 typically crystallizes under milder conditions. It was suggested that at higher temperatures (140 °C and 150 °C) zeolite Na-P1 is unstable and transforms into analcime. At higher pressure, alkali concentration of 1 M to 3 M NaOH, solid/liquid ratios 1:5 and 1:20 and reaction temperatures of 100 °C to 140 °C, the zeolite product was found to be only analcime with a percentage of crystallinity depending on reaction time. When the reactions are carried out under the influence of 3 M NaOH and 1:5 solid/liquid ratio at 140 °C, perlite is typically converted to a single phase of analcime with the highest yield. Cancrinite surprisingly favors formation with 3 M NaOH and 1:20 solid/liquid ratio at 140 °C.

Figures 4.4, 4.5 and 4.6 represent the XRD patterns of zeolite Na-P1, cancrinite and analcime, respectively. Zeolite Na-P1 shows 5 strong main peaks at  $2\theta = 12.5^\circ$  to  $33.5^\circ$ , while cancrinite as well as analcime shows all strong XRD patterns matching that of each of their literature values (Treacy and Higgins, 2001). However, only analcime was synthesized with the highest percent of crystallinity. This was confirmed by XRD pattern (figure 4.6) and SEM (figure 13).

**Table 4.3** Zeolite formation from perlite under various conditions.

Concentration (M)	Temperatures (°C)	Solid/Liquid (g/ml)	Time (hrs)	Products	
1	100*	1:5	24	ZeoliteNa-P <sub>1</sub>	
			48	ZeoliteNa-P <sub>1</sub>	
			72	ZeoliteNa-P <sub>1</sub>	
			96	ZeoliteNa-P <sub>1</sub>	
		1:20	24	ZeoliteNa-P <sub>1</sub>	
			48	ZeoliteNa-P <sub>1</sub>	
			72	ZeoliteNa-P <sub>1</sub>	
			96	ZeoliteNa-P <sub>1</sub>	
	100	1:5	168	Analcime	
			168	Analcime	
		1:20	120	Analcime	
			24	Analcime	
		140	1:5	48	Analcime
				72	Analcime
			1:20	96	Analcime
				96	Analcime
3	100*	1:5	24	ZeoliteNa-P <sub>1</sub>	
			48	ZeoliteNa-P <sub>1</sub>	
			72	ZeoliteNa-P <sub>1</sub>	
			96	ZeoliteNa-P <sub>1</sub>	
			120	ZeoliteNa-P <sub>1</sub>	
			144	ZeoliteNa-P <sub>1</sub>	
			1:20	24	ZeoliteNa-P <sub>1</sub>
				48	ZeoliteNa-P <sub>1</sub>
		72		ZeoliteNa-P <sub>1</sub>	
		96		ZeoliteNa-P <sub>1</sub>	
		120		ZeoliteNa-P <sub>1</sub>	
		144		ZeoliteNa-P <sub>1</sub>	

\* = atmosphere pressure

**Table 4.3** (Continued)

Concentration (M)	Temperatures (°C)	Solid/Liquid (g/ml)	Time (hrs)	Products
	100	1:5	168	Analcime
		1:20	168	Analcime
	120	1:5	24	Analcime
			48	Analcime
			72	Analcime
			96	Analcime
		1:20	24	Analcime
			48	Analcime
			72	Analcime
			96	Analcime
	140	1:5	24	Analcime
			48	Analcime
			72	Analcime
			96	Analcime
			120	Analcime
			144	Analcime
			168	Analcime
		1:20	96	Cancrinite
			120	Cancrinite
			144	Cancrinite
			168	Cancrinite

\* = atmosphere pressure

**Table 4.4.** Zeolite formation from perlite at periods of 12 hours under various conditions.

Concentration (M)	Temperatures (°C)	Solid/Liquid (g/ml)	Products	% Crystallinity
1	120	1:5	ZeoliteNa-P <sub>1</sub>	-
		1:10	ZeoliteNa-P <sub>1</sub>	-
	130	1:5	ZeoliteNa-P <sub>1</sub>	-
		1:10	ZeoliteNa-P <sub>1</sub>	-
	140	1:5	ZeoliteNa-P <sub>1</sub>	-
		1 :10	ZeoliteNa-P <sub>1</sub>	-
2	120	1:5	Analcime	11.1
		1:10	Analcime	17.8
	130	1:5	Analcime	19.6
		1:10	Analcime	31.2
	140	1:5	Analcime	44.4
		1 :10	Analcime	86.6
3	120	1:5	Analcime	18.2
		1:10	Analcime	21.5
	130	1:5	Analcime	21.7
		1:10	Analcime	32.3
	140	1:5	Analcime	100
		1 :10	Analcime	85.6

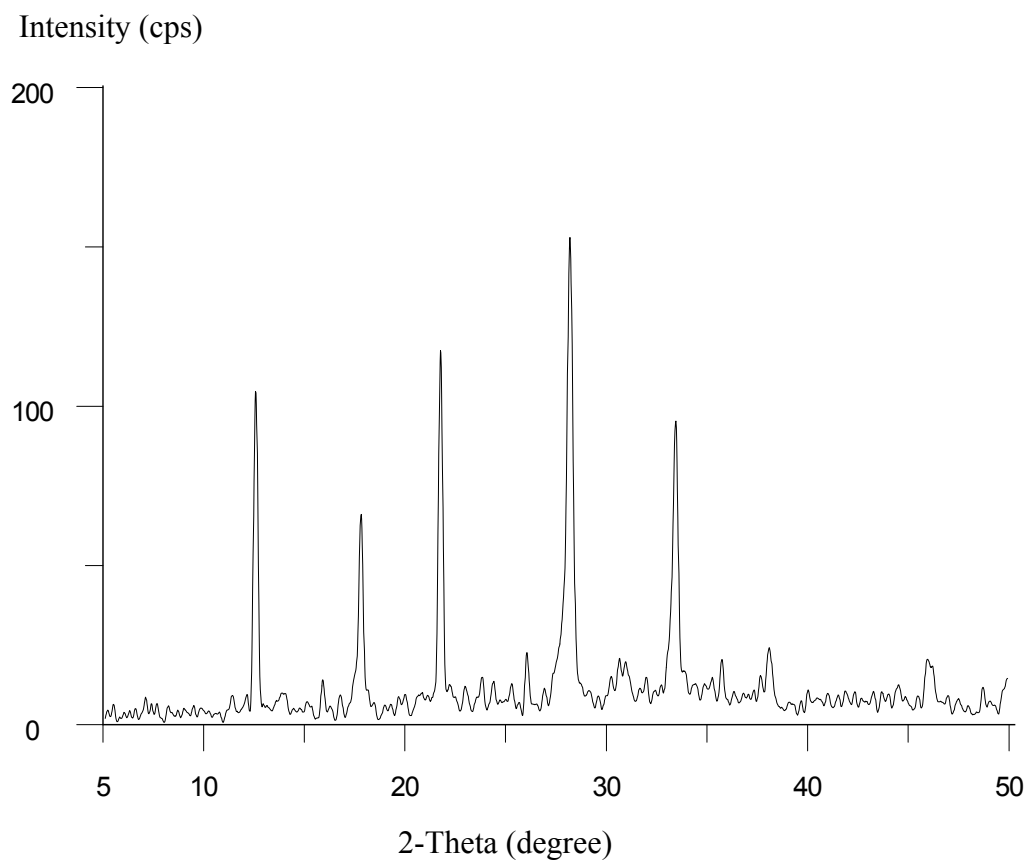


**Figure 4.4** X-ray diffractogram of zeolite Na-P1 obtained from perlite.

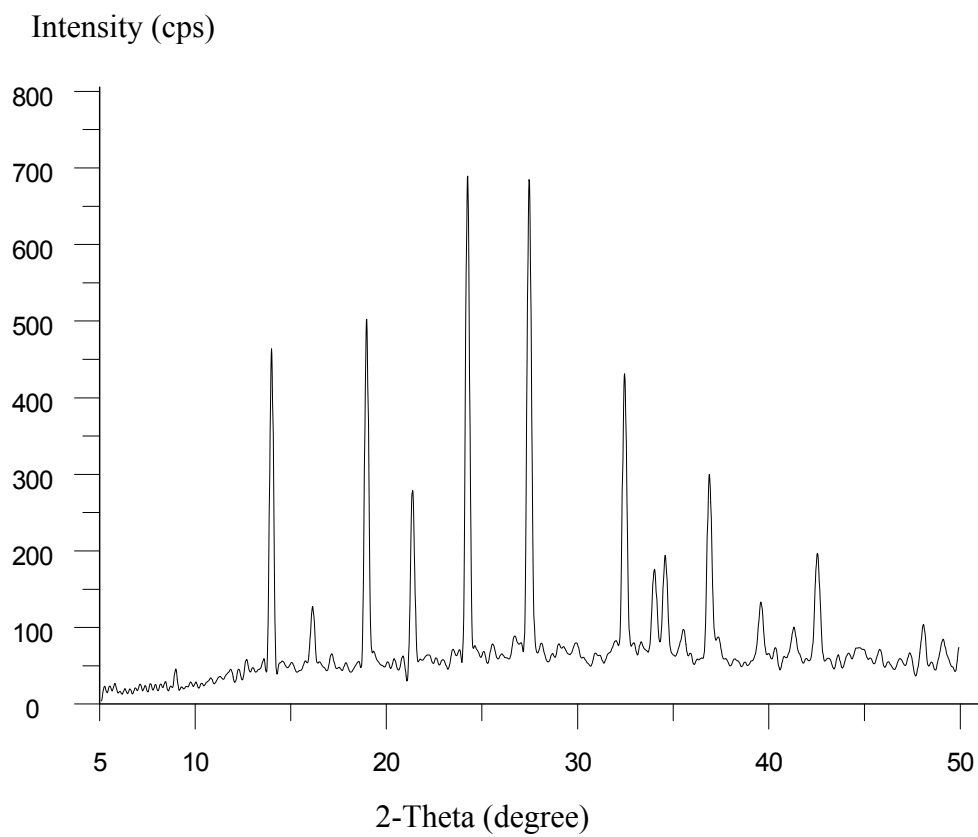


**Figure 4.5** X-ray diffractogram of cancrinite obtained from perlite.

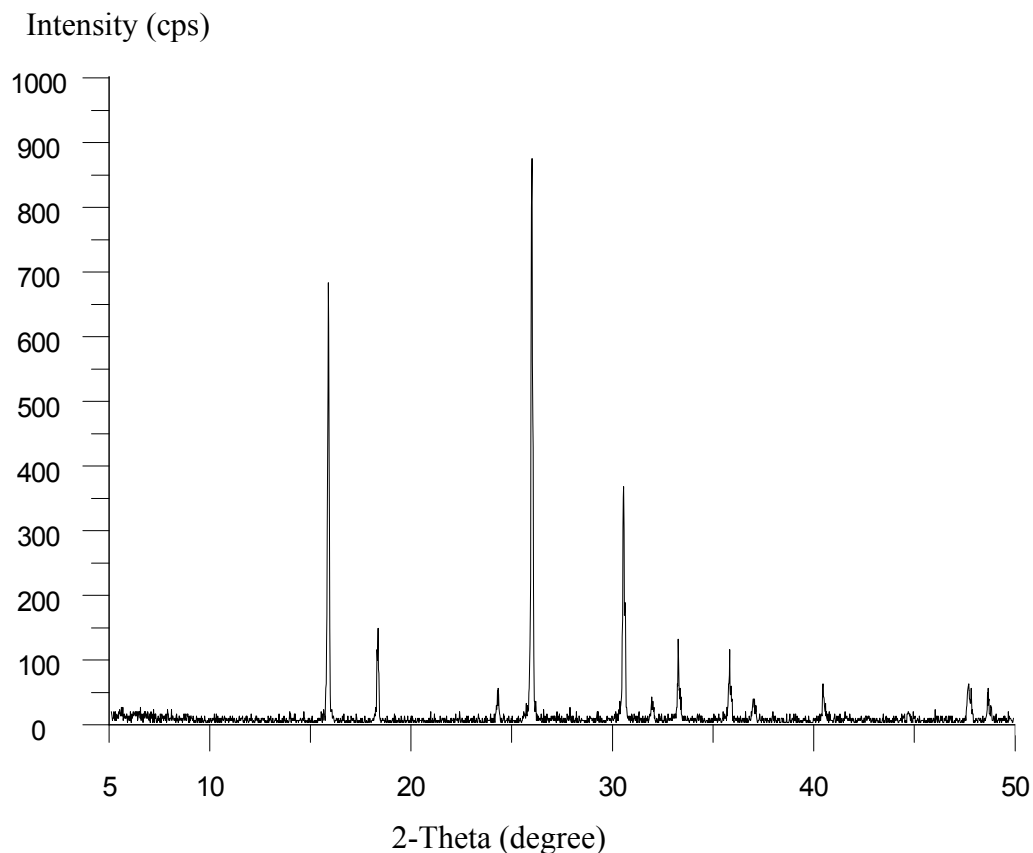


**Figure 4.6** X-ray diffraction pattern of analcime prepared from perlite.

A comparison of the IR spectra of raw perlite, zeolite Na-P1, cancrinite and analcime was shown in figure 4.7. Their IR spectra are also matched with fingerprints of wave number values (Flanigen *et al.*, 1971). In the region of OH stretching vibration, all samples show absorption bands around  $3440\text{ cm}^{-1}$ . Analcime showed a band at  $3622\text{ cm}^{-1}$ , attributed to free OH stretching vibration of water. Absorption bands at  $1640\text{ cm}^{-1}$  is due to bending vibration of adsorbed water molecules. Vibration in a region of  $\text{TO}_4$  tetrahedral (T = Si or Al) units of zeolite, bands at about  $1,020\text{ cm}^{-1}$ ,  $737\text{ cm}^{-1}$ ,  $619\text{ cm}^{-1}$  and  $444\text{-}460\text{ cm}^{-1}$  are assigned to asymmetric stretching,

symmetric stretching, double ring and T-O bending vibrations, respectively (Breck, 1974). However, infrared assignment of vibration framework of the three different zeolite products is shown in table 4.5. In the case of analcime, it found that the absorption band slightly differs from Flanigen *et al.* (1971). This may be due to the different ratio Si/Al present in the analcime framework.

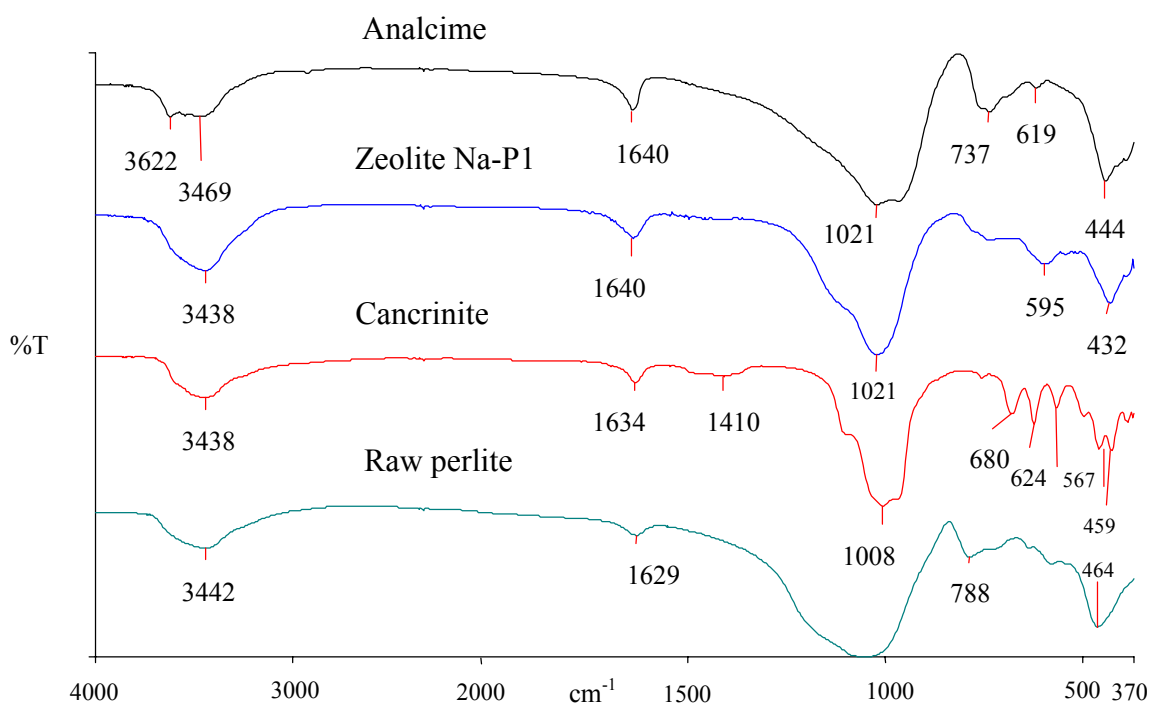


**Figure 4.7** FT-IR spectra of raw perlite and zeolite products of zeolite Na-P1, cancrinite and analcime.

**Table 4.5** Infrared assignment of vibrational framework of three different zeolite products.

Zeolite	Asymmetric stretching	Symmetric stretching	Double ring	T-O bending
Analcime	1,021, 925	740, 686	615	442
Cancrinite	1,000, 965	680	624, 567	458
Zeolite Na-P1	995-1,000	722, 670	600	435

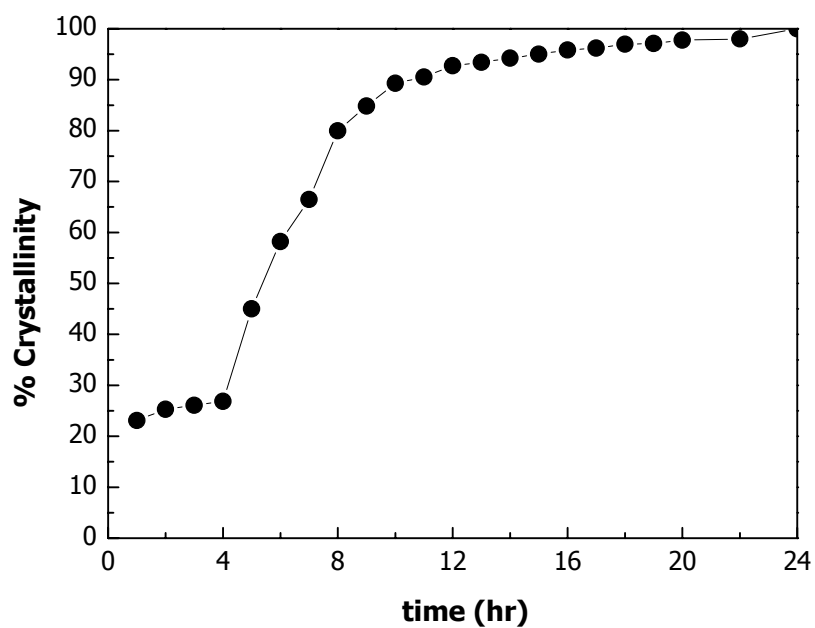


**Figure 4.8** Plot percent crystallinity of analcime against different crystallization periods of time at 140 °C.

The highest yield of analcime was obtained by the synthesis of 3 M NaOH 1:5 solid/liquid ratio at 140 °C. Under these conditions, the synthetic analcime was used as a standard (figure 4.8).

Figure 4.9 shows the SEM photographs of analcime obtained from perlite conversion with various crystallization periods from 1 to 7 days at 140 °C. SEM images of the reaction time of 1 to 5 days are slightly different in percent crystallization and crystal size (see figure 4.10 to 4.12) except at a period of 7 day, when analcime was unstable (figure 4.9(d)). The average particle size of analcime at different reaction times is very close (figure 4.12). The grain size decreases from 8 to 7  $\mu\text{m}$  with a reaction time of 1 to 7 days (figure 4.12).



**Figure 4.9** SEM photographs of kinetics of crystallization of analcime obtained by varying crystallization periods at 140 °C. (a) 1 day, (b) 3days, (c) 5 days and (d) 7 days.

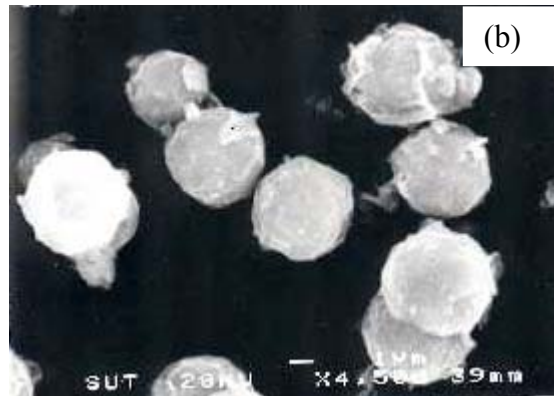
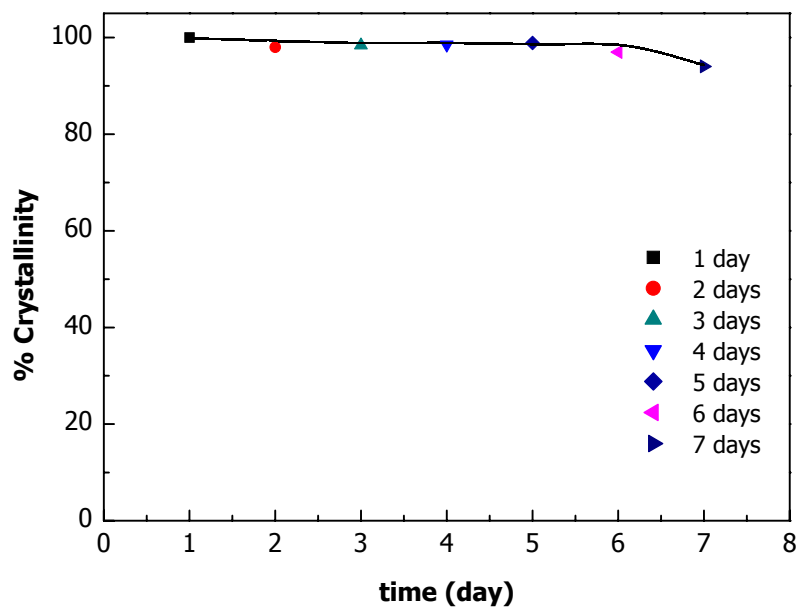
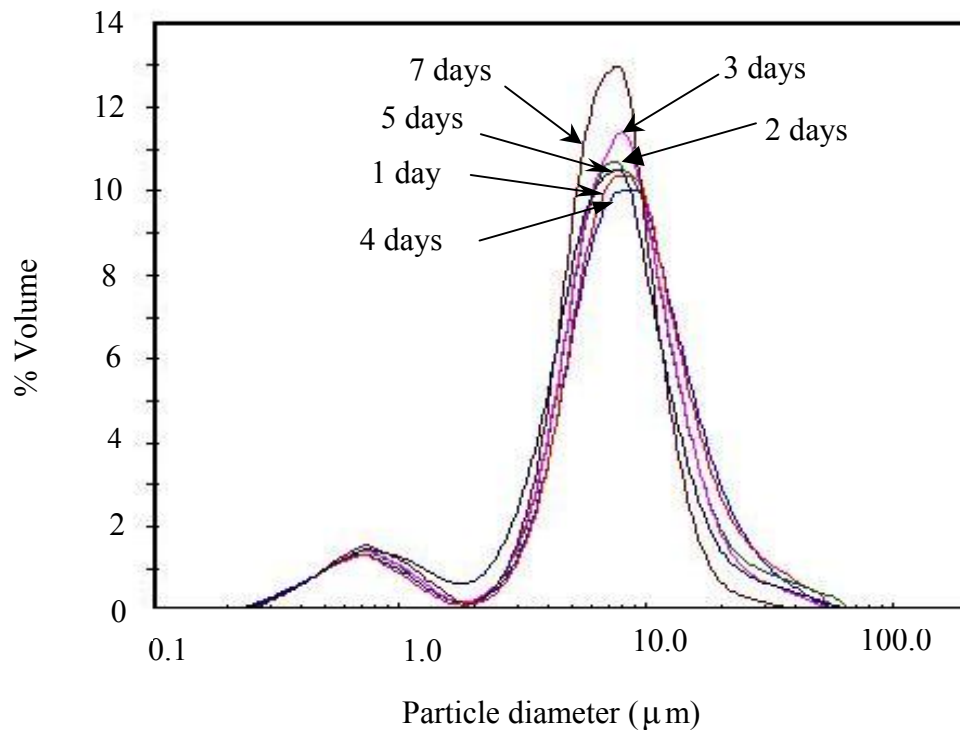


Figure 4.9 (Continued)



**Figure 4.10** Plot describing analcime crystals obtained by varying crystallization periods at 140 °C.



**Figure 4.11** Particle size distribution of analcime crystallites synthesized at different crystallization periods (1 to 7 days) at 140 °C.

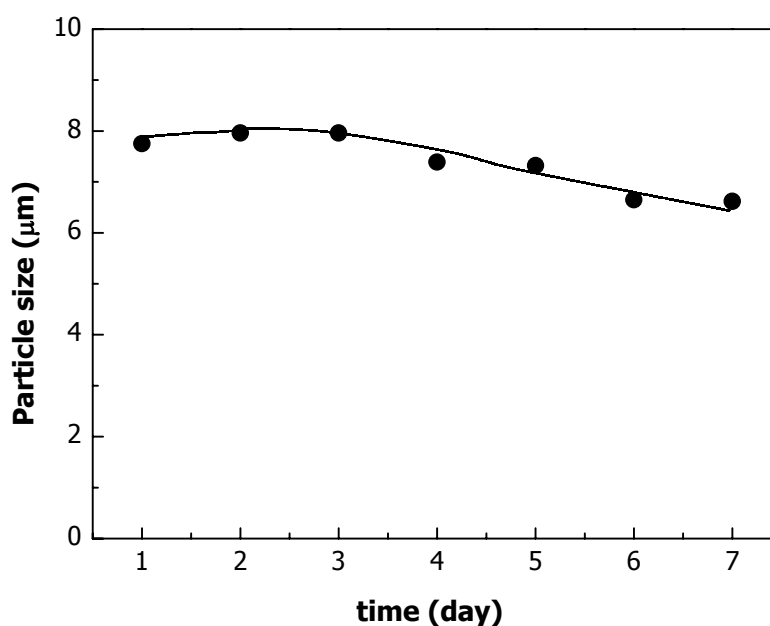


**Figure 4.12** Plot of particle size distribution trend of analcime crystallites synthesized at different crystallization periods (1 to 7 days) at 140 °C.

To summarize the inspection of zeolite crystallization from perlite under the conditions studied, the results (table 4.4) indicate that analcime was only obtained with the highest percent crystallinity under the influent of 3 M NaOH and 1:5 solid/liquid ratio at 140 °C for 24 hours. Under these conditions pure analcime was synthesized for further study of its diffusion and ion exchange properties. In addition, the crystallization kinetics of analcime was intensively studied at constant NaOH concentration and solid/liquid ratio with different temperatures.

### 4.3 Chemical, physical properties and pH tolerance of analcime

As shown, analcime was obtained with the highest percent crystallization under the condition studied, so the characteristic and properties of analcime were studied before it was used for the study of its diffusion and ion exchange applications. XRF and TGA-DTA were carried out to measure their chemical properties. Loss on ignition was investigated. The XRD, SEM, BET, CEC,  $^{29}\text{Si}$  MAS NMR, laser particle size analyzer and FT-IR were also used to investigate the physical properties of analcime. pH tolerance at pH range 1 to 12 and the effects of temperature in the range 100 °C, 200 °C and 300 °C on their structure were determined.

The chemical composition of synthetic analcime was compared to other studies as shown in table 4.6. The synthetic analcime samples for this study are slightly different in their main composition of  $\text{SiO}_2$ ,  $\text{Al}_2\text{O}_3$  and  $\text{Na}_2\text{O}$  contents when compared to other studies. Thermograms of the synthetic analcime are shown in figure 4.13. The analcime had a total mass loss of 8.5%, being close to the value of 8.4% due to water loss quoted in previous work (Todorovic *et al.*, 1987). Yusof (1984) reported that the water content obtained was around 8-9%. DTA showed the typical endothermic dehydration curve of analcime in the range 200 °C to 400 °C which corresponds to water loss in TGA data. The trace also showed that the structure of analcime was stable to at least 800 °C.

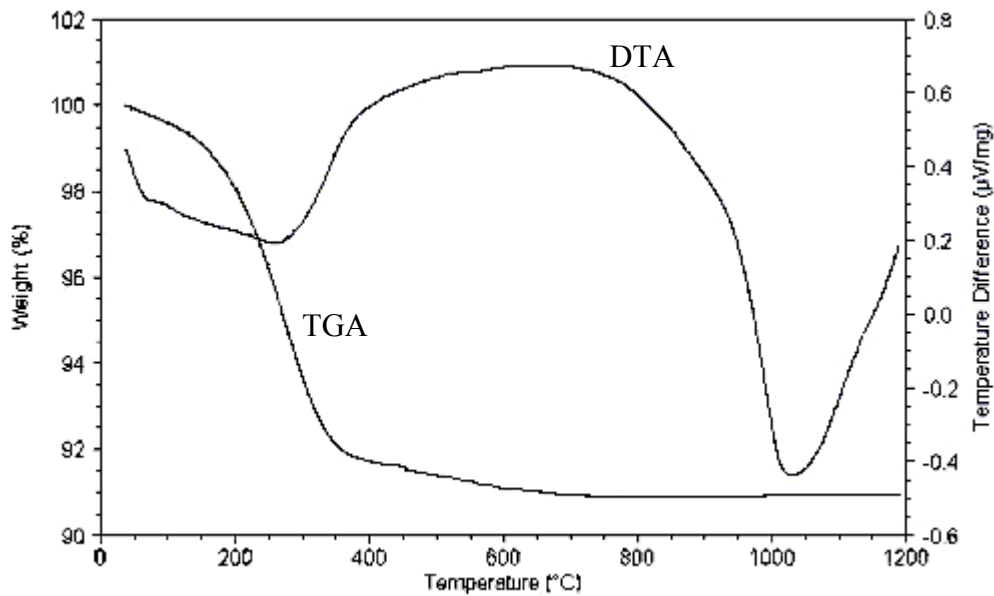


**Figure 4.13** TGA-DTA thermograms of a synthetic analcime sample.

**Table 4.6** Chemical composition of synthetic analcime in weight percentage.

Oxide	Analcime (this work)	Analcime Yusof (1984)	Analcime Yoder <i>et al.</i> , (1960)
SiO <sub>2</sub>	52.44	51.63	56.05
Al <sub>2</sub> O <sub>3</sub>	24.30	24.19	22.36
K <sub>2</sub> O	0.34	-	-
Na <sub>2</sub> O	12.53	13.98	13.44
CaO	0.28	-	-
Fe <sub>2</sub> O <sub>3</sub>	1.61	-	-
H <sub>2</sub> O	8.50	8.9	8.13
LOI	7.99	-	-

The synthetic analcime product is pure as confirmed by XRD pattern (figure 4.6), FT-IR spectra (figure 4.7) and again with SEM photographs. The SEM morphology of synthetic analcime crystals prepared from perlite is shown in figure 4.14. Table 4.7 shows the physical properties of synthetic analcime.

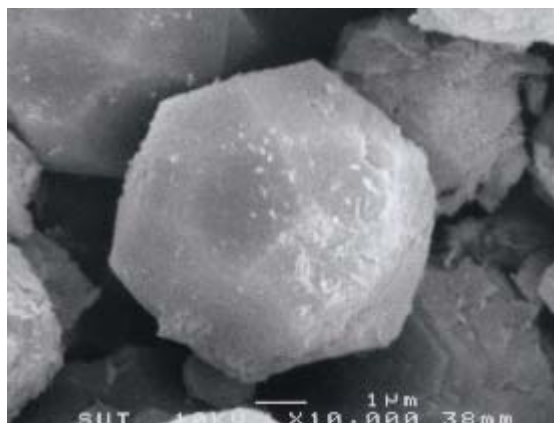


**Figure 4.14** SEM photographs of analcime crystals prepared from perlite.

**Table 4.7** Physical properties of synthetic analcime.

Physical properties	Analcime product
Surface area	
This work	18.92 m <sup>2</sup> g <sup>-1</sup>
Reference (Barrer, 1950)	21.0 m <sup>2</sup> g <sup>-1</sup>
CEC	
This work	4.16 meqg <sup>-1</sup>
Reference(Sherman, 1978)	4.9 meqg <sup>-1</sup>
Si/Al ( <sup>29</sup> Si MAS NMR)	1.97
Mean particle size	7.75 μm

The analcime had Si/Al of 1.97 (<sup>29</sup>SiMASNMR). The spectrum shows three major peaks at -91.6 ppm, -96.6 ppm and -101.9 ppm assigned to different silicon configurations Si(3Al), Si(2Al) and Si(1Al), respectively, as shown in figure 4.15 which is similar to those of previous studies (Cheng *et al.*, 2000). The relatively

broader centreband signals can be accounted for by the known iron content (table 4.6). Usually the Si/Al ratio of synthetic analcime, prepared by high temperature hydrothermal processes, has been found to be 1.5 to 3 (Balgord and Roy, 1971). The ion exchange capacity of the zeolite varies from 3 to 7 meqg<sup>-1</sup> depending on the Si/Al ratio. The smaller the Si/Al ratio, the greater the ion exchange capacity observed (Faghihian, 1990). In this study, cation exchange capacity (CEC) of the synthetic analcime was found to be 4.16 meqg<sup>-1</sup> and its specific surface area was determined by a BET surface area analyzer of 18.92 m<sup>2</sup>g<sup>-1</sup>. The value of the water content and CEC of the synthetic analcime will be used to construct the isotherms.

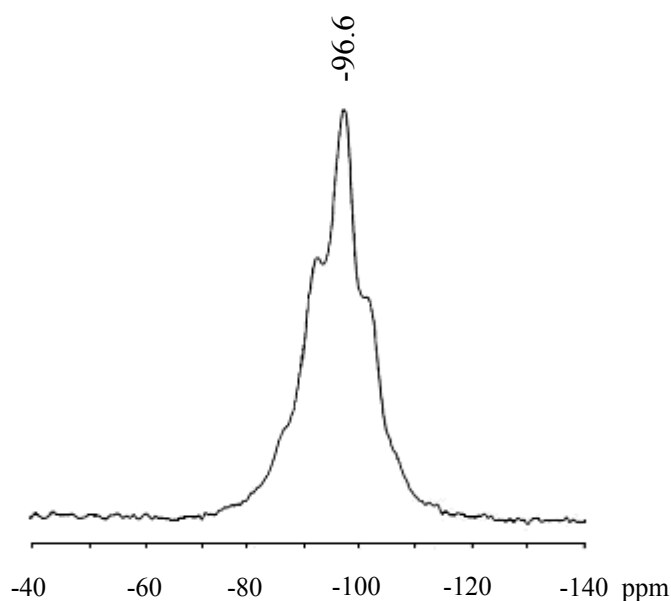


**Figure 4.15** <sup>29</sup>Si MAS NMR spectra of synthetic analcime prepared from perlite.

Figure 4.16 shows bimodal particle size distribution with the peak at less than 1  $\mu\text{m}$  and 7.75  $\mu\text{m}$ . The peaks at 7.75  $\mu\text{m}$  is due to analcime particles. This particle size value has been used to calculate the diffusion parameters. The peak at less than 1

$\mu\text{m}$  is due to the presence of very small amounts of an amorphous material (Ferchiche *et al.*, 2001).

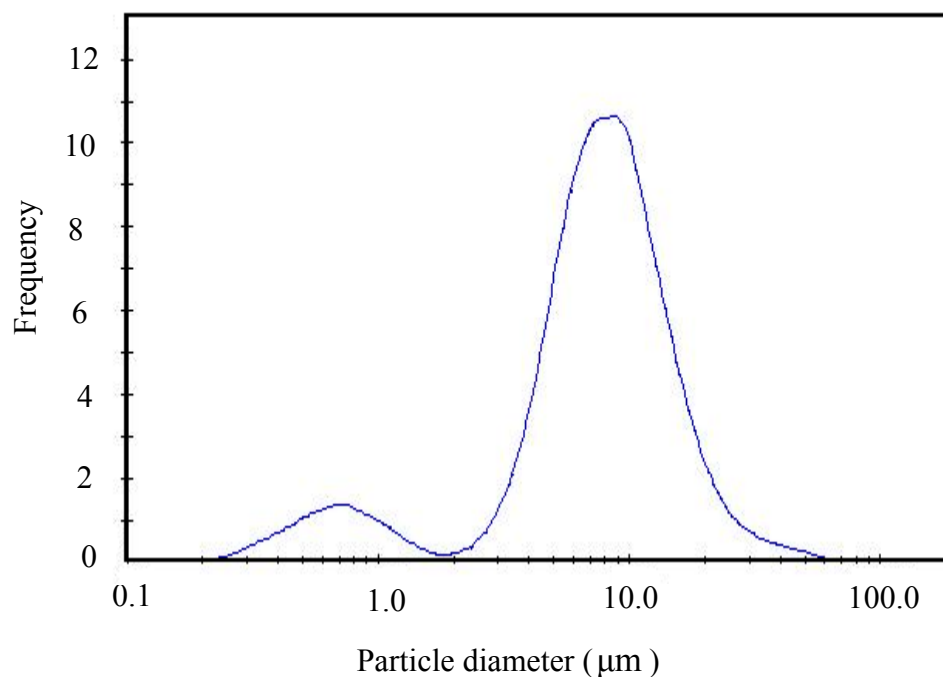


**Figure 4.16** Particle size distributions of analcime crystallites.

Figure 4.17 shows the change in the crystallinity percentage of analcime at various pH values from 1 to 13. pH also has a significant impact on the structure of analcime at pH range 1 to 3 with a decrease in percentage crystallization of analcime to 25 %. This demonstrates that at very low pH the structure of analcime is not stable and it will collapse. The structure of analcime remains stable at the pH range 4 to 13. X-ray patterns were also used to confirm the effects of pH on analcime structure (figure 4.18).

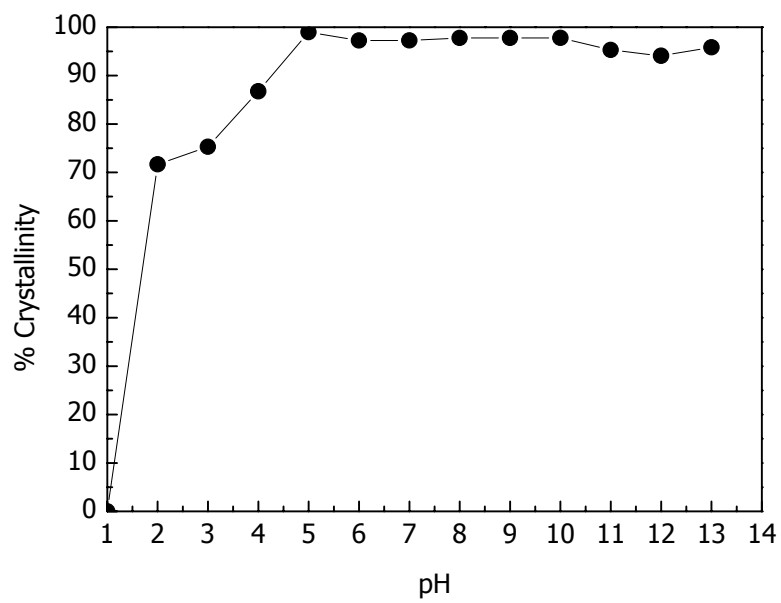


**Figure 4.17** Plot of percentage crystallinity of analcime samples at different pH treatments.

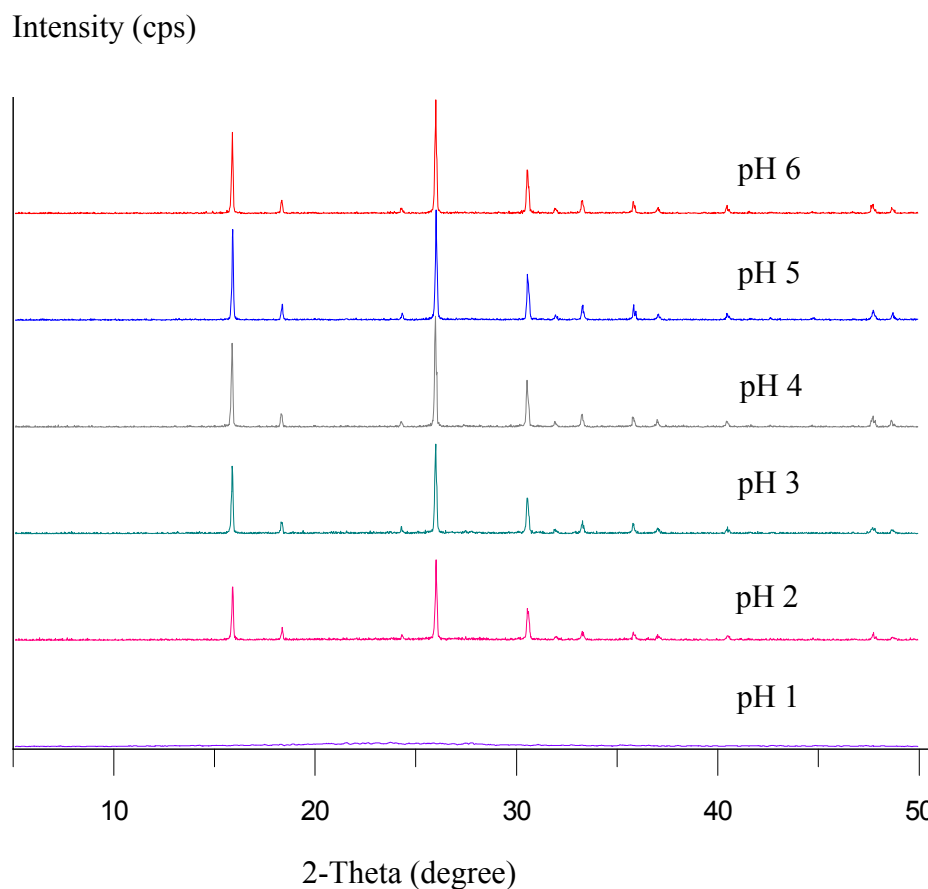


**Figure 4.18** X-ray diffractogram of analcime samples at different pH treatments.

The IR transmittance spectra of analcime heated for 24 hours at 100 °C, 200 °C and 300 °C in a KBr matrix were recorded in the range of 4000  $\text{cm}^{-1}$  to 370  $\text{cm}^{-1}$  (figure 4.19). As mentioned previously, analcime shows an absorption band at 3627  $\text{cm}^{-1}$  and a strong water absorption band at 3452  $\text{cm}^{-1}$  and 1638  $\text{cm}^{-1}$ . The absorption band at 3620  $\text{cm}^{-1}$  is assumed to be a band of Si-OH. The intensity of this band decreases with increasing temperature due to dehydroxylation of isolated silanol groups as shown in figure 4.19. The stretching vibration band of bound water in zeolite at 3448  $\text{cm}^{-1}$  shifts to a lower wave number at 3438  $\text{cm}^{-1}$  when there is an increase in temperature from 200 °C to 300 °C. This red shift indicates that waters in

zeolite at 300 °C forms a stronger hydrogen bond than that at 120 °C. While a blue shift appears for bending vibration of water with stronger hydrogen bonds. The adsorption band due to internal tetrahedra at 736  $\text{cm}^{-1}$  and 443  $\text{cm}^{-1}$  are not affected by heating at these temperatures.

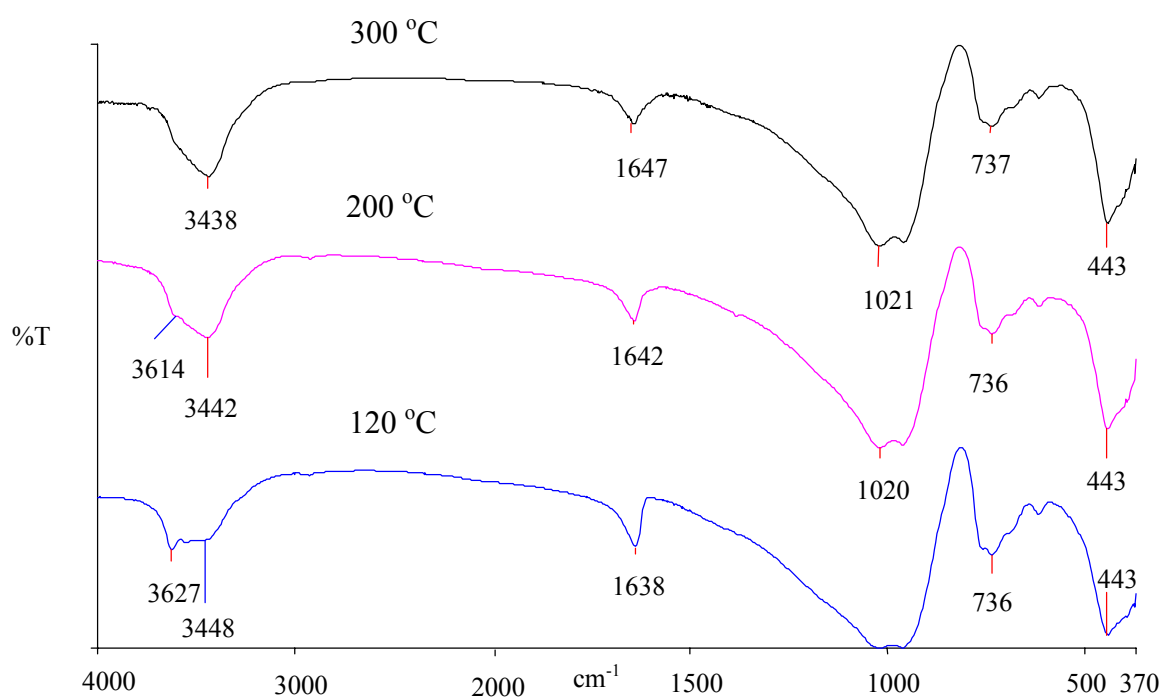


**Figure 4.19** FT-IR spectra of analcime samples calcined at different temperatures.

#### 4.4 Crystallization kinetics of analcime

The effect of reaction time and temperature on the crystallization of analcime synthesized from perlite was examined under fixed conditions at 3 M NaOH and 1:5 solid/liquid ratio in a temperature range from 130 °C to 145 °C. Percent of crystallinity is shown in table 4.8.

**Table 4.8** The kinetics of analcime formation from perlite at various reaction temperatures.

Concentration (M)	Temperatures (°C)	Solid/Liquid (g/ml)	Time (hrs)	Product	% Crystallinity
3	130	1:5	24	Analcime	85.8
	135	1:5	24	Analcime	89.7
	140	1:5	24	Analcime	100
	145	1:5	24	Analcime	95.7

The XRD patterns of solid phases obtained from the synthesis during different crystallization periods at 135 °C to 145 °C were shown in figure 4.20 to 4.23. These patterns showed that raw glass perlite remains XRD amorphous for the first of the treatment. After 4 hours some peaks of zeolite Na-P1 appeared and all the peaks of analcime appeared after 9 hours. The peak intensities slightly developed as the crystallization period increased. The broad amorphous peak from raw perlite gradually disappears as the glass is converted to zeolite. No other crystalline phase appeared in

the XRD peak of analcime after crystallization periods up to 14 hours. This change indicated that the percentage of crystallinity of analcime increased while amorphous evidence decreased. The greatest change in the extent of crystallization of the solid phase is observed between the 8<sup>th</sup> and the 14<sup>th</sup> hours for 130 °C to 140 °C and between the 5<sup>th</sup> and the 7<sup>th</sup> hours for 145 °C, as the results of temperature changes. Therefore, it is clear that analcime crystallization is highly dependent on temperature.

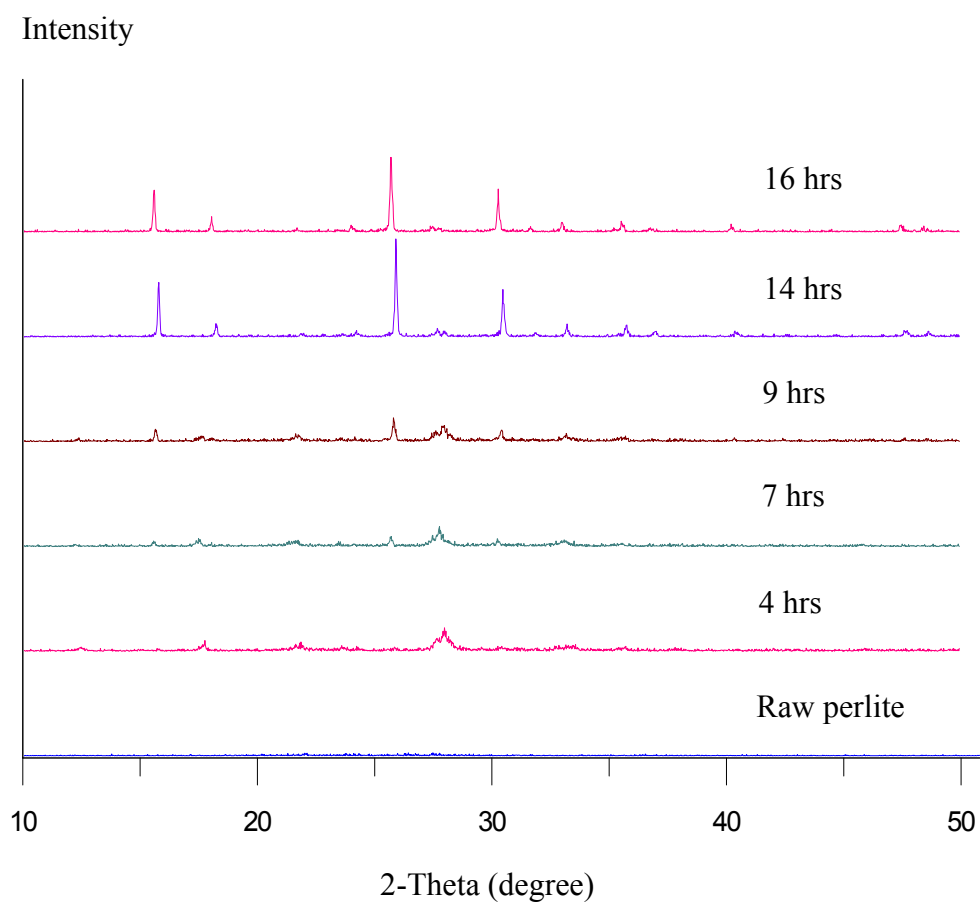


**Figure 4.20** X-ray diffraction patterns of raw perlite and analcime samples obtained at different crystallization periods at 130 °C.

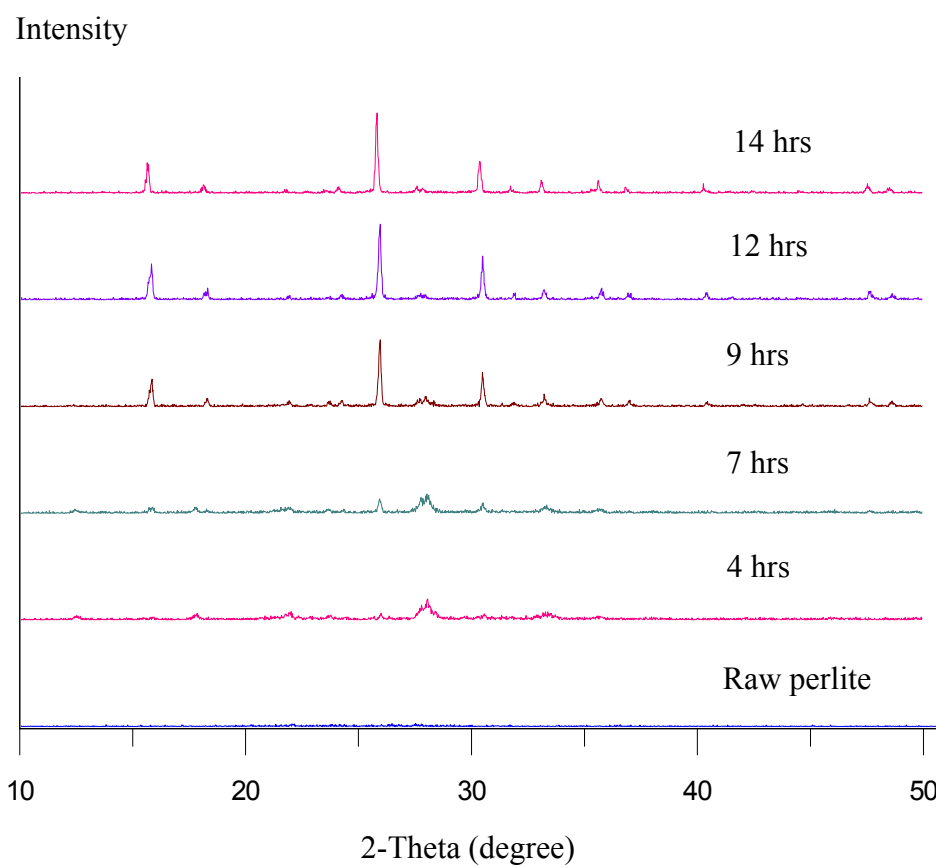


**Figure 4.21** X-ray diffraction patterns of raw perlite and analcime samples obtained at different crystallization periods at 135 °C.

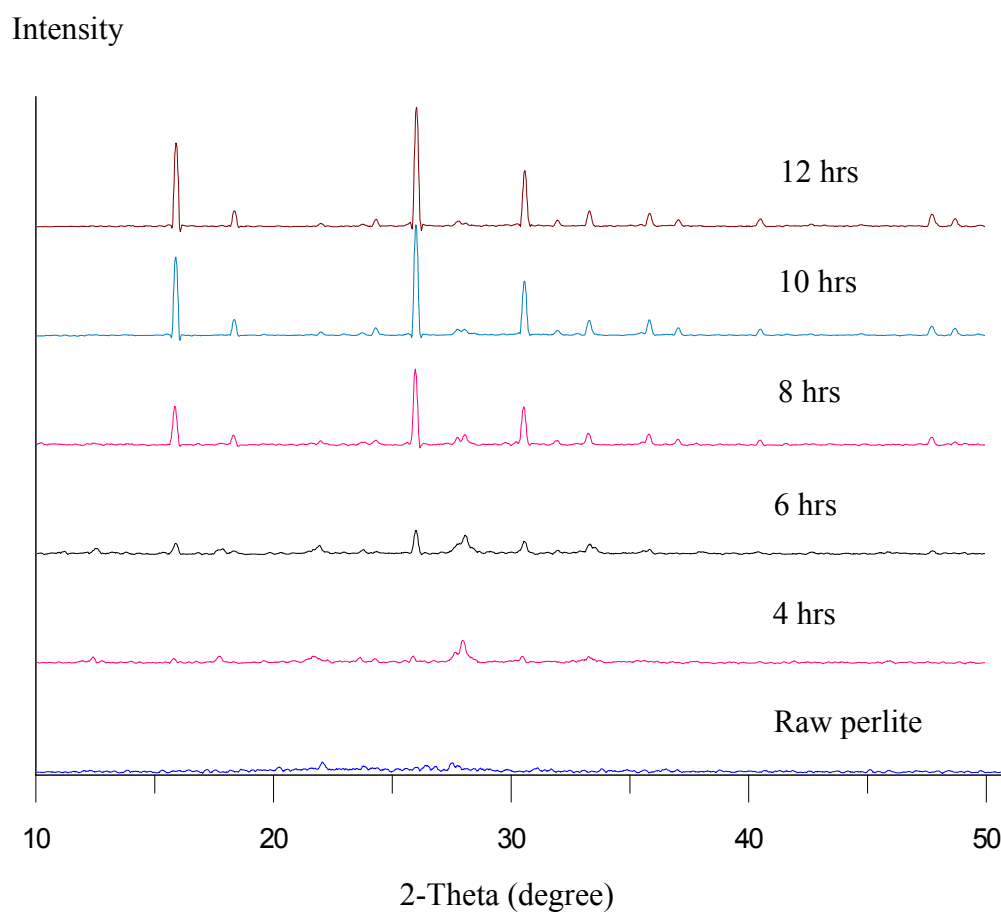


**Figure 4.22** X-ray diffraction patterns of raw perlite and analcime samples obtained at different crystallization periods at 140 °C.

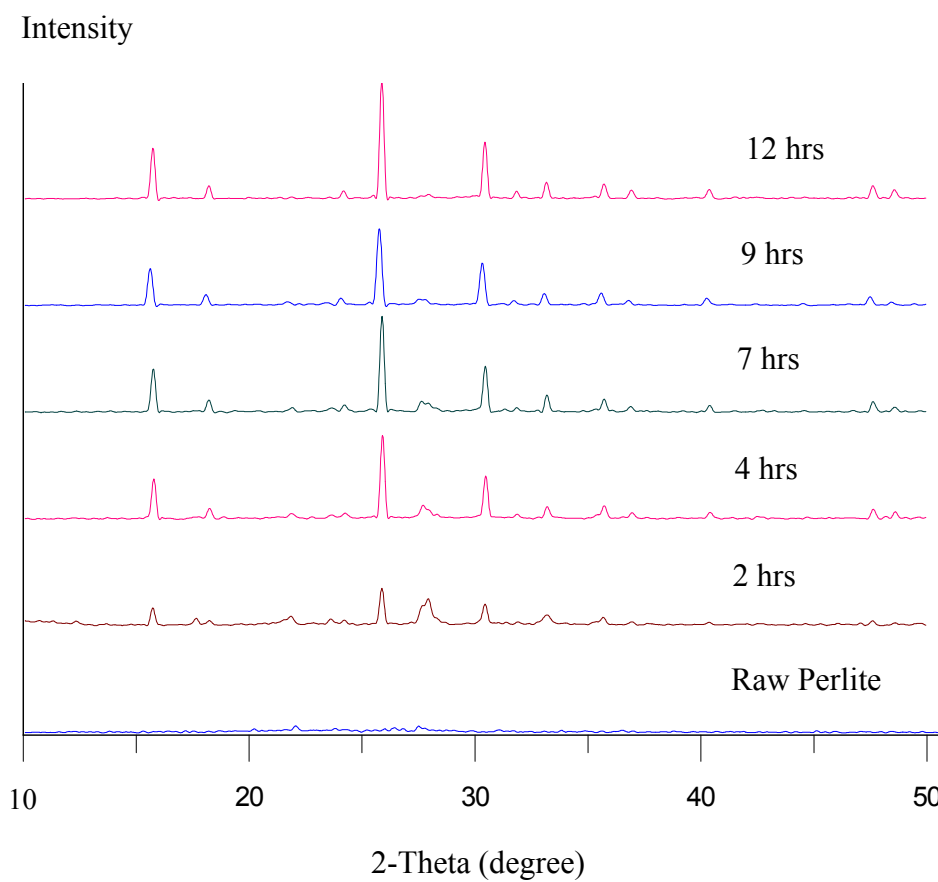


**Figure 4.23** X-ray diffraction patterns of raw perlite and analcime samples obtained at different crystallization periods at 145 °C.

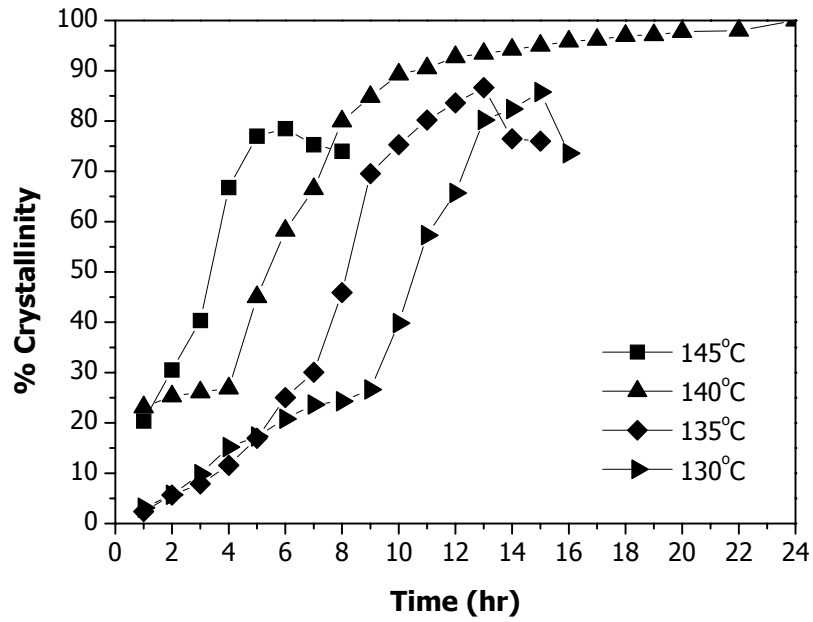


Figure 4.24 Kinetics of analcime crystallization at different temperatures.

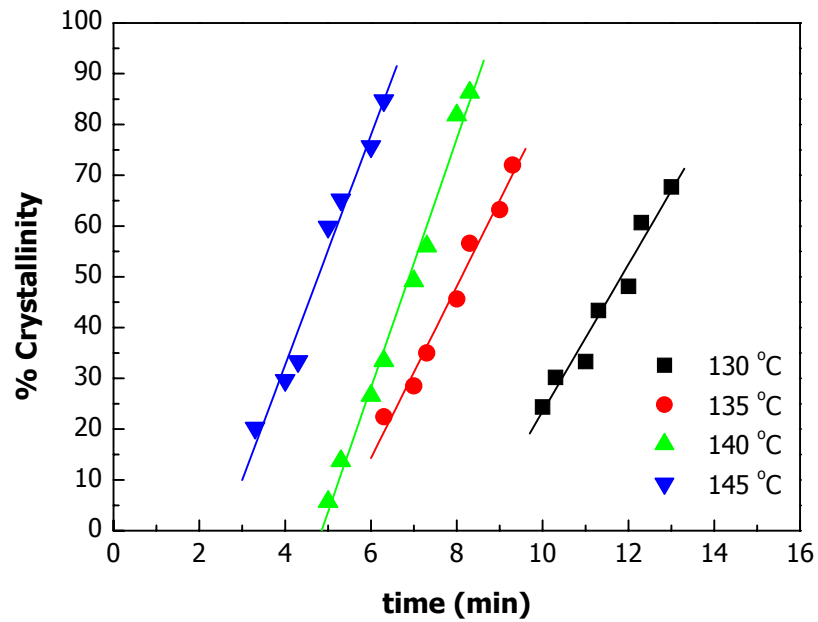
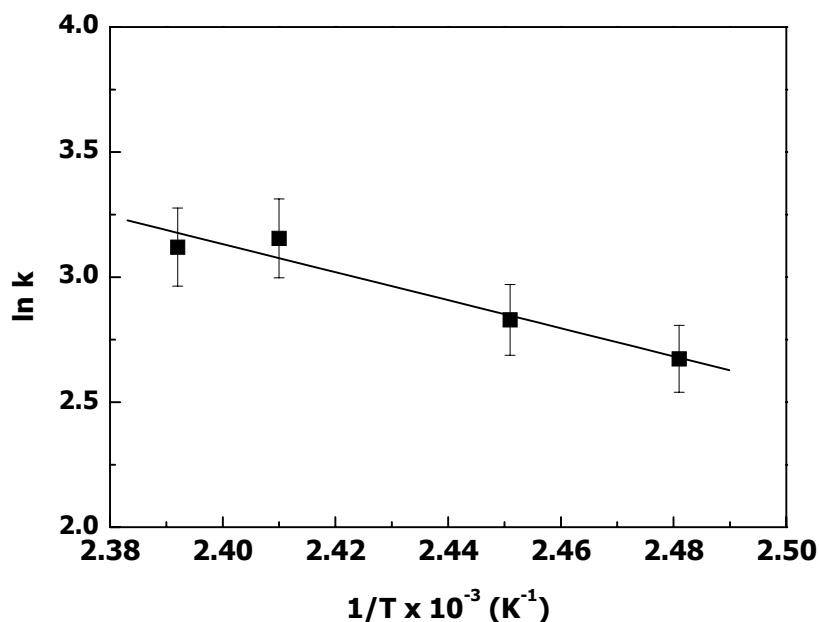


Figure 4.25 Crystallinity as a function of time.



**Figure 4.26** Arrhenius plot for analcime crystallization.

As the mechanism of zeolite crystallization referring to kinetics such as the autocatalysis of crystallization has been insufficiently studied, we attempted in this part to calculate the activation energy of crystallization from the Arrhenius equation and to fit the data on the nucleation growth model of Avrami. The plots of analcime crystallization at different temperature are shown in figure 4.24 and figure 4.25.

The activation energy ( $E_a$ ) of the process was extracted from the slope of the plot  $\ln k$  against  $1/T$  (K), derived from the general Arrhenius equation,  $k = Ae^{E_a/RT}$  as shown in figure 4.26. The pre-exponential factor (A) was extracted from the intercept of the line. The resulting values were shown in table 4.9. The  $E_a$  value was found to be  $11.2 \text{ kcal mol}^{-1}$ , which is in good agreement with the activation energy of other zeolites, as reported by Breck and Flanigen (1968). It was suggested that the activation energy is not related to the diffusion of crystal building units in solution but to the

condensation reaction between the crystal surface and the crystal building units (Van Bekkum *et al.*, 1991). Breck and Flanigen (1968) estimated the activation energy of the crystallization process for zeolites A, X, Y and mordenite (Domine and Quobex, 1968). The values obtained are 11, 14, 15 and 11 kcal mol<sup>-1</sup>, respectively. The values obtained for activation energy are important as energetic characteristics for the zeolite crystallization process.

The Avrami equation can provide a good empirical fit for the kinetic curves. However, the Avrami equation essentially describes solid-state reactions and not solution-mediated processes and it does not refer to any particular mechanism (Gualtievi *et al.*, 1997). According to the Avrami equation  $(-\ln(1-\alpha) = (kt)^n)$ , the reaction orders (n) were extracted from plots of  $\ln[-\ln(1-\alpha)]$  against  $\ln t$  is shown in figure 4.27. Where  $\alpha$  is the conversion factor ranging from 0 to 1. The order of the reaction is also derived from the slope of the regression line for each temperature experiment, whereas the rate constant k is derived from the intercept and the order parameters have been evaluated for each reaction temperature, and the results are shown in table 4.10.

Based on this model the n value is expected to vary between 1 and 4 depending on the dimensionality of the growth process and on the kinetic order of nucleation. The n values 3 and 4 can be interpreted as follows. With n = 3 the growth process in three dimensions is combined with zero order nucleation and n = 4 a similar process of crystal growth appears, but nucleation is first order. However the n value found in this study varies from 3.4 to 6.4 with a decrease in temperature from 145 °C to 130 °C except at 140 °C. The same trend of the n value was observed also in the synthesis of zeolite Na-A (Wongwiwattana and Rangriwatananon, 2002) and zeolite Na-X

(Thammavong and Rangriwatananon, 2003). It was suggested that  $n$  exceeds 4 crystallization of the amorphous phase should take place in the autocatalytic stage of the crystallization process under conditions where either the rate of nucleation or the rate of crystal growth increases (Zhdanov *et al.*, 1990). At 140 °C the  $n$  value is the highest, so it is assumed that the nucleation of analcime is favored this value rather than the other conditions as shown in table 4.8 indicating the percentage of analcime crystallinity.

**Table 4.9** Activation energy of analcime crystallization at reaction condition 3 M NaOH 140 °C 1:5 solid/liquid ratio.

Temperature (°C)	slope	R	Pre-exponential factor (A)	$E_a$ kcal K <sup>-1</sup> mol <sup>-1</sup>
130	14.50	0.98		
135	16.92	0.99	16.59	11.2
140	24.50	0.99		
145	22.65	0.99		

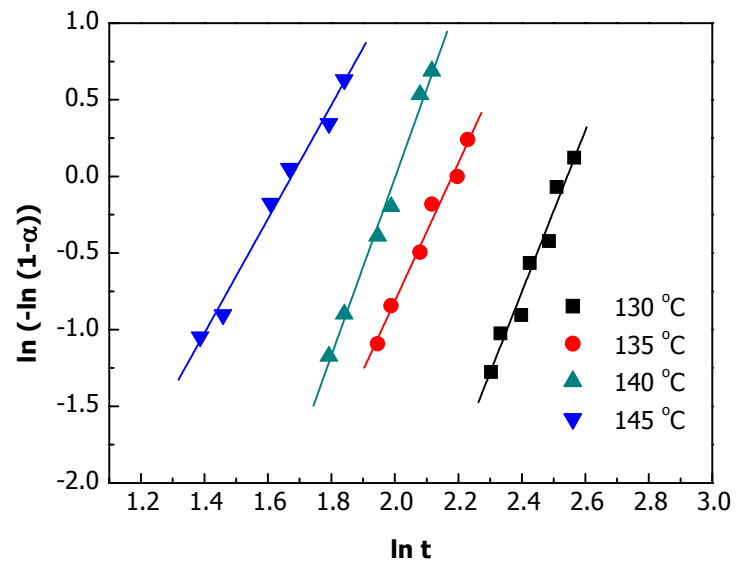


**Figure 4.27** The Avrami plot for  $\ln(-\ln(1-\alpha))$  against  $\ln t$  of analcime crystallization.

**Table 4.10** The Avrami exponent for analcime crystallization.

Temperature(°C)	130	135	140	145
n	5.3	4.2	6.4	3.4
R	0.98	0.99	0.99	0.99

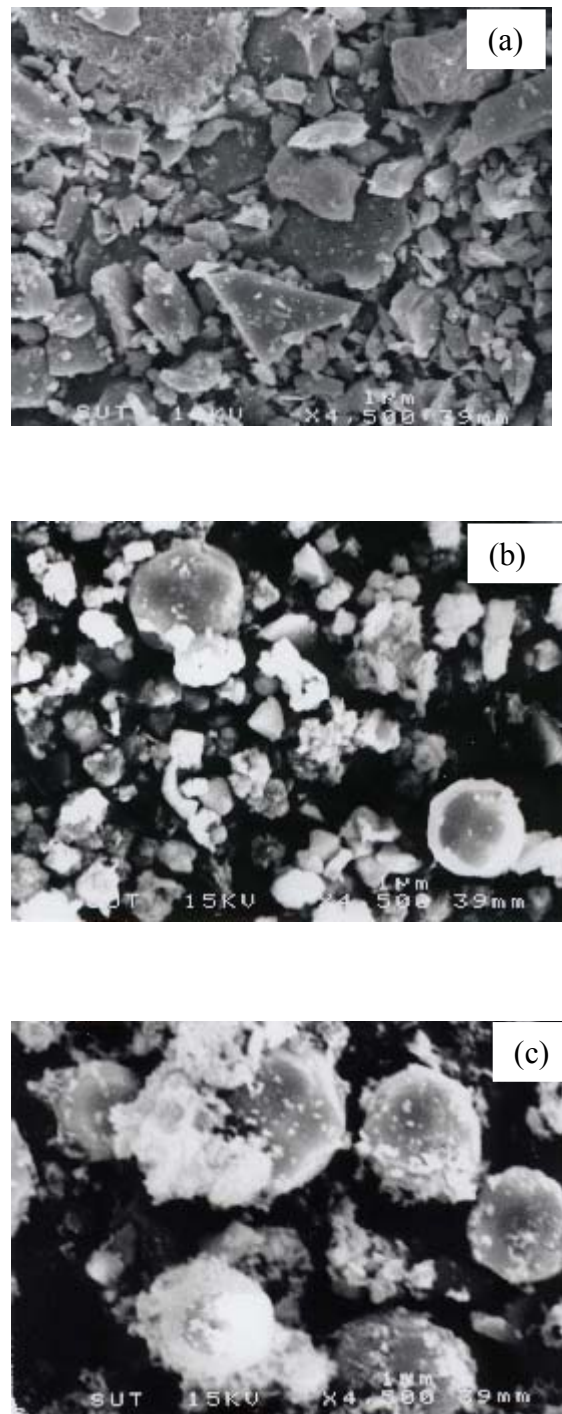


**Figure 4.28** SEM photographs of raw perlite and kinetics of crystallization of analcime obtained by varying crystallization periods at 140 °C. (a) raw perlite, (b) 6 hrs, (c) 8 hrs, (d) 10 hrs, (e) 14 hrs and (f) 24 hrs.

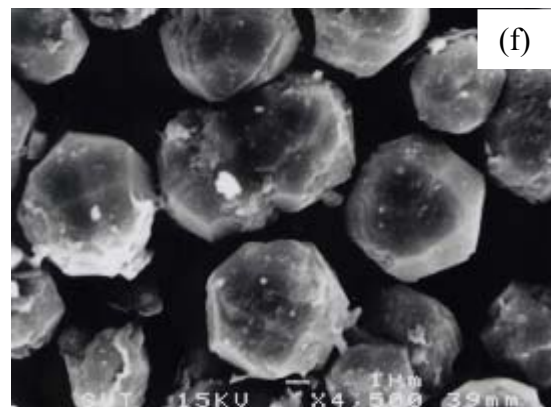
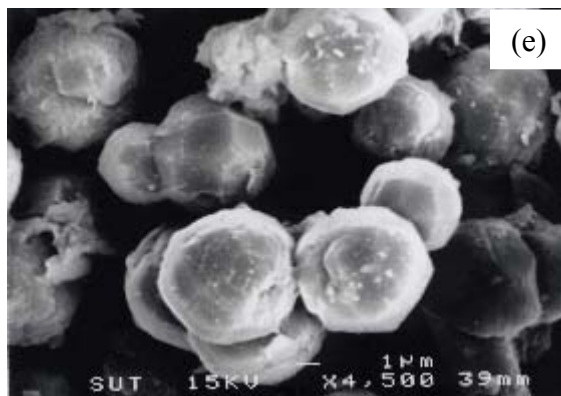
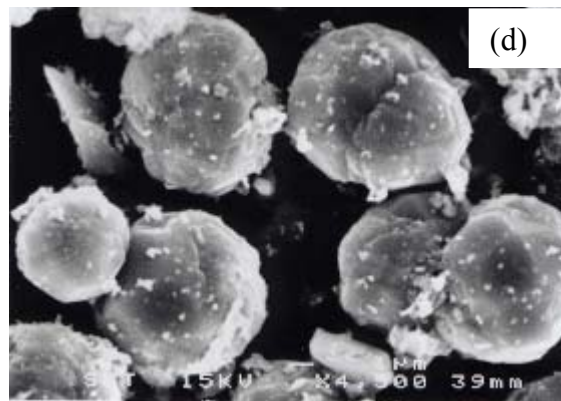
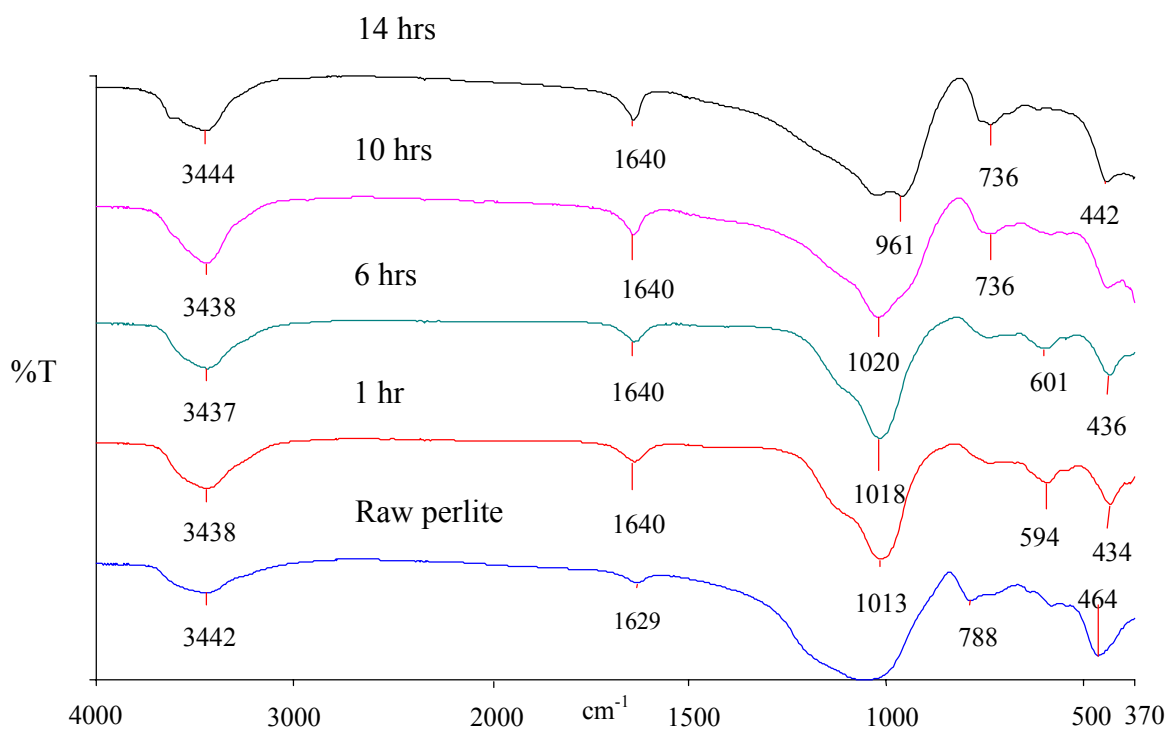


Figure 4.28 (continued)

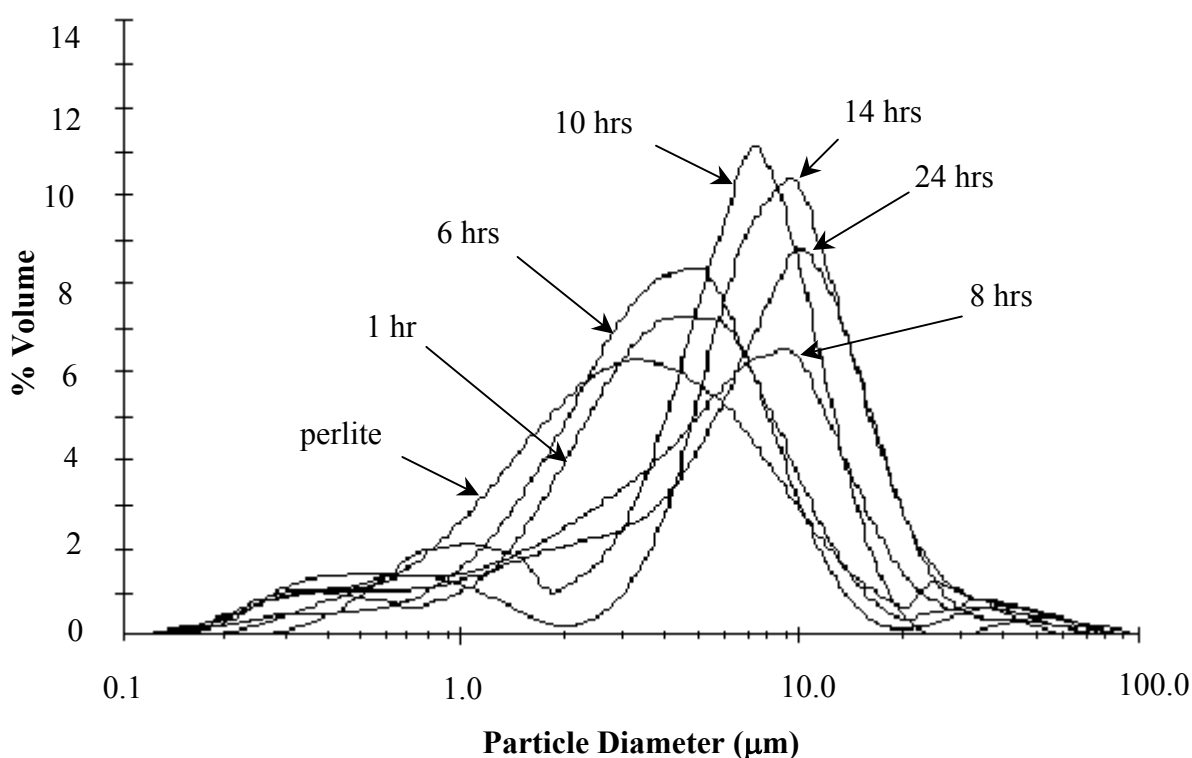
The corresponding SEM photographs of the analcime samples are shown in figure 4.28. The amorphous material gradually disappeared as the crystallization progressed and the amount of the crystalline phase increased. After 14 hours amorphous material disappeared completely which correlates to IR data (figure 4.29).



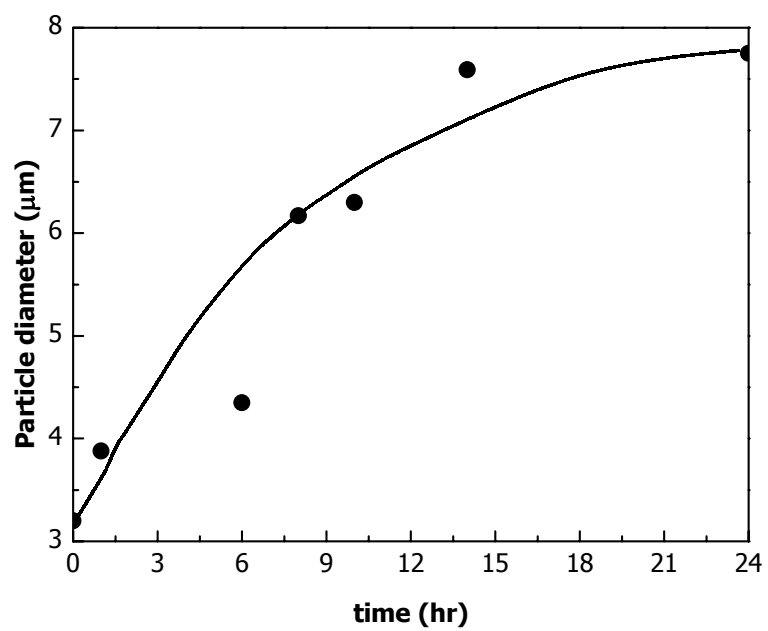
**Figure 4.29** FT-IR spectra of raw perlite and analcime samples obtained at different crystallization periods at 140 °C.

Figure 4.29 shows FT-IR spectra of raw perlite converted to analcime at crystallization periods of at 140 °C. The broad band of perlite at 1054  $\text{cm}^{-1}$  assigned to Si-O stretching of Si-O-Si shifted to the lower wave number according to the degree of crystallization of analcime. IR spectra of the glass perlite reflected only slightly

changes until the reaction time reached 14 hours correlates to XRD patterns (figure 4.22). The bands at  $1021\text{ cm}^{-1}$ ,  $736\text{ cm}^{-1}$ , and  $442\text{ cm}^{-1}$  indicates the complete crystalline structure of analcime. The particle size distribution depending on the crystallization periods are shown in figure 4.30. The average crystal sizes of the solid product at the synthesis periods of 1, 6, 8, 10, 14 and 24 hours were 3.2, 3.88, 4.35, 6.17, 6.3, 7.59 and 7.75  $\mu\text{m}$ , respectively (figure 4.31). The mean particle size gradually increased as the crystallization time increased which corresponds to previous studies (Ko and Ahn, 1999 and Cetin *et al.*, 2001).



**Figure 4.30** Particle size distribution of solid products at different crystallization periods at  $140\text{ }^{\circ}\text{C}$ .



**Figure 4.31** Plot of particle size distribution describing solid products at different crystallization periods at 140 °C.

## 4.5 Diffusion

The activity of filtrates for exchange diffusion of  $\text{Cu}^{2+}$ ,  $\text{Ni}^{2+}$ ,  $\text{Pb}^{2+}$  and  $\text{Zn}^{2+}$  into analcime synthesized from perlite at various temperatures and times is shown in tables 4.11 to 4.14. The  $W_t/W_\infty$  plots for the diffusion process are shown in figures 4.32 to 4.35. Plots of  $\ln D$  against  $1/T$  were of good linearity (figures 4.36 to 4.37).

**Table 4.11** Activity of filtrates for  $\text{Cu}^{2+}$  diffusion into analcime at various temperatures.

Time (min)	Activity of filtrates at various temperatures (cpm )		
	25 °C	40 °C	60 °C
15	62.03	76.77	94.77
30	65.55	85.46	111.13
60	74.10	96.91	138.49
120	85.95	86.04	145.41
240	93.68	119.03	180.11
360	101.41	131.61	215.11
900	120.33	153.93	224.25
1440	121.23	160.99	268.82

**Table 4.12** Activity of filtrates for Ni<sup>2+</sup> diffusion into analcime at various temperatures.

Time (min)	Activity of filtrates at various temperatures (cpm )		
	25 °C	40 °C	60 °C
15	50.81	57.69	66.80
30	54.09	59.88	82.70
60	56.07	68.88	89.25
120	60.85	74.73	116.63
240	67.98	83.63	138.17
360	70.59	94.35	155.65
900	83.05	109.91	205.23
1440	92.27	112.65	214.64

**Table 4.13** Activity of filtrates for Pb<sup>2+</sup> diffusion into analcime at various temperatures.

Time (min)	Activity of filtrates at various temperatures (cpm )		
	25 °C	40 °C	60 °C
15	75.15	87.96	107.32
30	77.78	72.77	129.72
60	82.39	102.34	176.97
120	91.21	110.05	151.41
240	103.53	128.02	188.51
360	107.19	149.23	246.48
900	128.05	153.05	347.98
1440	128.13	159.01	369.95

**Table 4.14** Activity of filtrates for  $Zn^{2+}$  diffusion into analcime at various temperatures.

Time (min)	Activity of filtrates at various temperatures (cpm )		
	25 °C	40 °C	60 °C
15	56.71	61.41	75.42
30	46.95	67.42	86.08
60	60.51	68.51	99.59
120	63.41	81.54	117.63
240	73.35	93.35	125.43
360	74.90	104.44	153.10
900	88.17	118.86	183.48
1440	94.16	128.93	275.53

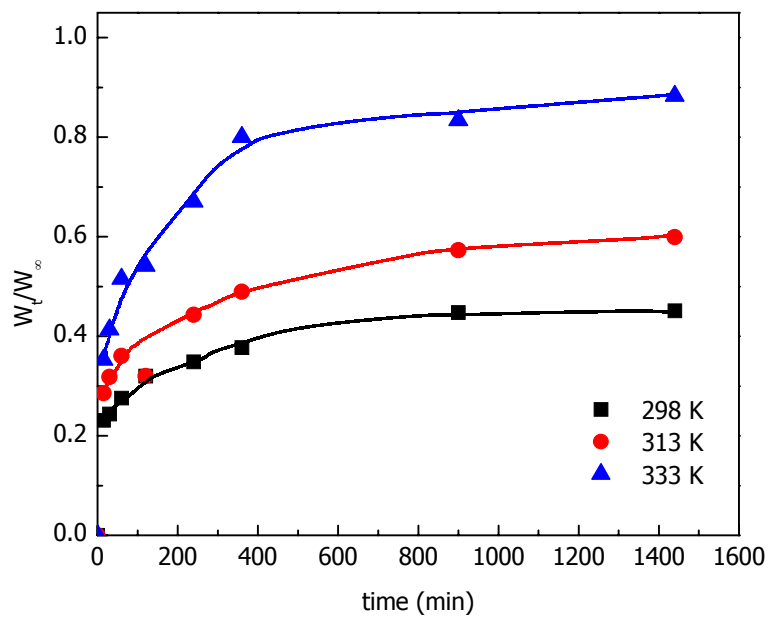


**Figure 4.32** Plots of  $W_t/W_\infty$  against time ( $t$ ) for  $\text{Na}/\frac{1}{2}\text{Cu}^{2+}$  exchange in analcime, in the range of 298-333 K.

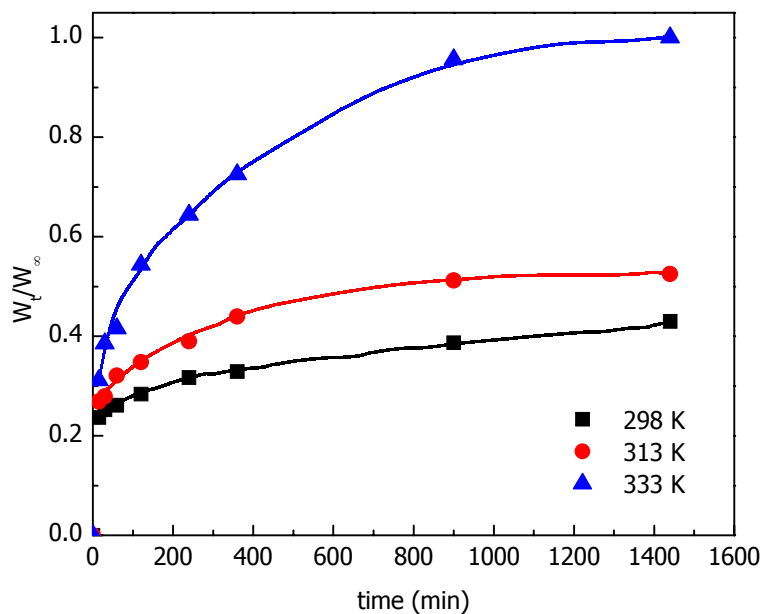


**Figure 4.33** Plots of  $W_t/W_\infty$  against time ( $t$ ) for  $\text{Na}/\frac{1}{2}\text{Ni}^{2+}$  exchange in analcime, in the range of 298-333 K.

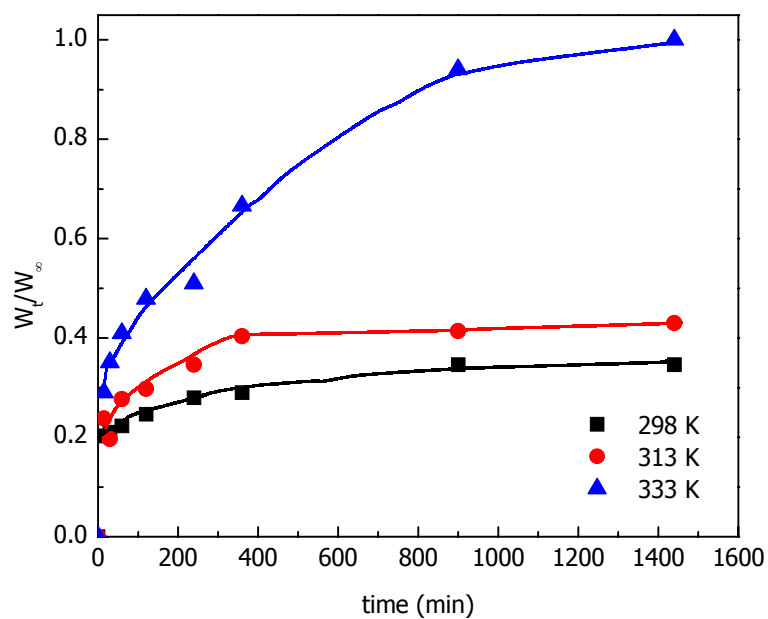


**Figure 4.34** Plots of  $W_t/W_\infty$  against time ( $t$ ) for  $\text{Na}/\frac{1}{2}\text{Pb}^{2+}$  exchange in analcime, in the range of 298-333 K.

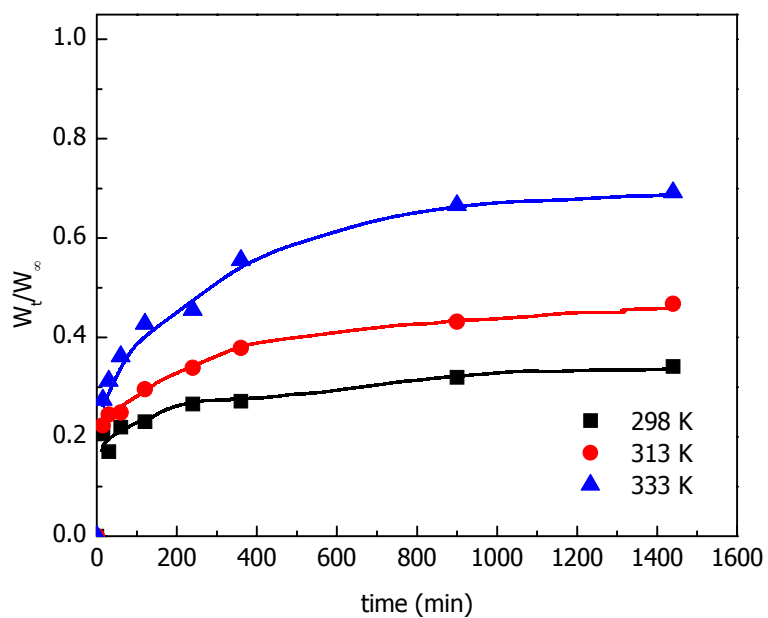


**Figure 4.35** Plots of  $W_t/W_\infty$  against time ( $t$ ) for  $\text{Na}/\frac{1}{2}\text{Zn}^{2+}$  exchange in analcime, in the range of 298-333 K.

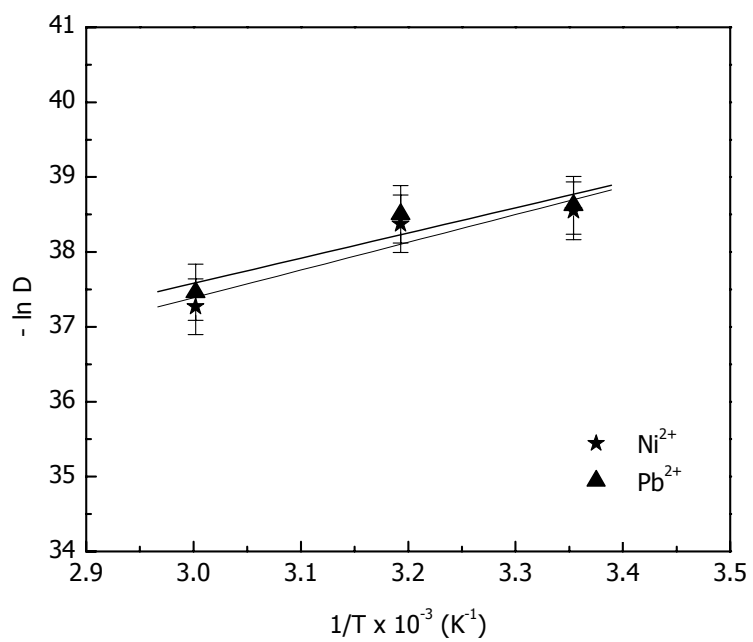


**Figure 4.36** Arrhenius plots for exchange diffusion of  $\text{Ni}^{2+}$  and  $\text{Pb}^{2+}$  in analcime, in the range 298-333 K.

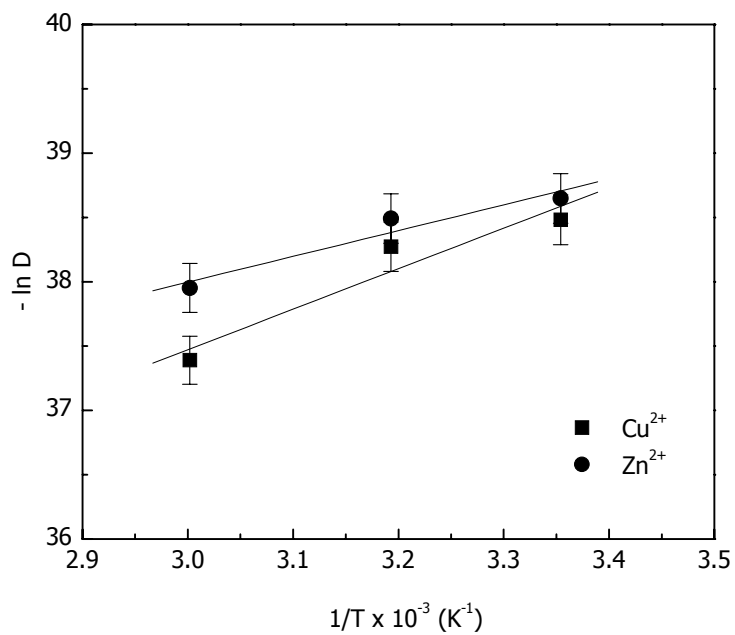


**Figure 4.37** Arrhenius plots for exchange diffusion of  $\text{Cu}^{2+}$  and  $\text{Zn}^{2+}$  in analcime, in the range 298-333 K.

In-going cations slightly affected XRD d-spacings in the fully exchanged analcimes, prepared separately, and also caused small changes in their intensities. The baselines of their XRD patterns, however, remained almost linear. Figure 4.38 shows a plot of percentage crystallinity against cation radius. The percentage of crystallinity was reduced by only 2-10% even though treatments were performed, several times, with a 0.5 M excess of in-going cations. This confirmed that the structure of analcime will remain unchanged during those diffusion studies carried out using 0.01M of in-going cation solutions.

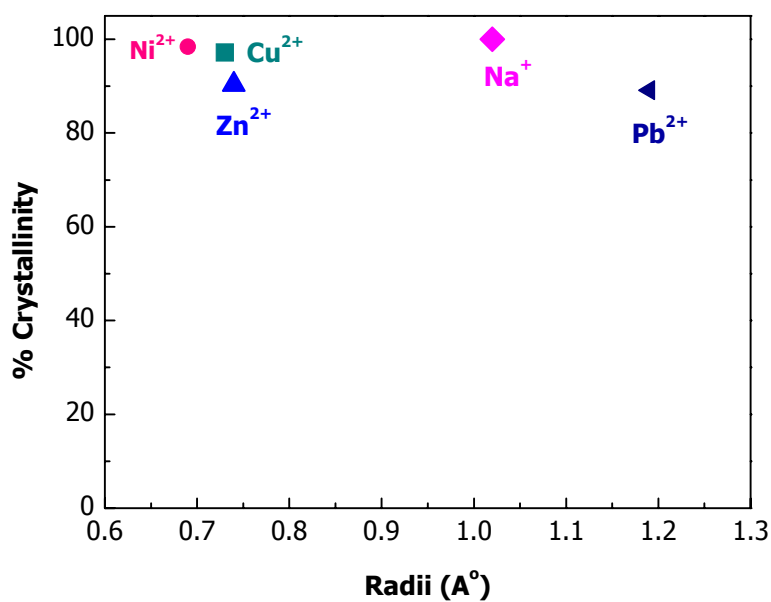


**Figure 4.38** Plot of percentage of crystallinity against cation radii for cation exchanged analcime.

Table 4.15 shows the thermodynamic parameters for the diffusion of cations into Na analcime at different temperatures. Exchange diffusion coefficients for  $\text{Cu}^{2+}$ ,  $\text{Ni}^{2+}$ ,  $\text{Pb}^{2+}$  and  $\text{Zn}^{2+}$  in analcime are of the order of  $10^{-17} \text{ m}^2\text{s}^{-1}$ . This is consistent with previous work that found sodium and potassium self-diffusion coefficients in analcime to be  $10^{-16}$  to  $10^{-17} \text{ m}^2\text{s}^{-1}$  at 293 K (Yusof, 1984).

The free energies of exchange suggest that similar processes are being followed for the different cations and, again, are of the same order of magnitude as those measured for  $\text{Na}^+$  and  $\text{K}^+$  self-diffusion in analcime (Dyer and Yusof, 1987).

**Table 4.15** Thermodynamic parameters for the diffusion of cations into Na-analcime.

Cation	Temperature (K)	$E_a$ (kJ mol <sup>-1</sup> )	$\Delta S^*$ (JK <sup>-1</sup> mol <sup>-1</sup> )	$\Delta H^*$ (kJ mol <sup>-1</sup> )	$\Delta G^*$ (kJ mol <sup>-1</sup> )
$\text{Cu}^{2+}$	298		-136		64.5
	313	26.2	-137	23.7	66.6
	333		-138		69.3
$\text{Ni}^{2+}$	298		-122		64.5
	313	30.8	-123	28.3	66.6
	333		-124		69.3
$\text{Pb}^{2+}$	298		-132		65.0
	313	28	-133	25.4	66.0
	333		-134		69.6
$\text{Zn}^{2+}$	298		-169		64.8
	313	17	-170	14.2	67.4
	333		-171		70.8

Values for the energies of activation for the cation exchanges follow the series  $\text{Zn} < \text{Cu} < \text{Pb} < \text{Ni}$ , and recourse to figure 4.39 shows that the value recorded for lead is

lower than expected from its bare ion size. This reflects the polarisability of the  $\text{Pb}^{2+}$  cation, i.e. it can “squeeze” into the narrow analcime channels more readily than would be expected from its size. The order of the activation energies for the other cations follows that of bare cation size, coupled with d electron shells, so it seems that the waters of hydration are lost prior to migration into the analcime structure. This is reflected in the high negative entropy values concomitant with release of water molecules from cation hydration spheres, with  $\text{Zn}^{2+}$  being the most hydrated cation and having no outer d electrons, showing the most negative entropy change.

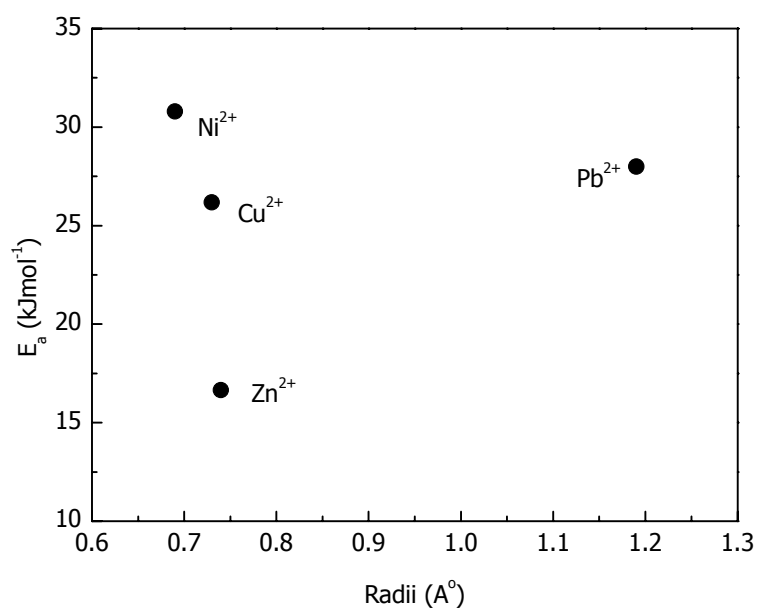


**Figure 4.39** Plot of the activation energy ( $E_a$ ) against cation radii for diffusion processes.

The activation energies are, in general, lower than those encountered by sodium and potassium cations as they move through the analcime structure, which is in accord with their larger and less hydrated cations. Similarly entropy changes for sodium and potassium self-diffusion processes in analcime are less negative than those measured herein. The extents of exchange seen in figures 4.32 to 4.35 suggest that all exchange sites in analcime structure are available to the in-going cations, in the temperature range studied, apart from when zinc is considered. It seems that, up to 333 K, only sites in 2 of the 3 channels are taken up by zinc. This may arise from a size restriction caused by zinc moving as a partially hydrated cation thus hindering its progress into the smallest channel of the analcime structure.

Comparison to thermodynamic diffusional parameters measured for cation exchanges in clinoptilolite (Dyer and White, 1999), using the BBK equation, show that exchanges in this zeolite are more facile ( $\Delta G^* = 29-48 \text{ kJ mole}^{-1}$  for Na/NH<sub>4</sub>, K/Na, and Na/1/2 Ca ion pairs). Energy barriers fall in the range 17 to 42 kJ mole<sup>-1</sup>, and changes in entropy are much lower than those measured here, as expected from relatively unhydrated cations moving through the clinoptilolite framework.

## 4.5 Ion exchange

After the equilibrium time, ion exchange isotherms were checked for their activity of filtrates (cpm) by a liquid scintillation counter (LSC) which was used to calculate the thermodynamic parameters. The activity of filtrates for  $\text{Cu}^{2+}$ ,  $\text{Pb}^{2+}$ ,  $\text{Ni}^{2+}$  and  $\text{Zn}^{2+}$  in analcime at various temperatures is shown in tables 4.16 to 4.19.

**Table 4.16** Activity of filtrates for  $\text{Cu}^{2+}$  exchanged by Na analcime.

Volume of solution (ml)		Activity of filtrates at various temperatures (cpm)		
$\text{Cu}^{2+}$	$\text{NaNO}_3$	25 °C	40 °C	60 °C
20	0	63.81	77.65	92.41
19	1	88.09	97.22	113.82
18	2	110.65	122.19	145.34
16	4	147.05	171.69	182.88
14	6	207.81	208.93	199.09
12	8	251.25	210.84	267.78
10	10	287.99	293.63	295.01
8	12	333.30	329.57	338.48
6	14	365.84	356.32	368.97
4	16	398.32	393.29	389.95
2	18	425.21	403.29	404.97
1	19	438.60	419.61	423.01
0	20	450.11	450.11	450.11

**Table 4.17** Activity of filtrates for  $\text{Pb}^{2+}$  exchanged by Na analcime.

Volume of solution (ml)		Activity of filtrates at various temperatures (cpm)		
$\text{Pb}^{2+}$	$\text{NaNO}_3$	25 °C	40 °C	60 °C
20	0	63.91	89.88	122.43
19	1	84.02	95.70	135.45
18	2	112.71	130.56	160.45
16	4	156.84	173.55	197.75
14	6	204.00	222.17	201.09
12	8	240.26	259.09	268.39
10	10	283.13	306.29	302.17
8	12	326.43	339.47	318.91
6	14	349.65	369.95	322.00
4	16	374.87	410.25	399.62
2	18	393.91	419.75	404.89
1	19	422.13	433.51	412.19
0	20	450.11	450.11	450.11

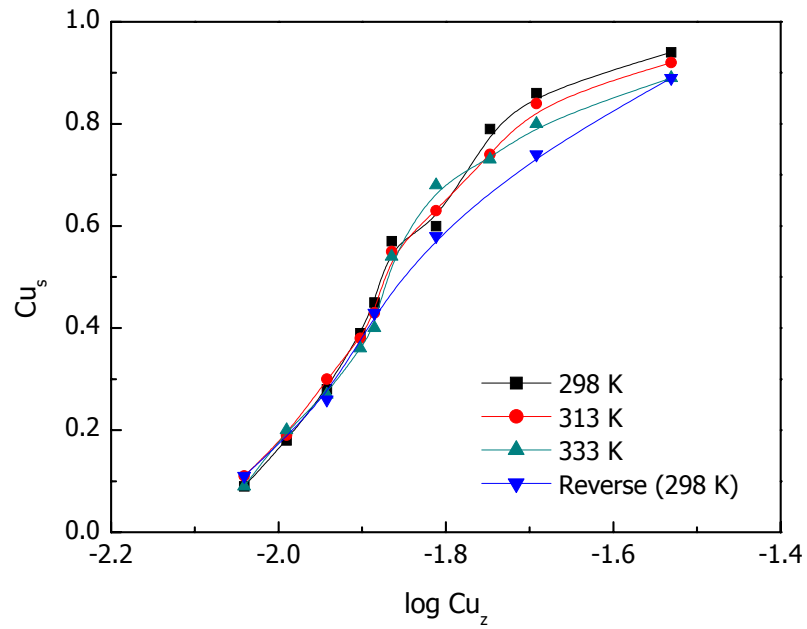
**Table 4.18** Activity of filtrates for  $\text{Ni}^{2+}$  exchanged by Na analcime.

Volume of solution (ml)		Activity of filtrates at various temperatures (cpm)		
$\text{Ni}^{2+}$	$\text{NaNO}_3$	25 °C	40°C	60 °C
20	0	51.89	61.47	86.85
19	1	75.21	81.78	107.35
18	2	100.40	111.19	127.75
16	4	147.65	157.86	167.07
14	6	194.75	201.18	217.04
12	8	236.91	221.03	258.53
10	10	280.75	286.67	288.25
8	12	322.17	323.20	299.08
6	14	363.33	350.31	366.27
4	16	389.35	361.92	389.75
2	18	421.01	397.12	406.95
1	19	432.84	420.54	426.08
0	20	450.11	450.11	450.11

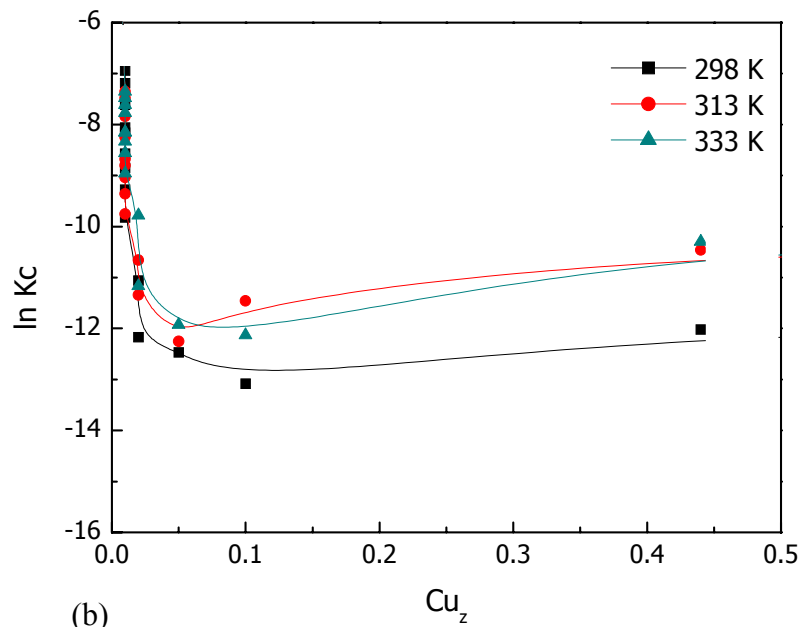
**Table 4.19** Activity of filtrates for Zn<sup>2+</sup> exchanged by Na analcime.

Volume of solution (ml)		Activity of filtrates at various temperatures (cpm)		
Zn <sup>2+</sup>	NaNO <sub>3</sub>	25 °C	40 °C	60 °C
20	0	47.70	68.31	104.14
19	1	70.24	89.54	121.29
18	2	94.79	118.27	146.15
16	4	149.22	153.65	188.21
14	6	190.49	212.96	230.29
12	8	236.96	253.37	266.50
10	10	271.87	288.19	303.63
8	12	311.23	293.77	348.56
6	14	347.38	361.21	376.59
4	16	364.97	389.22	390.73
2	18	373.87	406.99	415.96
1	19	403.51	424.49	426.76
0	20	450.11	450.11	450.11

The ion exchange isotherm for Na<sup>+</sup> with four heavy metal ions exchanged in Na analcime and their Kielland plots of  $\ln K_c$  against  $A_z$  are shown in figures 4.40 to 4.43. Changes in isotherm shape are small illustrative of the absence of exchange sites of differing energy. They also show good reversibility.



(a)



(b)

**Figure 4.40** Ion exchange isotherm for  $\text{Na}^+ \leftrightarrow 1/2\text{Cu}^{2+}$  exchange in analcime at

$T_N = 0.01\text{N}$  (a). and their Kielland plots (b).

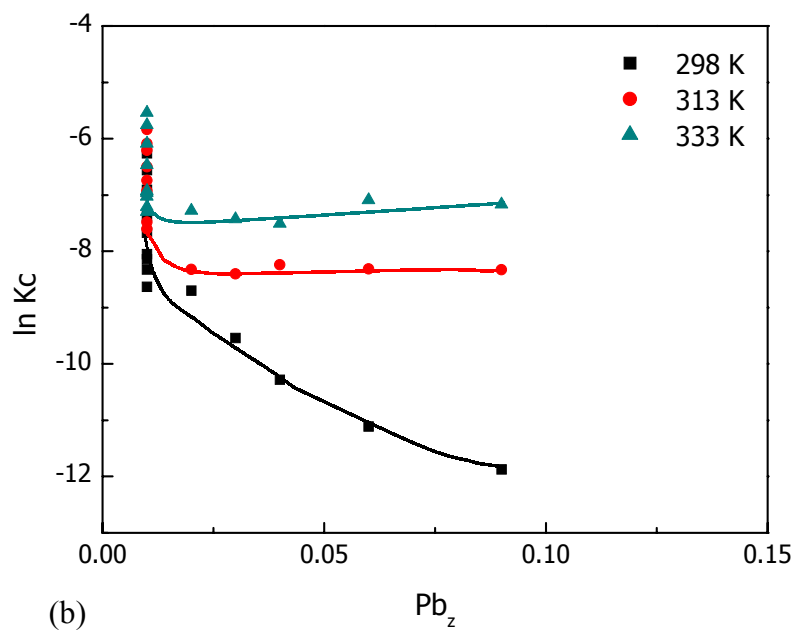
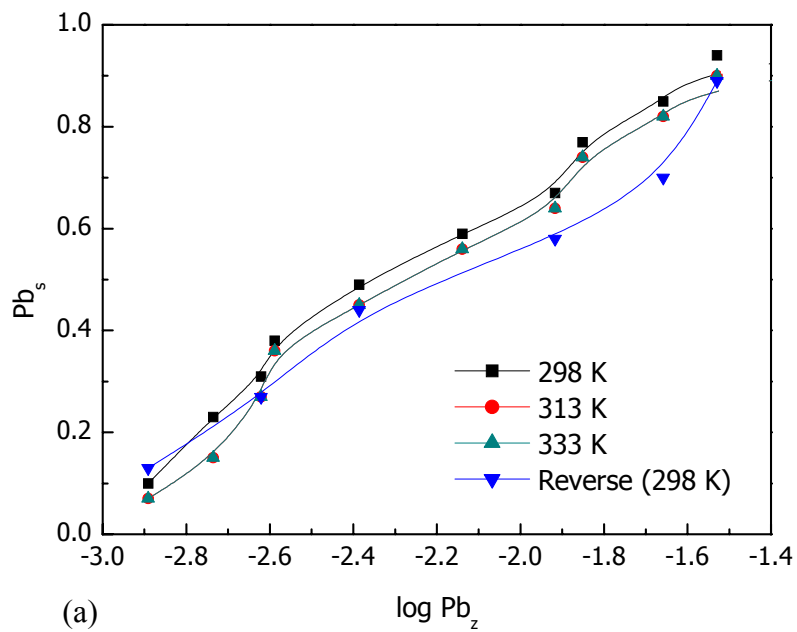
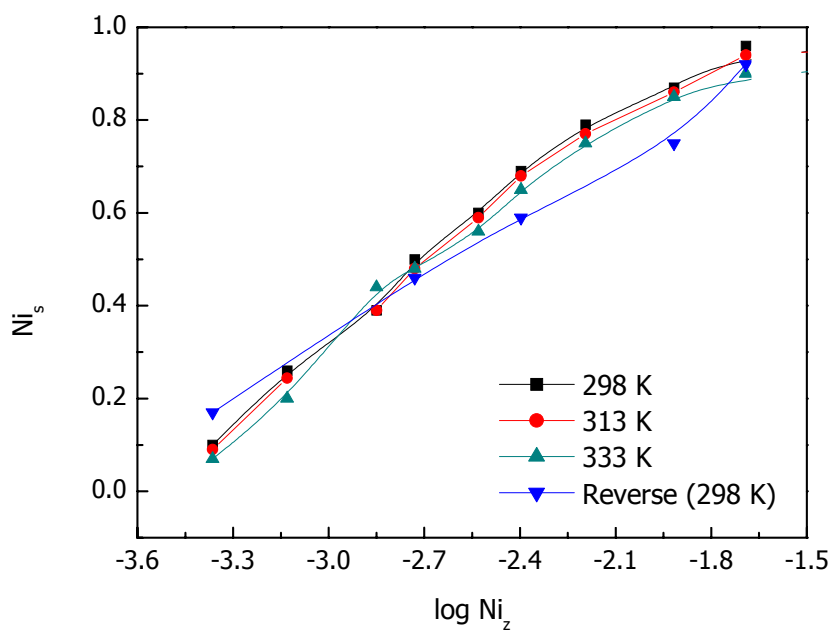
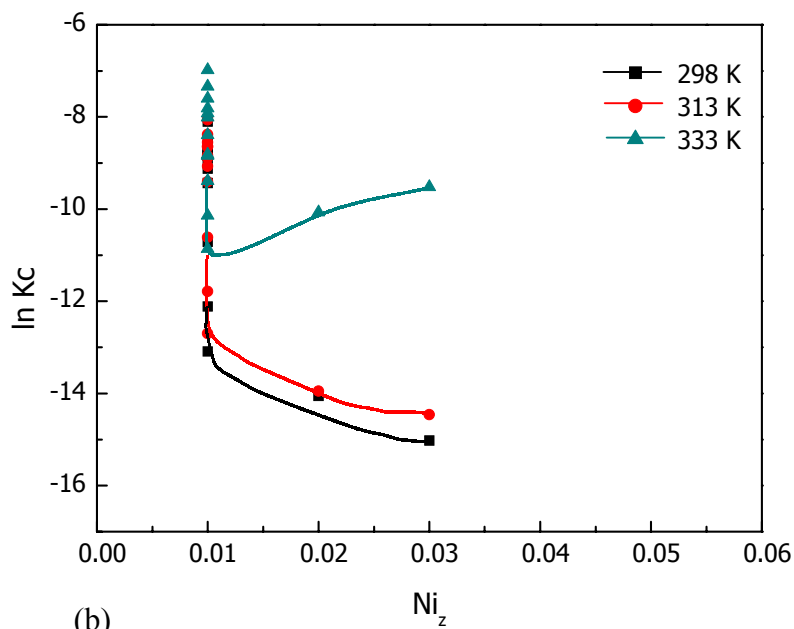


**Figure 4.41** Ion exchange isotherm for  $\text{Na}^+ \leftrightarrow 1/2\text{Pb}^{2+}$  exchange in analcime at  $T_N = 0.01\text{N}$  (a). and their Kielland plots (b).



(a)



(b)

**Figure 4.42** Ion exchange isotherm for  $\text{Na}^+ \leftrightarrow 1/2\text{Ni}^{2+}$  exchange in analcime at

$T_N = 0.01\text{N}$  (a). and their Kielland plots (b).

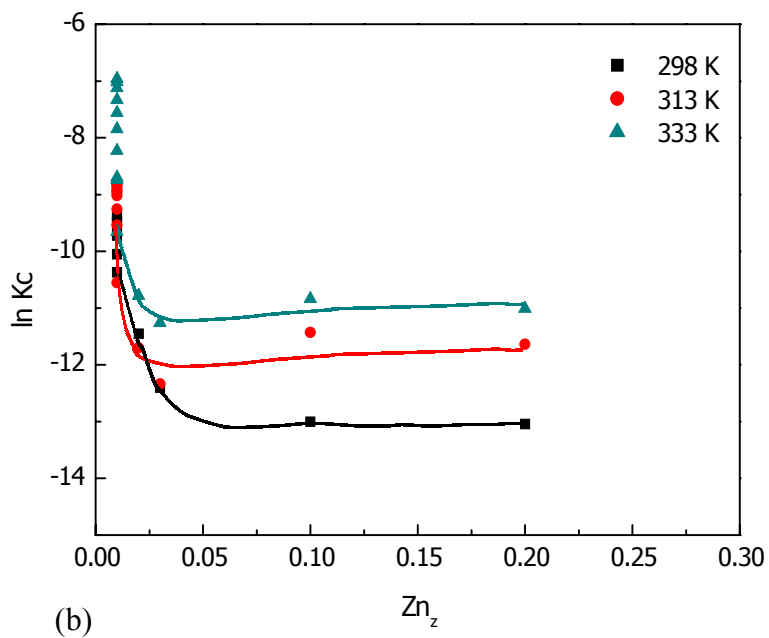
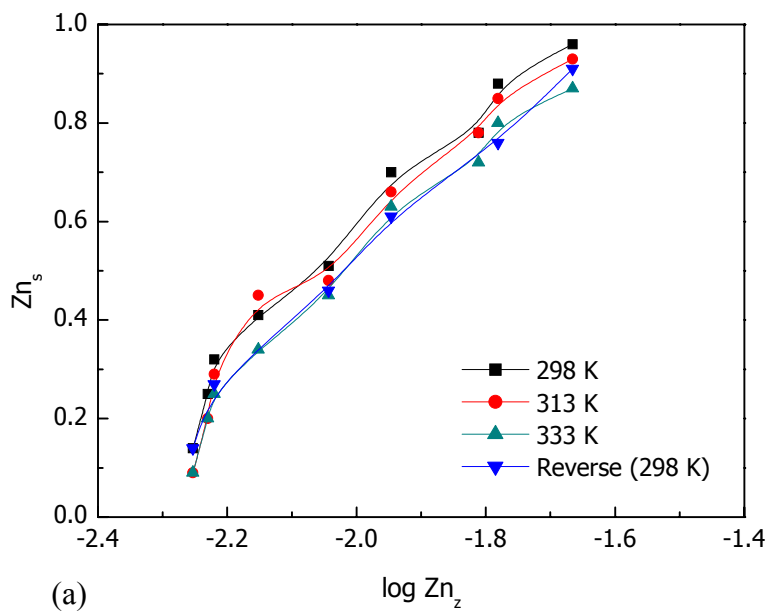


**Figure 4.43** Ion exchange isotherm for  $\text{Na}^+ \leftrightarrow 1/2\text{Zn}^{2+}$  exchange in analcime at  $T_N = 0.01N$  (a). and their Kielland plots (b).

The  $\Delta G^\circ$  values (table 4.20) enable the construction of a cation selectivity series, which shows that the cation exchange selectivities of the analcime synthesized from natural Thai perlite for the cations studied was;  $\text{Pb}^{2+} > \text{Cu}^{2+} > \text{Zn}^{2+} > \text{Ni}^{2+}$ .  $\text{Pb}^{2+}$  had the lowest  $\Delta G^\circ$  value despite its large radii, which is a reflection of its ease of polarisability coupled with the lowest enthalpy of cation hydration,  $-1480 \text{ kJ mol}^{-1}$  (Wulfsberg, 2000), among the cations considered. This result corresponds to that of Ahmed *et al.*, who reported that ions with low charge densities are present in a less hydrated environment and so interact more strongly with the zeolite framework (Ahmed *et al.*, 1998). In addition, Barrer and coworkers (1979) also found that the larger, less strongly hydrated, cations tend to concentrate in the zeolite in contrast to the smaller ions, which tend to remain in solution.

Analcime has less preference for the smaller  $\text{Ni}^{2+}$  cation with its stronger ability to hold water molecules around it as shown by its high enthalpy of hydration ( $-2106 \text{ kJ mol}^{-1}$ , (Wulfsberg, 2000)) compared with the other three in-going cations

Contributions to  $\Delta S^\circ$  values come from changes in the degree of cation solvation of ions sited in the aqueous and solid phases (Barrer *et al.*, 1968). Entropy changes (table 4.20) thus are related to changes in water content created during the exchange. These changes arise when cations with differing hydration spheres move between the solution and solid phases (Yoder and Weir, 1960). In addition, Barrer *et al.* (1968) reported that positive entropy changes occur when divalent ions in solution displace two monovalent ions in zeolite phase. The negative entropy changes observed here for  $\text{Cu}^{2+}$ ,  $\text{Pb}^{2+}$ ,  $\text{Ni}^{2+}$  and  $\text{Zn}^{2+}$ , as they exchange for  $\text{Na}^+$ , arise from the release of waters of hydration from of these cations from their tightly bound hydration sphere as they move from solid to solution phase to replace the relatively unhydrated sodium

cation. This will be enhanced by the replacement of two sodium cations for the zeolite phase by the in-going divalent metal cations (Dyer and Zubair, 1998).

**Table 4.20** Thermodynamic parameters for Na<sup>+</sup>/heavy metal ions exchange in analcime at various temperatures.

In-going Cation	T (K)	K <sub>a</sub>	ΔG <sup>o</sup> (kJ mol <sup>-1</sup> )	ΔH <sup>o</sup> (kJ mol <sup>-1</sup> )	ΔS <sup>o</sup> (JK <sup>-1</sup> mol <sup>-1</sup> )
Cu <sup>2+</sup>	298	2.0 x 10 <sup>-6</sup>	16.3	11.7	-15.4
	313	6.2 x 10 <sup>-6</sup>	14.9		-10.2
	333	6.6 x 10 <sup>-6</sup>	14.8		-9.3
Ni <sup>2+</sup>	298	1.1 x 10 <sup>-7</sup>	19.9	53.9	-114.1
	313	1.7 x 10 <sup>-7</sup>	19.3		-110.5
	333	1.9 x 10 <sup>-5</sup>	13.5		-121.3
Pb <sup>2+</sup>	298	3.3 x 10 <sup>-6</sup>	15.7	37.2	-72.2
	313	9.5 x 10 <sup>-5</sup>	11.5		-82.1
	333	1.4 x 10 <sup>-4</sup>	11.0		-78.7
Zn <sup>2+</sup>	298	2.5 x 10 <sup>-7</sup>	18.9	33.8	-50.0
	313	3.4 x 10 <sup>-6</sup>	15.6		-58.1
	333	7.2 x 10 <sup>-6</sup>	14.7		-57.4

Table 4.21 lists selectivity series for other zeolites for the cations under study. They are seen to be broadly similar despite variations in zeolite structure and Si/Al ratio. The relatively poor removal of Ni<sup>2+</sup> by zeolites has been ascribed by Sherry (1969) to the high stability of its aqueous complex. Cu<sup>2+</sup> and Zn<sup>2+</sup> cations slightly differ in the order of their replacement (Ouki *et al.*, 1997, Mondele *et al.*, 1995 and Semmens and Seyforth, 1976) in chabazite and clinoptilolite. This may be because

both the zeolite samples examined in the references cited are natural zeolites of sedimentary origin, with high Si/Al frameworks.

**Table 4.21** Comparison selectivity series for ion exchange of heavy metals in this work to other works.

Zeolites	Selectivity series	References
Analcime	Pb>Cu>Zn>Ni	This work
Mordenite	Cu>Zn>Ni	Barrer and Townsend, 1975
Clinoptiolite	Pb>Zn≥Cu Pb>Cu>Zn>Ni Pb>Zn≥Cu>>Ni	Semmens and Seyforth, 1976 Ouki <i>et al.</i> , 1997 Mondele <i>et al.</i> , 1995
Chabazite	Pb>Zn>Cu>Ni	Ouki <i>et al.</i> , 1997
Linde X	Cu>Zn>Ni	Maes and Cremers, 1975
Linde Y	Cu>Zn>Ni Pb>Cu>Ni	Maes and Cremers, 1975 Joshi <i>et al.</i> , 2000
Zeolite Na-Pc	Pb>Zn>Ni	Moirou <i>et al.</i> , 2000

Exchanges of Na<sup>+</sup> by Cu<sup>2+</sup>, Pb<sup>2+</sup>, Ni<sup>2+</sup> and Zn<sup>2+</sup> are endothermic. Figure 4.43 plots  $\Delta G^{\circ}$  values against  $\Delta H^{\circ}_{\text{hyd}}$  for Na<sup>+</sup> exchanges with Pb<sup>2+</sup>, Cu<sup>2+</sup>, Zn<sup>2+</sup> and Ni<sup>2+</sup>. Unfortunately,  $\Delta G^{\circ}$  values of K<sup>+</sup>, Rb<sup>+</sup>, Cs<sup>+</sup>, Tl<sup>+</sup>, Mg<sup>2+</sup> and Co<sup>2+</sup> for ion exchange in Na-analcime have never been reported. When their  $\Delta H^{\circ}_{\text{hyd}}$  values are plotted as in figure 4.44, it can be seen that Mg<sup>2+</sup> and Co<sup>2+</sup> exchange in Na-analcime can be expected to be very low as experienced by Balgord and Roy (1971). On the other hand, when the hydration energies of K<sup>+</sup> (-321 kJ mol<sup>-1</sup>), Rb<sup>+</sup> (-296 kJ mol<sup>-1</sup>), Cs<sup>+</sup> (-263 kJ mol<sup>-1</sup>), and Tl<sup>+</sup> (-326 kJ mol<sup>-1</sup> (Wulfsberg, 2000)) are compared to that of Na<sup>+</sup> (-405

$\text{kJ mol}^{-1}$ ), full exchange into analcime is observed (Barrer and Hinds, 1953 and Barrer and Sammon, 1961), as expected from figure 4.44.

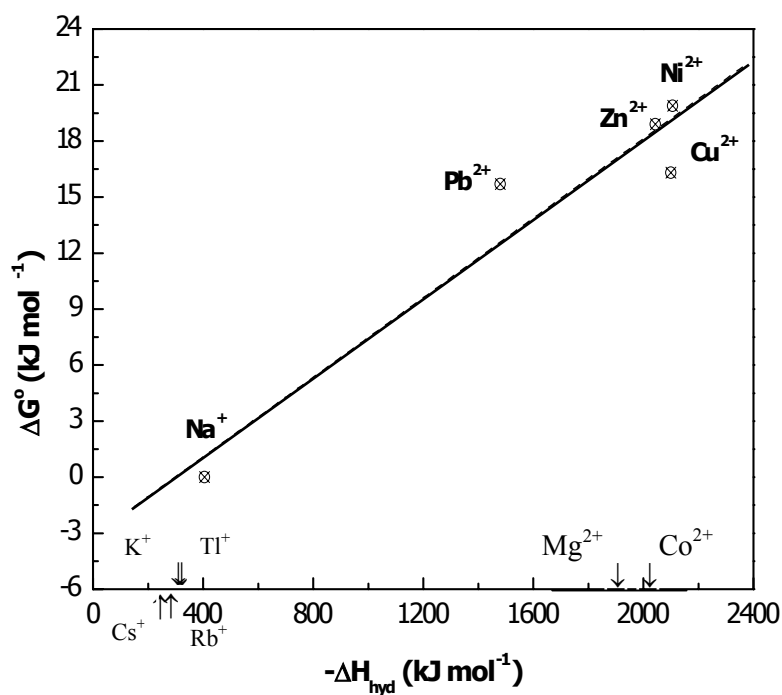


**Figure 4.44** Plots of  $\Delta G^\circ$  ( $\text{kJ mol}^{-1}$ ) against  $\Delta H_{\text{hyd}}$  ( $\text{kJ mol}^{-1}$ ) for  $\text{Na}^+$  with  $\text{Cu}^{2+}$ ,  $\text{Ni}^{2+}$ ,  $\text{Pb}^{2+}$  and  $\text{Zn}^{2+}$  exchange in analcime at 298 K.

Figure 4.45 represents the XRD diffractogram of the parent analcime and the solid products of ion exchange. After exchange treatments were performed the XRD pattern remained unchanged.

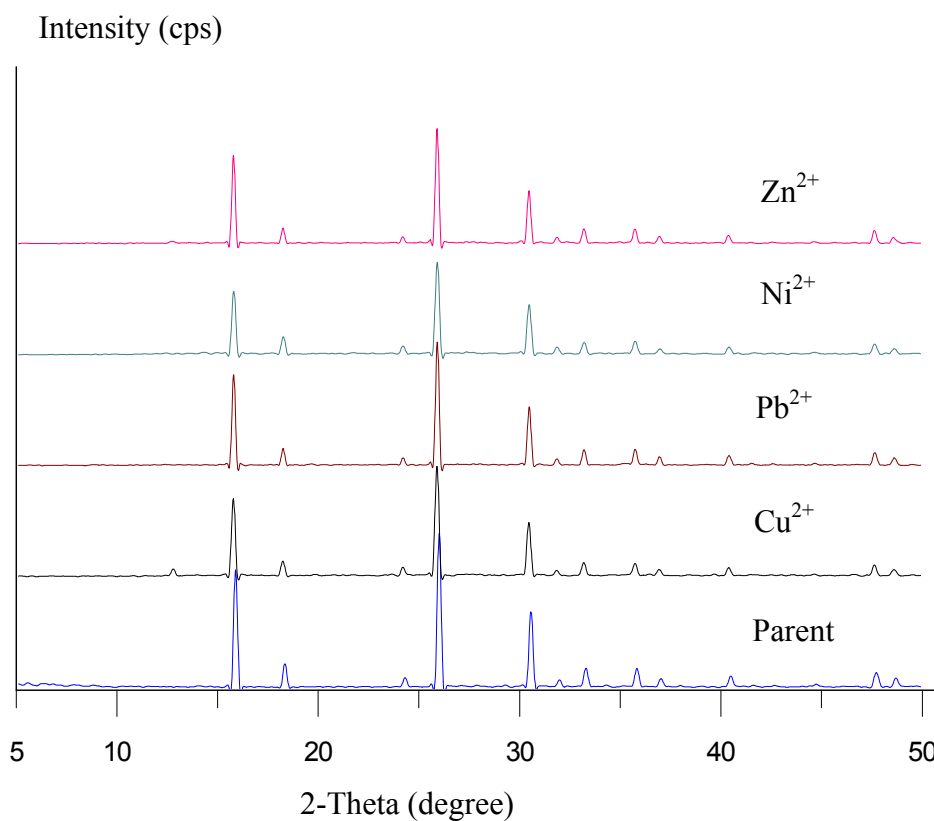


**Figure 4.45** XRD diffractogram of the parent analcime and the solid products of ion exchange.

The pattern obtained from the TGA thermograms indicated loss of weight in samples due to the exclusion of water as shown in figure 4.46. The TGA result correlated to DTA with weight loss at about 150 °C to 400 °C. Loss of water of the

parent analcime and  $\text{Cu}^{2+}$ ,  $\text{Pb}^{2+}$ ,  $\text{Ni}^{2+}$  and  $\text{Zn}^{2+}$  are very similar, the percentage of water loss being found to be from 8.5 to 9.

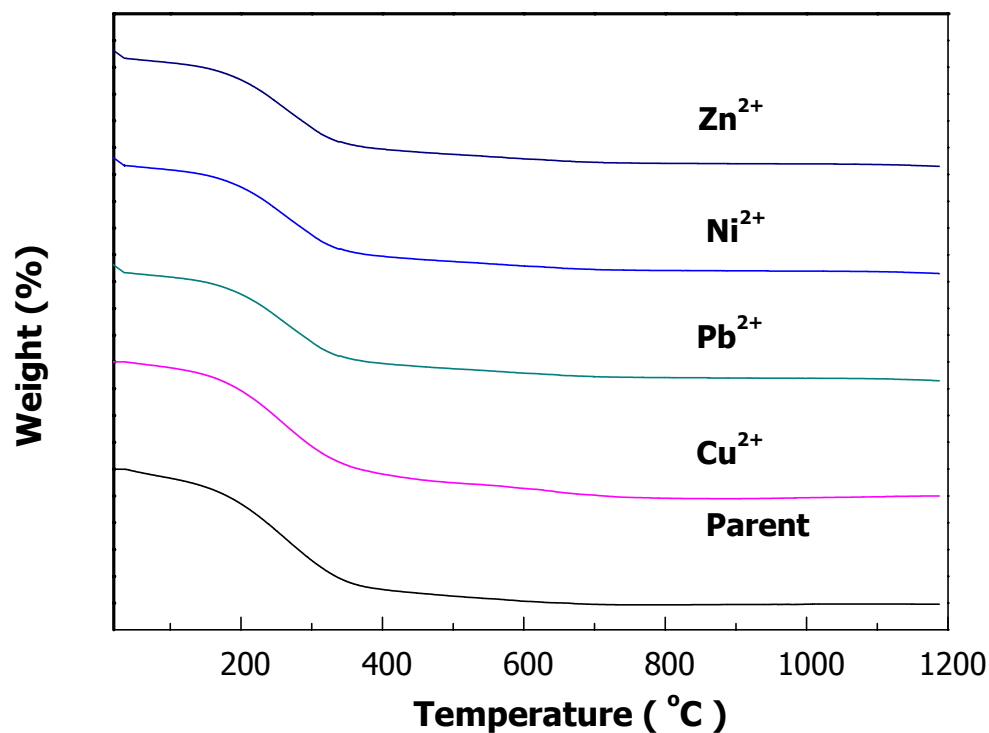


**Figure 4.46** TGA curves for the parent analcime and the solid products of ion exchange.

The DTA curves of the analcime parent and analcime with other ions are shown in figure 4.47. The broad endothermic of analcime with other ions decreases from the analcime parent which may be due to the interaction of water in zeolite with cation. The broad band at about 150 °C to 400 °C was ascribed to the loss of adsorbed water. The large broad endothermic around 1000 °C is due to the zeolite structure. The

stability of the analcime structure depends on the amount of cation occupying the zeolite framework. This result reflects that the broad endothermic of analcime parent is less stable than analcime with other ions, where the maximum peak shift varies with the interaction of analcime with cation.

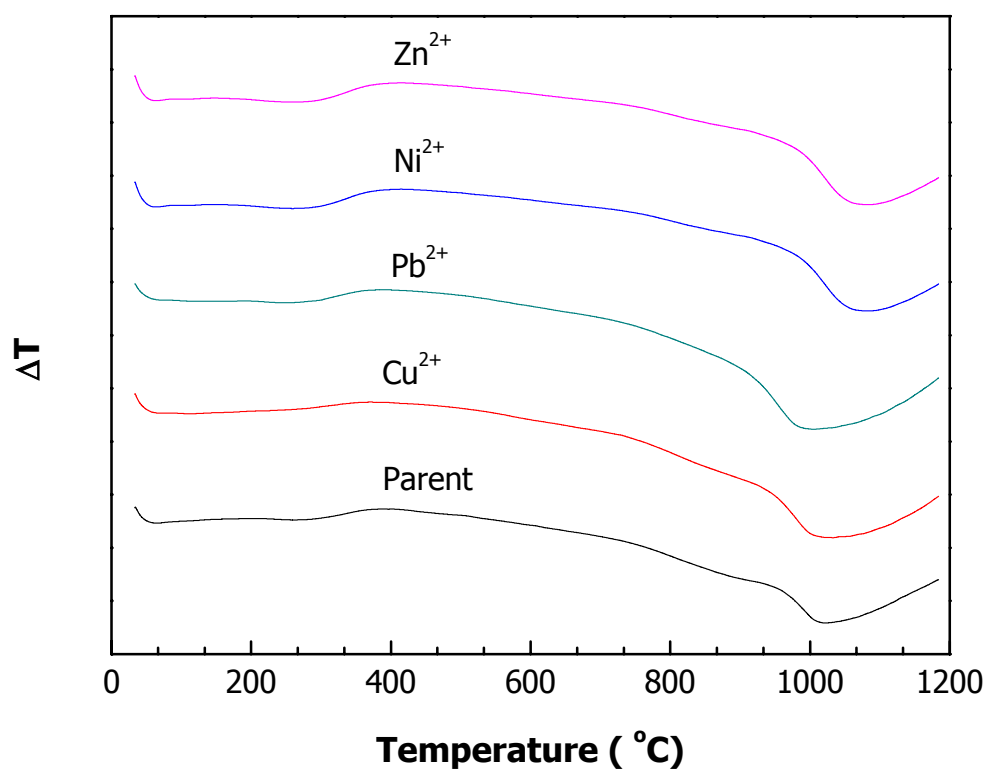


**Figure 4.47** Differential thermal analysis curves for the parent analcime and the solid products of ion exchange.

## Chapter V

### Conclusion

Raw perlite collected from Lopburi Province in Central Thailand was first characterized to overview its characteristics and properties before being used as starting the material. The zeolite crystallization from perlite was studied under the conditions, such as the concentration of alkalinity (1 to 3 M NaOH), the reaction temperatures (100 °C to 140 °C), the reaction times (1 to 7 days) and the solid/liquid ratios (1:5 to 1:20), in a 500 ml high pressure/high temperature stirred reactor (Parr Instrument). The results showed that at 100 °C and 20 psi the perlite prefers to convert to zeolite Na-P1, while at 100-140 °C and 20-50 psi the major zeolite product obtained was analcime. Under the influence of 3 M NaOH and 1:5 solid/liquid ratio at 140 °C for 24 hrs, perlite was mainly converted to analcime. Cancrinite favored formation with 3 M NaOH and 1:20 solid/liquid ratio at 140 °C.

Since the analcime was the major product under the studied conditions, therefore it was selected for further study on the crystallization kinetics. Additionally, the physical and chemical properties of analcime were determined. It was found that the surface area, particle size, Si/Al ( $^{29}\text{Si}$  MAS NMR) and CEC was  $18.92 \text{ m}^2\text{g}^{-1}$ ,  $7.75 \mu\text{m}$ , 1.97 and  $4.16 \text{ meqg}^{-1}$ , respectively. Next, the diffusion kinetics and the ion exchange of  $\text{Cu}^{2+}$ ,  $\text{Ni}^{2+}$ ,  $\text{Pb}^{2+}$  and  $\text{Zn}^{2+}$  into analcime were determined.

The kinetics of analcime was studied at different temperatures. It was found that the rate of crystallization increases with increasing reaction temperatures. The

activation energy was found to be  $11.2 \text{ kcal mol}^{-1}$ ; this value can be connected with the dehydration of silicate and aluminate ion in solution to form crystal building and condensation reaction between the crystal surfaces. The Avrami exponent ( $n$ ) was obtained in the range of 3.4 to 6.4 which reflected that the reaction is governed by autocatalytic nucleation and crystallization.

The diffusion exchange of  $\text{Cu}^{2+}$ ,  $\text{Ni}^{2+}$ ,  $\text{Pb}^{2+}$  and  $\text{Zn}^{2+}$  with  $\text{Na}^+$  in the synthetic analcime was investigated in the temperature range 25-60 °C. The diffusion coefficients ( $D$ ) were calculated using the Barrer, Barri and Klinowski equation.  $E_a$ ,  $\Delta S^*$  and  $\Delta G^*$  values showed that all the channel sites were involved in the observed diffusion processes. Analcime acts as a potentially useful material for the uptake of heavy metals from aqueous solution. The energy barriers to cation movements into the zeolite framework represents movements of bare ions into analcime, except for zinc which may ingress as a partially hydrated moiety. Although lead is the largest ion studied it is able to enter the narrow analcime structure, because of its high polarisability. The measured entropy values reflect the change in hydration state as the ions move from the solution to the solid.

The ion exchange of  $\text{Cu}^{2+}$ ,  $\text{Ni}^{2+}$ ,  $\text{Pb}^{2+}$  and  $\text{Zn}^{2+}$  in analcime was investigated at 25-60 °C. The selectivity sequence for ions entering analcime was  $\text{Pb}^{2+} > \text{Cu}^{2+} > \text{Zn}^{2+} > \text{Ni}^{2+}$ , which is indicated by the values of  $\Delta G^0$ .  $\text{Pb}^{2+}$  had the lowest value of  $\Delta G^0$  despite its large radii, which is a reflection of its ease of polarisability coupled with the lowest enthalpy of cation hydration. Analcime has less preference for the smaller  $\text{Ni}^{2+}$  cation with its stronger ability to hold water molecules around it as shown by its high enthalpy of hydration. Entropy changes are related to changes in water content created during the exchange. Exchange processes are also endothermic with positive

values for  $\Delta H^\circ$ . The changes in the ion exchange isotherm shape are very small assuming that the ions have the same valence. A comparison of the selectivities of Pb, Cu, Ni, and Zn cations in analcime with the other zeolites shows quite a similar trend overall to other zeolites. It is confirmed that the selectivity of zeolites for heavy metals can be determined by cation size and hydration energy.

## **References**

## References

- Ahmed, S., Chughtai, S., and Keane, M.A. (1998). The removal of cadmium and lead from aqueous solution by ion exchange with Na-Y zeolite. **Sep. Purif. Technol.** 13: 57-64.
- Akcay, H., Kilinc, S., and Karakas, R. (1998). Preparation of a chromatographic solid support on the basis of perlite and separation of Uranium on a TBP-loaded perlite column. **J. Radioanal. Nucl. Chem.** 230: 83-89.
- Ali, J.A.M. (1987). **Liquid phase adsorption of n-paraffins on 5A molecular sieve**, Ph.D thesis, Aston University, UK.
- Allen, P. A., Evan, A. M., and Goudie, A. S. (1993). **The Encyclopedia of the Solid Earth Sciences**. Blackwell Scientific:Oxford. p. 461.
- Alloyway, B. C., and Ayres, D. C. (1997). **Chemical Principles of Environmental Pollution**. Blackie Academic & Professional. p 204.
- Amazorb. (2000). **What are Zeolites**. [On-line]. Available:<http://www.amazorb.com/zeolites.htm>.
- Arrhenius (1988) in Yusof, A.M. (1984). **The mobility of water in heteroionic analcites**. Ph.D thesis, The University of Salford, UK.
- Balgord, W.D., and Roy, R. (1971). Molecular sieve Zeolites I, **Amer. Chem. Soc. Adv. Chem. Series**. 101: 140.
- Balgord, W., and Roy, R. (1971). Crystal chemical relationships in the analcime

- family. **Adv. Chem. Ser. Amer. Chem. Soc.** 101: 140-146.
- Barth-Wirsching, U, Holler, H., Klammer, D., and Konrad, B. (1993). Synthetic zeolites formed from expanded perlite; Type, formation conditions and properties. **Mineralogy and Petrology.** 48: 275-294.
- Barrer, R.M. (1950). The hydrothermal chemistry of silicates. Part II  
**J. Chem. Soc.** 2342.
- Barrer, R.M., Barri, S.A.I., and Klinowski, J. (1980). **J. Chem. Soc., Faraday trans I.** 76: 1038.
- Barrer, R.M., and Townsend, R.P. (1975). Transition metal exchange in zeolite Part I: Thermodynamics of exchange of hydrated  $Mn^{2+}$ ,  $Co^{2+}$ ,  $Ni^{2+}$ ,  $Cu^{2+}$  and  $Zn^{2+}$  ion in ammonium mordenite. **J. Chem. Soc. Faraday. Trans I.** 72: 661-673.
- Barrer, R.M. in Sand, L.B., and Mumpton, F.A.(1978). **Natural Zeolite/ Occurrence, Properties and Uses.** Pergamon. 392.
- Barrer, R.M., and Ree, L.V.C. (1960). Self diffusion of alkali metals in analcime.  
**Trans. Faraday Soc.** 56: 709-721.
- Barrer, R.M., and Hinds, L. (1953). Ion exchange in crystal of analcite and leucite.  
**J. Chem. Soc.** 1879-1888.
- Barrer, R.M., and Sammon, D.C. (1961). **Alkali metal ion separation using zeolite: U.S. Patent 3.** 010: 785.
- Barrer, R.M., Davies, J.A., and Ree, L.V.C. (1968). Thermodynamics and thermochemistry of cation exchange in zeolite Y. **Org. Nucl. Chem.** 30: 3333-3349.
- Barrer, R.M., Barri, S., and Klinowski, J. (1979). Zeolite RHO. Part II Cation exchange equilibria and kinetics. **Chem. Soc. Faraday Trans I.** 1038-1051.

- Barrer, R.M., and Hinds, L. (1953). Ion exchange in crystals of Analcite and Leucite. **Faraday Soc.** 1879-1888.
- Barrer, R.M. (1971). Intracrystalline diffusion. In **Molecular Sieve Zeolite-II**, **Amer. Chemical Society**. Washington. D.C. pp. 1-36.
- Barrer, R.M., Buser, W. and Grutter, W.F. (1956). Synthetischer faujasite. **Chim. Act.** 39: 518.
- Barrer, R.M., and Baynham, J.W. (1956). Hydrothermal Chemistry of Silicates Part III. Synthetic potassium aluminosilicates. **J. Chem. Soc.** 2882.
- Barrer, R.M. (1978) in Sand, L.B., Mumpton, F.A. **Natural Zeolite Occurrence**, Pergamon, New York. pp. 385-395.
- Beatties, I.R. (1954). **Trans. Faraday. Soc.** 50: 581.
- Bous, V.A., Bororce, Z., Cimbalnikova, A., Kraus, I., Lajcakova, A., and Pacesova, M. (1993). **Natural Glasses**. Ellis Horwood. p. 97.
- Breck, D.W. and Flanigen, E.M. (1968). **Molecular sieve**. Society of the chemical industry. London, UK. p. 47.
- Breck, D. W. (1974). **Zeolite Molecular Sieves**. Wiley. New York. 529-536.
- Bruce King, R. (1994). **Encyclopedia of Inorganic Chemistry**. John Wiley & Sons. Athens. pp. 4363-4391.
- Cepeda, J. C. (1994). **Introduction to Minerals and Rocks**. Macmillan College. p. 123.
- Cetin, T., Tather, M., Erdem-Senatalar, A., Demirler, U., and Urgan, M. (2001). Lower temperatures for the preparation of thinner zeolite A coatings. **Microporous Mesoporous Mater.** 47: 1-14.
- Cheng, X., Zhao, P., and Stebbins, J.F. (2000). **Amer. Mineral.** 85: 1030-1037.
- Cheetham, A. K., and Day, P. (1992). **Solid State Chemistry Compounds**. Oxford. 226.

- Christidis, G. E., Paspaliaris, I., and Kontopoulos, A. (1999). Zeolitisation of perlite fine: Mineralogical characteristics of the end products and mobilization of chemical elements. **Appl. Clay Sci.** 15: 305-324.
- Christidis, G. E., Paspaliaris, I., Kontopoulos, A., Moirou, A., and Vaxevanidou, E. (1996). **Synthesis zeolite from perlite waste: Production environmental applications.** Proceedings SWEMP '96' Italy, 7-11 October. pp. 1135-1142.
- Crank, J. (1956). **Mathematics of Diffusion**, Oxford University, UK.
- Curkovic, V., Cerjan-Stefanovic, S., and Filinpan, T. (1996). **Metal Ion Exchange by Natural and Modified Zeolites.** Elsevier Science. 1379–1382.
- Dogan, M., Alkan, M., and Cakir, U. (1997). Electrokinetic properties of perlite. **J. Colloid Interface Sci.** 192: 114-118.
- Domine, D., and Quobex, J. (1968). **Molecular sieve. Society of the chemical industry.** London. UK. p. 78.
- Do, D.D. (1998). **Adsorption analysis: Equilibria and kinetics.** Imperial College, London, UK. pp. 91-92.
- Dyer, A., and White, K.J. (1999). Cation diffusion in the natural zeolite clinoptiolite. **Thermochim. Acta.** 341: 340-341.
- Dyer, A., and Yusof, A.M. (1987). Diffusion in heteroionic analcimes. Part I Sodium-potassium-water-system. **Zeolites.** 7: 196.
- Dyer, A., and Zubair, M. (1998). Ion–Exchange in Chabazite. **Microporous Mesoporous Mater.** 22: 135–150.
- Dyer, A. (1984). **Use of Natural Zeolites.** Chemistry and Industry. UK. 241-245.
- Dyer, A. (1988). **An Introduction to Zeolite Molecular Seives.** John Wiley & Sons. Chichester. UK.

- Dyer, A., and Molyneux, A. (1968). **Inorg. Nucl. Chem.** 30: 829.
- Dyer, A., and Keir, D. (1989). Ion exchange and PH tolerance in Molecular sieve zeolites. **J. Radioanal. Nucl. Chem.** 132: 423-441.
- Dyer, A. (2001) **Royal Society of Chemistry, Analytical Division Radiochemical Methods Group**, Workshop in liquid Scintillation Counting, September 24<sup>th</sup>-28<sup>th</sup>. p. 2.
- Dean, J.A. (1995). **Analytical Chemistry Handbook**. McGraw-Hill. New York. 11. p.19.
- Faghihian, H. (1990). **Studies on the ion exchange and water diffusion in the natural zeolites, natrolite and stilbite**. Ph.D. Thesis. University of Salford, UK.
- Faiia, A.M., and Feng, X. (2000). **Geochim. Cosmochim. Acta.** 64(18): 3181- 3188.
- Farrauto, R. J. (1997). **Fundamentals of Industrial Catalytic Processes**. London: Blackie Academic. p. 65.
- Ferchiche, S., Warzywoda, J., and Sacco Jr, A. (2001). Direct synthesis of zeolite Y with large particle size. **International Journal of Inorganic Materials.** 3: 733-780.
- Fletcher, P., and Townsend, R. P. (1981). Transition Metal Ion Exchange in Zeolites. **J. Chem. Soc; Faraday Trans.** 77: 497-509.
- Fletcher, P. and Townsend, R.P. (1982). **J. Chem. Soc., Faraday Trans. I**, 78: 1741.
- Gates, B. C. (1992). **Catalytic Chemistry**. John Wiley & Sons. p. 270.
- Ghosh, B., Agrawal, D.C., and Bhatia, S. (1994). Synthesis of zeolite A from calcined diatomaceous clay : Optimum studies. **Ind. Eng. Chem. Res.** 33(9): 107-110.
- Giordano, N., Recupero, V., Pino, L., and Bart, J. C. J. (1987). Zeolitisation of perlite : A prospective route. **Ind. Miner.** 86-95.

- Girolam. G.S., Rauchfuss.T.B., and Angelici, R.J. (1999).**Synthesis and technique in inorganic chemistry.** University Science. USA.
- Gonthier, S., Gora, L., Güray, I., and Thompson. RW. (1993). Further comments on the role of autocatalytic nucleation in hydrothermal zeolite synthesis. **Zeolites.**13: 414-418.
- Gualtieri, A.F. (2001). Synthesis of sodium zeolites from a natural halloysite. **Phys. Chem. Minerals.** 28: 719-728.
- Gualtieri, A., Norby, O., Artioli., G., and Hanson, J. (1997) Kinetics of formation of zeolite Na-A [LTA] from natural kaolinites. **Phys. Chem. Materials.** 24: 191-199.
- Gude,A.I., and Sheppard, R.A. (1966). Silica-rich Chabazite from the Barstow Formation. **Amer. Miner.** 51: 909.
- Güray, I., Warzywoda, J., Bac, N. and Sacco Jr, A. (1999). Synthesis of zeolite MCM-22 under rotating and static conditions. **Microporus Mesoporous Mater.** 31: 241-251.
- Haines, P.J. (2002). **Principles of thermal analysis and calorimetry.** The Royal Society of Chemistry.UK. pp 166-168.
- Harben, P. W., and Bates, L. (1990). **Industrial Minerals Geology and World Deposits.** Metal Bulletin: London. p. 184.
- Holmes, G.G., and Pecover, S.R. (1987). **Natural Zeolite Department of mineral resources.** UK. pp. 16-28.
- Incon corporation. (2000). **Perlite Handbook.** [On-line].Available: <http://www.info@incon-corp.com>.
- Jolley, W.L. (1991). **Modern Inorganic Chemistry.** 2<sup>ed</sup>.McGraw-Hill Book.New York. pp. 592-597.

- Joshi, U.D., Joshi, U.N., Stamhamkar, S., Joshi, V.P., Idage, B.B., Joshi, V.V., and Shiralkar, V.P. (2000). **Thermochim. Acta.** 378: 121-130.
- Kallo, D. (2001). in Natural Zeolites: Occurrences, Properties, Applications, eds. Bish, D.L., and Ming, D.W. Reviews in **Mineralogy and Geochemistry** 45, **Mineralogical Society of America.** Washington, DC. p. 519.
- Karlsson, H.R., and Clayton, R.N. (1990). Oxygen isotope fractionation between analcime and water: An experimental study. **Geochim. Cosmochim. Acta.** 54: 1
- Karge, H.G., and Weitkamp, J. (1998). **Molecular Sieve Science and Technology.** Springer.1.
- Keinath, T.M., and Wanielista, M.P. (1975) in Amin, S. (1991). **Surface Barriers on synthetic zeolite.** Ph.D thesis. The University of Salford.UK.
- Khodabanden, S., and Davis, M. E. (1997). Alteration of perlite to calcium zeolites. **Microporous Mater.** 9: 161-172.
- Kim, Y., and Kirkpatrick, R.J. (1998). High-temperature multinuclear NMR investigation of analcime. **Am. Mineral.** 83: 339-347.
- Ko, Y.S., and Ahn, W.S. (1999). Synthesis and Characterization of zeolite L. **Bull. Korean Chem. Soc.** 20: 1-6.
- Laidler, K.J., and Meiser, J.H. (1999). **Physical Chemistry.** 4<sup>ed</sup>. Houghton Mifflin. USA. pp. 299-303.
- Larsen, E.M., and Vissers, D.R. (1960). **J. Phys. Chem.** 64: 1732.
- Lide, D.R. (1995). **CRC Handbook of Chemistry and Physics.** 80<sup>th</sup>. Chemical rubber.USA. pp. 5-94-5-100.
- Maes, A., and Cremers, A. (1975). **J. Chem. Soc. Faraday Trans I.** 71: 265-277.
- Manahan, S E. (1991). **Environmental Chemistry.** 5<sup>ed</sup>. Lewis. USA. pp. 145–152.

- Malliou, E, Loizidou, M., and Spyrellis, N. (1994). Uptake of lead and cadmium by Clinoptiolite. **Sci. Total Environ.** 149: 139-144.
- Marcus, B. K. and Cormier, W. E. (in press). **Zeolyst International**. [Online]. Available: <http://www.beormie@pqcorp.com>.
- Marel, H.W., and Beutelspacher, H. (1976). **Atlas of Infrared Spectroscopy of Clay Minerals and their Admixtures**, New York. p. 476.
- Mendham, J., Denney, R.C., Barnes, J.D., and Thomas, M. (2000). **Vogel's: Textbook of quantitative chemical analysis**. Pearson Education.UK. p. 475.
- Moirou, A., Vaxevanidou, E., Christidis, G. E., and Paspaliaris, I. (2000). Ion exchange of zeolite Na-Pc with  $Pb^{2+}$ ,  $Zn^{2+}$  and  $Ni^{2+}$  ions. **Clays Clay Miner.** 48: 563-571.
- Meier, W.M., Olson, D.H., and Baerlocher, C. (1996). **Atlas of Zeolite Structure Types**. Butterworth-Heinemann, Stoneham, MA, 4<sup>th</sup> Ed. pp. 42-43.
- Mondele, K.D., Carland, R.M., and Aplan, F.F. (1995). **Miner. Eng.** 8: 535-548.
- Otonello, G. (1997). **Principles of Geochemistry**. Columbia University. New York. p. 496.
- Ouki, S.K., and Kavanagh, M. (1997). **Performance of natural zeolite for the treatment of mixed metal-contaminated effluents**. Waste Management and Research. 15: 384-394.
- Qureshi, M. and Varshney, K.G. (1991). **Inorganic ion exchangers in chemical analysis**. CRC.USA. pp. 40-41.
- Rayner-Canham, G. (2000). **Descriptive Inorganic Chemistry**. 2<sup>ed</sup>. Michelle Russel Julet. New York. p. 569.

- Rouessac, F., and Rouessac, A. (2000). **Chemical Analysis, Modern instrument methods and techniques**. 4<sup>ed</sup>. John Wiley & Son. UK.
- Rodriguez, G., and A. Herrera-Gómez. (2003) **J. Food Eng.** 59: 79-84.
- Ruthven, D. M. (1997). **Encyclopedia of Separation Technology**. 2<sup>ed</sup>. John Wiley. New York. p. 1059.
- Saha, P. (1959). Geochemical and X-ray investigation of natural and synthetic analcite. **Amer. Mineral.** 44: 300-313.
- Sand, L.B. (1968). **Molecular sieve**. Society of the Chemical Industry. London. UK. p. 71.
- Schundler, company. (2000). **Perlite Plant Guide**. [Online]. Available: <http://www.Schundler.com>.
- Semmens, J.M., and Seyforth, M. (1976). **Zeolite' 76 Conference**. Tucson. Ariz. (June 6-14, 1976).
- Sig Ko, Y., and Seung Ahn, W. (1999). Synthesis and characterization of zeolite L. **Bull. Korean Chem. Soc.** 20: 1-6.
- Sherman, J.D.C. (1978). Ion Exchange Separations with Molecular Sieve Zeolite. **The American Institute of Chemical Engineer.** 74(179): 99.
- Sherry, H.S. (1969). The ion exchange properties of zeolite, in J.A Marinsky, **Ion exchange**, New York. 2: 89.
- Sodeyama, K., Sakka, Y., and Kamino, Y. (1999). Preparation of fine expanded perlite. **J. Mater. Sci.** 34: 2461-2468.
- Subotic, B., and Graovac, A. (1985). Kinetic analysis of autocatalytic nucleation during crystallization of zeolites. In Gualtieri, A., Norby, O., Artioli, G., and Hanson, J. (1997). **Phys. Chem. Materials.** 24: 191-199.

- Szostak, R. (1992). **Handbook of Molecular Sieves**. Van Nostrand Reinhold, New York. pp 70-73.
- Szostak, R. (1998). **Molecular Sieves Principles of Synthesis and Identification**. Van Nostrand Reinholds: New York. p. 3.
- Takaishi, T. (1998). Ordered distribution of Al atoms in the framework of analcimes. **J. Chem. Soc., Faraday Trans.** 94: 1507-1518.
- Taylor, W.H. (1930). The structure of analcite. **Z. kristallogr.** 74: 1-19.
- Thammavong, S., and Rangsiwatananon, K. (2003). Synthesis, kinetics and particle size study of zeolite Na-X from Thai koalin. **29<sup>th</sup> congress on science and technology of Thailand**. October 20-22, 2003. p. 160-161.
- Todorovic, M., Radak-Jovanovic, Z., Gal, I.J., and Dyer, A. (1987). The release of tritiated water from synthetic analcime into surrounding water. **Colloids Surf. Sci.** 23: 350.
- Treacy, M.M.J., and Higgins, J.B. (2001). **Collection of simulated XRD powder patterns for zeolites**. Behalf of the structure Commission of the International Zeolite Association. 4<sup>ed</sup>.
- Van Bekkum, H., Flanigen, E. M., and Jensen, J. C. (1991). **Introduction to Zeolite Science and Practice**. Elsevier Science. 58. pp. 18-19.
- Vaughan, D.E.W.(1978). in Sand, L.B. and Mumpton, F.A. **Natural zeolite, Occurrence, properties, use**. Pergamon. New York.
- Wachinski, A. M., and Etzel, J. E. (1997). **Environmental Ion Exchange**. Lewis. New york. pp. 27-28.

- Walton, R.I., Millange, F., Hare, D., Davies, I.A., Sankar, G., and Catlow, R.A. (2001) An in Situ energy-dispersive x-ray diffraction study of the hydrothermal crystallization of zeolite A. 1. Influence of reaction conditions and transformation into sodalite. **J. Phys. Chem. B.** 105: 83-90.
- Wathanakul, P., Meesuk, L. and Sindhusen, P. (1995). **Zeolitisation of Lopburi perlite- A preliminary study.** International conference on geotechnology and mineral resources of Indochina(Geo-Indo'95).Thailand. 267-273.
- Wilson, M.J. (1994). **Clay mineralogy : Spectroscopic and chemical determinative methods.** Champman and Hall. UK.
- Wulfsberg, G. (2000). **Inorganic Chemistry.** University science books. USA. p. 57.
- Yang, P., Stolz, J., Armbuster, J.T. and Gunter, M. (1997). **Amer. Mineral.** 82:517.
- Yang, S., Vlessidis, A.G. and Elvmiridis, N.P. (1997). Influence of gel composition and crystallization conditions on the conventional synthesis of zeolites. **Ind. Eng. Chem. Res.** 36: 1622-1631.
- Yusof, A.M. (1984) **The mobility of water in heteroionic analcites.** Ph.D thesis, The University of Salford, UK.
- Yoder, H.S. and Weir, C.E. (1960). **Amer. J. Sci.** 258: 420.
- Zhdanov, S. P, khvoshchev, S. S, and Feoktistova, N. N. (1990). **Synthetic Zeolites.** Gordon and Breach Science. p. 1.
- Zhdanov, S.P., and Buntar, N.N. (1962). **Synthetic zeolite.** Nauka.Moscow. p. 105.

## **Appendices**

## **Appendix A**

### **Isotherm construction calculations**

## **Isotherm construction calculations**

### **1. Mathematical treatment for the ion exchange isotherm**

A Microsoft Excel spreadsheet was designed specifically for the calculations of the mathematical data obtained. The process for this program is detailed below:

1. Convert the counting data to be calculated into ionic fractions (via molalities) for both the solution and the solid phase exchange ions by using equations 1 to 10 and equations 11 and 12.
2. Isotherms are plotted with the ionic fractions of the out-going ion ( $\text{Na}^+$ ) in the solid and solution phase as the abscissa and ordinate respectively.
3. Manually draw a line of best fit through the isotherm points and read off the new values for the ionic fractions of  $\text{B}^{z_b^+}$  in the solution phase at regular intervals for the ionic fractions of  $\text{B}^{z_b^+}$  in the solid phase. This procedure makes it easier to interpret smooth the experimental data later. Re-enter this data into the spreadsheet.
4. Turn ionic fractions for the solution exchange into molalities. An equation 2.13 Kielland was used first to attempt to describe the ion exchange equilibrium. This equation was developed from a theoretical equation that was extended finally by Gaines and Thomas in 1953. The abstract thermodynamic approach resembles the Kielland approach to ion exchange equilibrium. The thermodynamic treatment for

the isotherm is near the rational scale. Combine data for the ionic fractions for the solid phase and the corrected solution phase molalities and using equations 19 and 20 to give the selectivity coefficients for the in-going ion ( ${}^A K_c$ ).

4. Plot the in-going ion ( $B^{Z_{B^+}}$ ) ionic fraction data against the selectivity coefficients  ${}^A K_c$ , as abscissa and ordinate respectively.
5. Use a spreadsheet (like 'excel') to fit polynomials (up to six) to this data so that a smooth mathematical trend describes the selectivity coefficient as a function of the fraction of the solid ionic phase. It may be necessary to fit three such equations for more complex trends.
6. Integrate these polynomials over the ionic fraction ranges they cover and sum the area together.
7. Calculate the equilibrium constant ( ${}^A K_a$ ) and the Gibbs free energy ( $\Delta G^\circ$ ) (equations 2.31 and 2.32) respectively.

## 2. Isotherm construction calculations for solution and solid phases

This calculation is based on the assumption that  $Na^+$  is the out-going radio-labelled ion.

$$IF_f^{B^{Z_{B^+}(s)}} = \frac{(A_f - A_b)}{60.w.A_s.N} (Q.w + N.F_{B^{Z_{B^+}}} . V) \quad (1)$$

$$IF_f^{B^{Z_{B^+}(z)}} = \left[ 60.w.A_s - \frac{(A_f - A_b)V}{60.w^2.A_s.Q} \right] (Q.w + N.F_{B^{Z_{B^+}}} . V) \quad (2)$$

$$IF_r^{B^{Z_{B^+}(s)}} = \frac{\left\{ \left[ \eta \cdot N \cdot w \cdot A_s - \frac{A_1}{60} (Q \cdot w + N \cdot F_{B^{Z_{B^+}}} \cdot V) \right] \cdot \psi \cdot V + (Q \cdot w + N \cdot F_{B^{Z_{B^+}}} \cdot V) \cdot A_s \cdot w \right\}}{A_s \cdot w \cdot N (60 \cdot w \cdot A_s - \psi \cdot A_1 \cdot V)} \cdot A_2 \quad (3)$$

$$IF_r^{B^{Z_{B^+}(z)}} = \frac{(60 \cdot w \cdot A_s - V(\psi \cdot A_1 + A_2)) \cdot \left[ w \left( \frac{Q(\psi \cdot A_1 \cdot V - 60wA_s) -}{60N \cdot V \cdot A_s} (F_{B^{Z_{B^+}}} + \eta\psi) \right) + \psi \cdot A_1 V^2 F_{B^{Z_{B^+}}} \cdot N \right]}{60 \cdot w^2 \cdot A_s \cdot Q(-60 \cdot w \cdot A_s + \psi \cdot A_1 \cdot V)} \quad (4)$$

$$IF_{f/r}^{A^{Z_{A^+}(s)}} = 1 - IF_{f/r}^{B^{Z_{B^+}(s)}} \quad (5)$$

$$IF_{f/r}^{A^{Z_{A^+}(z)}} = 1 - IF_{f/r}^{B^{Z_{B^+}(z)}} \quad (6)$$

Where:

$\psi$  = A fraction of the solution is removed in order to perform the reverse isotherm (0 to1)

$\eta$  = A fraction of the total normality of the out-going ion is added

$A_1$  = Background corrected solution activity after forward equilibration

( $\equiv A_f \cdot A_b$ )(cpm/ml)

$A_i$  = Initial radioactivity of the solution phase (cpm/ml)

$A_f$  = Final radioactivity of the solution phase after equilibrium (cpm/ml)

$A_b$  = background radioactivity of the solution phase (cpm/ml)

$A_2$  = Background corrected solution activity after reverse equilibration

(cpm/ml)

$V$  = Volume of isotherm solution used (ml)

$w$  = Mass of the exchanger phase (g)

$Q$  = Cation exchange capacity ( $\text{meqg}^{-1}$ )

$N$  = Isotherm solution normality(N)

$F_{B^{Z_{B^+}}}$  = Fraction of  $B^{Z_{B^+}}$  (out-going ion,  $\text{Na}^+$ ) in the isotherm

$IF_{f/r}^{A^{Z_{A^+}}}$  = Ionic fractions of ion  $A^{Z_{A^+}}$  in the solution phase in either the forward or reverse isotherm, respectively

$IF_{f/r}^{B^{Z_{B^+}}(s)}$  = Ionic fractions of ion  $B^{Z_{B^+}}$  in the solution phase in either the forward or reverse isotherm, respectively

$IF_{f/r}^{A^{Z_{A^+}}(z)}$  = Ionic fractions of ion  $A^{Z_{A^+}}$  in the solid phase in either the forward or reverse isotherm, respectively

$IF_{f/r}^{B^{Z_{B^+}}(z)}$  = Ionic fractions of ion  $B^{Z_{B^+}}$  in the solid phase in either the forward or reverse isotherm, respectively

## 2.1 Cation exchange capacity (CEC)

When the solid (zeolite) is solely in the  $\text{Na}^+$  form then CEC ( $Q$ ) can be found as:

$$Q = K_d M_{\text{Na}^+(s)} \quad (7)$$

Where;

$$K_d = \frac{[(A_i - A_b) - (A_f - A_b)]}{(A_f - A_b)} \cdot \frac{V}{w} \quad (8)$$

Where;

$A_i$  = Initial radioactivity of the solution phase (cpm/ml)

$A_f$  = Final radioactivity of the solution phase after equilibrium (cpm/ml)

$A_b$  = background radioactivity of the solution phase (cpm/ml)

$V$  = Volume of the solution phase (ml)

$w$  = Mass of the exchanger phase (g)

$M_{Na^+ (s)}$  = Total molar strength of  $Na^+$  ions in the closed system (0.01)

## 2.2 Conversion of concentration units

These formulas assume two ionic species are present and that there are no deviations from ideality, and that the solutions are dilute.

To convert molarity to molality as follows:

$$M_{\text{molality}} = \frac{1000M_i}{1000D - (M_i E)} \quad (9)$$

To convert molarity to ionic fraction as follow:

$$IF = \frac{\left( \frac{z_i M_i}{V} \right)}{\left( \sum_i \frac{z_i M_i}{V} \right)} \quad (10)$$

Where:

$M_{\text{molality}}$  = Molality of species in the solution or solid phase at equilibrium  
respectively (mole/kg)

$M_i$  = Molarity of species  $i$  in the solution phase at equilibrium (mol/l)

$E$  = Molecular weight of solute ( $\text{gmol}^{-1}$ )

$D$  = Density of solution ( $\text{gml}^{-1}$ )

$z_i$  = Charge on species  $i$

Note that the change in molarity with loading of the exchanger phase was taken into account by:

$$A_Z^{Z_B} = \left( \frac{z_A \bar{m}_A}{z_A \bar{m}_A + z_B \bar{m}_B} \right)^{z_B} \quad (11)$$

$$B_Z^{Z_A} = \left( \frac{z_B \bar{m}_B}{z_B \bar{m}_B + z_A \bar{m}_A} \right)^{z_A} \quad (12)$$

Where:

$A_Z, B_Z$  = Equivalent fractions of ions  $A^{z_{A+}}$  and  $B^{z_{B+}}$  respectively,  $B^{z_{B+}}$  in the exchanger phase

$z_A, z_B$  = Modulus of the charge of the ions  $A^{z_{A+}}$  and  $B^{z_{B+}}$  respectively

$\bar{m}_A, \bar{m}_B$  = The concentration of ions  $A^{z_{A+}}$  and  $B^{z_{B+}}$  in the exchanger phase (moles $kg^{-1}$ )

As before the thermodynamic equilibrium constant is:

$${}^A_B K_a = \frac{a_{A(z)}^{z_B} a_{B(s)}^{z_A}}{a_{A(s)}^{z_B} a_{B(z)}^{z_A}} \quad (13)$$

Where:

${}^A_B K_a$  = Rational thermodynamic equilibrium constant.

$a$  = Activity of the subscripted ion in the relevant phase, i.e. solution or solid, raised to power of the modulus of the valency of the counter ion.

The thermodynamic equilibrium constant can be separated into equivalent fractions (solid phase), concentration (solution phase) and activity coefficients.

$${}^A_B K_a = {}^A_B K_m \left( \frac{\gamma_B^{z_A} f_A^{z_B}}{\gamma_A^{z_B} f_B^{z_A}} \right) = {}^A_B K_c \left( \frac{f_A^{z_B}}{f_B^{z_A}} \right) \quad (14)$$

Where:

$\gamma_A, \gamma_B$  = Activity corrections for ions  $A^{z_A+}$  and  $B^{z_B+}$  in solution respectively

$f_A, f_B$  = Activity corrections for ions  $A^{z_A+}$  and  $B^{z_B+}$  in the exchanger phase

respectively

${}^A_B K_m$  = Mass action quotient on the rational scale and

$${}^A_B K_m = \frac{m_B^{z_A} A_z^{z_B}}{m_A^{z_B} B_z^{z_A}} \quad (15)$$

Where:

$m_A, m_B$  = Molality of the  $A^{z_A+}$  and  $B^{z_B+}$  in the solution phase(moleskg<sup>-1</sup>)

respectively

$A_z, B_z$  = Equivalent fractions of ions  $A^{z_A+}$  and  $B^{z_B+}$  respectively,  $B^{z_B+}$  in the

exchanger phase

$z_A, z_B$  = Modulus of the charge of the ions  $A^{z_A+}$  and  $B^{z_B+}$  respectively

### 2.3 Activity correction for the solution species

The method used for the correction of activity of the solution ion species has been presented in full by Fletcher and Townsend. The problem lies with the actual

values of  $\gamma_A^{z_B}$  and  $\gamma_B^{z_A}$  which can not be calculated individually. However, their ratio ( $\Gamma$ ) can be found from the mean molal stoichiometric activity coefficients in a mixed solution of the salts.

$$\Gamma = \frac{\gamma_B^{z_A}}{\gamma_A^{z_B}} = \left[ \frac{(\gamma_{\pm BX}^{AX})^{z_A(z_B + z_x)}}{(\gamma_{\pm AX}^{BX})^{z_B(z_A + z_x)}} \right]^{\frac{1}{z_x}} \quad (16)$$

Where:

$\Gamma$  = Ratio of the mean molal activity coefficients

$\gamma_{\pm BX}^{AX}$  = Mean molal stoichiometric activity coefficient of salt BX in presence of salt AX

$\gamma_{\pm AX}^{BX}$  = Mean molal stoichiometric activity coefficient of salt AX in presence of salt BX

$\gamma_B^{z_A}, \gamma_A^{z_B}$  = Activity of ion  $B^{z_B+}$  and  $A^{z_A+}$  raised to the power of the modulus of the valency of the counter ion.

$z_x$  = Modulus of the valency of the anion present.

Therefore, the thermodynamic equilibrium constant becomes;

$${}^A K_B = {}^A K_C \left( \frac{f_A^{z_B}}{f_B^{z_A}} \right) \quad (17)$$

Where:

$f_A, f_B$  = Activity corrections for ions  $A^{zA+}$  and  $B^{zB+}$  in the solid phase respectively

and:

$${}^A_B K_c = {}^A_B K_m \Gamma \quad (18)$$

Where:

${}^A_B K_c$  = Mass action quotient corrected for solution species activities by the

Kielland quotient.

${}^A_B K_m$  = Mass action quotient on the rational scale.

$\Gamma$  = Ratio of the mean molal stoichiometric activity coefficients.

This work has only one anionic species and only two cationic species present

in solution, to calculate  $\gamma_{\pm BX}^{AX}$  and  $\gamma_{\pm AX}^{BX}$  the following equation can be used:

$$\log \gamma_{\pm AX}^{BX} = \log \gamma_{\pm AX} + \frac{1}{4I(Z_A + Z_X)} \left[ \sum_{i=2}^m m_A \left( \begin{array}{l} \xi_{A_1} \log \gamma_{\pm AX} + \xi_{A_2} \log \gamma_{\pm AX} \\ + \\ \xi_{A_3} A \left( 1 + \frac{I}{2} \right)^{-1} + (\xi_{A_1} + \xi_{A_2}) \log Q \end{array} \right) \right] \quad (19)$$

$$\log \gamma_{\pm BX}^{\text{AX}} = \log \gamma_{\pm BX} + \frac{1}{4I(Z_B + Z_X)} \left[ \sum_{i=2}^m m_B \left\{ \begin{aligned} &\xi_{B_1} \log \gamma_{\pm BX} + \xi_{B_2} \log \gamma_{\pm BX} \\ &+ \\ &\xi_{B_3} A \left( 1 + I \frac{1}{2} \right)^{-1} + (\xi_{B_1} + \xi_{B_2}) \log Q \end{aligned} \right\} \right] \quad (20)$$

(These values can then be used in equation (16) to obtain the ratio of the mean molal stoichiometric activity coefficients.) The derivation of the equations come from Rodney Townsend's papers (Fletcher, P., Townsend, R. P., J. Chem. Soc., Faraday T., 2, 77, 955 963, (1981), Fletcher, P., Townsend, R. P., J. Chem. Soc., Faraday T., 2, 77, 965 980, (1981), Fletcher, P., Townsend, R. P., J. Chem. Soc., Faraday T., 2, 77, 2077 2089, (1981), Fletcher, P., Townsend, R. P., J. Chem. Soc., Faraday T., 2, 79, 419 432, (1983)).

Where;

$$Q = 1 + 0.018 \sum v_s m_s$$

Where;

$v_s$  = Number of moles formed in the ionization of species, if species is  $\text{NaNO}_3$

$$\text{hen } v_s = 2$$

$m_s$  = Molality of species s.

$\sum v_s m_s$  = The summation is made over all species present

$$\xi_{A_1} = (z_{A_1} + z_{x_1})(z_{A_1} - 2z_{A_1} - z_{x_1})$$

$$\xi_{A_2} = z_{A_1} (z_{A_1} + z_{x_1})^2$$

$$\xi_{A_3} = z_{A_1} z_{A_2} z_{x_1} (z_{A_1} + z_{A_2})^2$$

$$\xi_{A3} = z_{A1} (z_{A1} + z_{x1}) (z_{x1} - 2z_{x1} - z_{A1})$$

$$\xi_{B2} = z_{x1} (z_{x1} + z_{A1})^2$$

$$\xi_{B3} = z_{x1} z_{x2} z_{A1} (z_{x1} + z_{x2})^2$$

Where;

$\xi$  = a correction term in the activity coefficient

$z_{A1}$  = Modulus of the charge on the cationic ion of salt AX which is being corrected  
for

$z_{A1}$  = Modulus of the charge on the cationic ion of salt BX  $z_{A1}$ , i.e. the counter ion

$z_{x1}$  = Modulus of the charge on the anionic ion of salt AX which is being corrected  
for

$z_{x1}$  = Modulus of the charge on the anionic ion of salt BX, i.e. the counter ion

$I$  = Ionic strength

Where;

$$I = \frac{1}{2} \sum_i z_i^2 m_i \quad (21)$$

Where;

$m_i$  = Molality of species

$Z_i$  = Charge on species i, positive for cations and negative for anions.

Where;

$$A = \frac{1}{2} \sqrt{\left(\frac{500N}{16\pi^2}\right) \left(\frac{e^2}{\epsilon kT}\right)^2} \quad (22)$$

Where;

A = Debye-Huckel constant for aqueous solutions is taken as  $\sim 0.509 \text{ (mol}^{-1/2}\text{dm}^{3/2}\text{)}$

N = Avogadro's constant ( $6.02213673 \times 10^{23} \text{ mol}^{-1}$ )

e = Single proton charge ( $1.6021773349 \times 10^{-19} \text{ C}$ )

k = Boltzman's constant ( $1.38065812 \times 10^{-23} \text{ JK}^{-1}$ )

T = Absolute temperature (K)

$\epsilon$  = Permittivity of the solution is taken as constant at  $6.959 \times 10^{-10} \text{ (J}^{-1}\text{C}^2\text{m}^{-1}\text{)}$

From equation 18

$${}^A_B K_c = {}^A_B K_m \Gamma$$

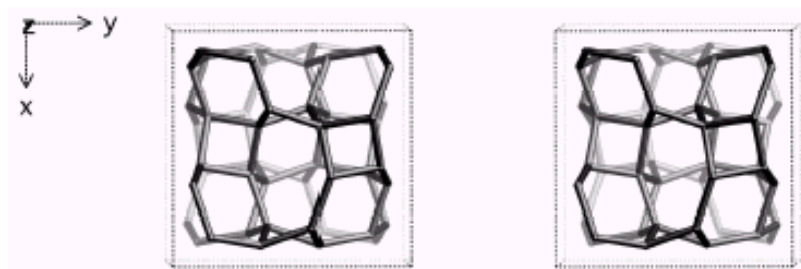
Where  ${}^A_B K_c$  is the Kielland coefficient related to  ${}^A_B K_a$  by the Gaines-Thomas relationship;

$$\ln K_a = (Z_B - Z_A) + \int_0^1 \ln K_c dA_Z \quad (23)$$

## **Appendix B**

### **Atlas of zeolite structure types**

(<http://www.iza-structure.org/databases/>)

**ANA****Framework Type****la $\bar{3}$ d***framework viewed along [001]*

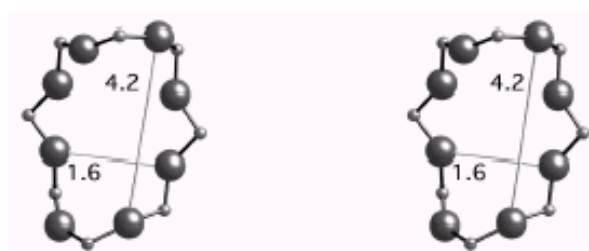
<b>Idealized cell constants:</b>	cubic, la $\bar{3}$ d, a = 13.6Å	
<b>Coordination sequences and vertex symbols:</b>	T <sub>1</sub> (48, 2)    4   10   22   39   60   87   118   154   196   242	4-4-6-6-8 <sub>4</sub> -8 <sub>4</sub>
<b>Secondary building units:</b>	6-2 or 6 or 4	
<b>Loop configuration of T-Atoms:</b>		
<b>Isotypic framework structures:</b>	*Analcime <sup>(1-3)</sup> [Al-Co-P-O]-ANA <sup>(4)</sup> [Al-Si-P-O]-ANA <sup>(5)</sup> [Ga-Ge-O]-ANA <sup>(6)</sup> [Cs-Na-(H <sub>2</sub> O)] [Ga-Si-O]-ANA <sup>(7)</sup> [Cs <sub>16</sub> ][Cu <sub>8</sub> Si <sub>40</sub> O <sub>96</sub> ]-ANA <sup>(8)</sup> [K]-[B-Si-O]-ANA <sup>(9)</sup> AlPO <sub>4</sub> -24 <sup>(10)</sup> AlPO <sub>4</sub> -pollucite <sup>(11)</sup> Ammonioleucite <sup>(12)</sup> Ca-D <sup>(13)</sup> Cs beryllsilicate pollucite <sup>(14)</sup>	Cs,Fe silicate pollucite <sup>(15)</sup> Hsianghualite <sup>(16)</sup> Kehoeite <sup>(17)</sup> Leucite <sup>(18)</sup> Na-B <sup>(19)</sup> Pollucite <sup>(20)</sup> Synthetic analcime <sup>(21)</sup> Synthetic hsianghualite <sup>(22)</sup> Synthetic wairakite <sup>(23)</sup> Wairakite and additional compositional variants <sup>(24)</sup>
<b>Alternate designation:</b>	Analcite	

**References:**

- (1) Taylor, W.H. *Z. Kristallogr.*, **74**, 1-19 (1930)
- (2) Knowles, C.R., Rinaldi, F.F. and Smith, J.V. *Indian Mineral.*, **6**, 127- (1965)
- (3) Ferraris, G., Jones, D.W. and Yerkess, J. *Z. Kristallogr.*, **135**, 240-252 (1972)
- (4) Feng, P.Y., Bu, X.H. and Stucky, G.D. *Nature*, **388**, 735-741 (1997)
- (5) Artioli, G., Pluth, J.J. and Smith, J.V. *Acta Crystallogr.*, **C40**, 214-217 (1984)
- (6) Bu, X., Feng, P., Gier, T.E., Zhao, D. and Stucky, G.D. *J. Am. Chem. Soc.*, **120**, 13389-13397 (1998)

Analcime	Type Material	ANA
----------	---------------	-----

<b>Crystal chemical data:</b>	$[\text{Na}^+_{16}(\text{H}_2\text{O})_{16}] [\text{Al}_{16}\text{Si}_{32}\text{O}_{96}]$ -ANA cubic, $la\bar{3}d$ , $a = 13.73\text{\AA}$ <sup>(3)</sup>
<b>Framework density:</b>	18.5 T/1000 $\text{\AA}^3$
<b>Channels:</b>	irregular channels formed by highly distorted 8-rings

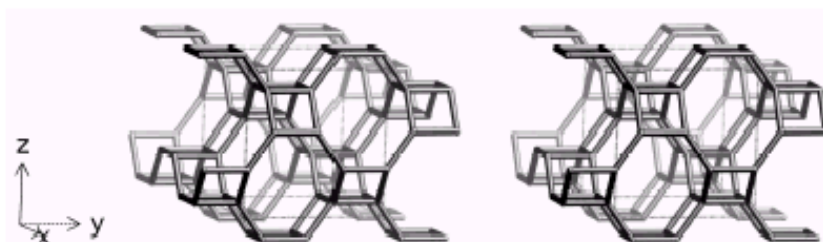


distorted 8-ring viewed along  $[110]$

**References (cont.):**

- (7) Yelon, W.B., Xie, D., Newsam, J.M. and Dunn, J. *Zeolites*, **10**, 553-558 (1990)
- (8) Heinrich, A.R. and Baerlocher, Ch. *Acta Crystallogr.*, **C47**, 237-241 (1991)
- (9) Millini, R., Montanari, L. and Bellussi, G. *Microporous Materials*, **1**, 9-15 (1993)
- (10) Wilson, S.T., Lok, B.M., Messina, C.A., Cannan, T.R. and Flanigen, E.M. *J. Am. Chem. Soc.*, **104**, 1146-1147 (1982)
- (11) Keller, E.B. *Ph.D. Thesis, ETH, Zürich, Switzerland*, (1987)
- (12) Hori, H., Nagashima, K., Yamada, M., Miyawaki, R. and Marubashi, T. *Am. Mineral.*, **71**, 1022-1027 (1986)
- (13) Ames, L.L. and Sand, L.B. *Am. Mineral.*, **43**, 476-480 (1958)
- (14) Torres-Martines, L.M., Gard, J.A., Howie, R.A. and West, A.R. *J. Solid State Chem.*, **51**, 100-103 (1984)
- (15) Kopp, O.C., Harris, L.A., Clark, G.W. and Yakel, H.L. *Am. Mineral.*, **48**, 100-109 (1963)
- (16) Wen-Hui, H., Saho-Hua, T., Kung-Hai, W., Chun-Lin, C. and Cheng Chi, Y. *Am. Mineral.*, **44**, 1327-1328 (1959)
- (17) McConnell, D. and Foreman Jr., D.W. *Can. Mines*, **12**, 352- (1974)
- (18) Peacor, D.R. *Z. Kristallogr.*, **127**, 213-224 (1968)
- (19) Barrer, R.M. and White, E.A.D. *J. Chem. Soc.*, 1561-1571 (1952)
- (20) Nel, H.J. *Am. Mineral.*, **29**, 443-451 (1944)
- (21) Ghobarkar, H. and Franke, W. *Cryst. Res. Technol.*, 1071-1075 (1986)
- (22) Ghobarkar, H., Schaefer, O. and Knauth, P. *Annal. Chimie, Science Matériaux*, **24**, 209-215 (1999)
- (23) Ghobarkar, H. *Cryst. Res. Technol.*, K90-92 (1985)
- (24) Takeuchi, Y., Mazzi, F., Haga, N. and Galli, E. *Am. Mineral.*, **64**, 993-1001 (1979)

**GIS** **Framework Type** **I4<sub>1</sub>/amd**



framework viewed along [100]

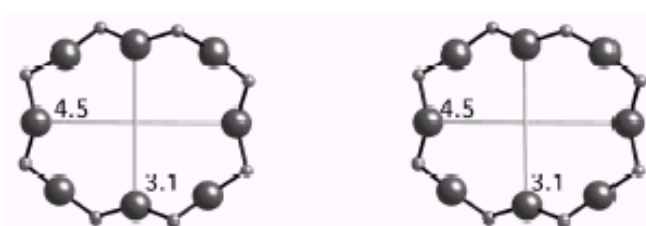
<b>Idealized cell constants:</b>	tetragonal, I4 <sub>1</sub> /amd (origin choice 2), a = 9.8Å, c = 10.2Å	
<b>Coordination sequences and vertex symbols:</b>	T <sub>1</sub> (16, 2)	4 9 18 32 48 67 92 120 150 185 4-4-4-8 <sub>2</sub> -8-8
<b>Secondary building units:</b>	8 or 4	
<b>Loop configuration of T-Atoms:</b>		
<b>Isotypic framework structures:</b>	*Gismondine <sup>(1)</sup> [Al-Co-P-O]-GIS <sup>(2)</sup> [Co-Al-P-O]-GIS <sup>(3)</sup> [Co-Ga-P-O]-GIS <sup>(4)</sup> [Co-P-O]-GIS <sup>(5)</sup> [Ga-Si-O]-GIS <sup>(6)</sup> [Mg-Al-P-O]-GIS <sup>(3)</sup> [Zn-Ga-P-O]-GIS <sup>(7)</sup> [(NH <sub>4</sub> ) <sub>4</sub> ][Zn <sub>4</sub> B <sub>4</sub> P <sub>8</sub> O <sub>32</sub> ]-GIS <sup>(8)</sup> [Cs <sub>4</sub> ][Zn <sub>4</sub> B <sub>4</sub> P <sub>8</sub> O <sub>32</sub> ]-GIS <sup>(8)</sup> [Rb <sub>4</sub> ][Zn <sub>4</sub> B <sub>4</sub> P <sub>8</sub> O <sub>32</sub> ]-GIS <sup>(8)</sup> Amicite <sup>(9)</sup> Garronite <sup>(10,11)</sup>	Gobbinsite <sup>(12)</sup> High-silica Na-P <sup>(13)</sup> Low-silica Na-P (MAP) <sup>(14)</sup> MAPO-43 <sup>(15)</sup> MAPSO-43 <sup>(16,17)</sup> Na-P1 <sup>(18)</sup> Na-P2 <sup>(19)</sup> SAPO-43 <sup>(20)</sup> Synthetic Ca-garronite <sup>(21)</sup> Synthetic amicite <sup>(22)</sup> Synthetic garronite <sup>(22)</sup> Synthetic gobbinsite <sup>(22)</sup> TMA-gismondine <sup>(23)</sup>
<b>Alternate designation:</b>	Gismondite (discredited) synthetic zeolite B (disused)	

**References:**

- (1) Fischer, K. and Schramm, V. *Adv. Chem. Ser.*, **101**, 250-258 (1971)
- (2) Feng, P.Y., Bu, X.H. and Stucky, G.D. *Nature*, **388**, 735-741 (1997)
- (3) Feng, P., Bu, X., Gier, T.E. and Stucky, G.D. *Microporous and Mesoporous Materials*, **23**, 221-229 (1998)
- (4) Cowley, A.R. and Chippindale, A.M. *Chem. Commun.*, 673-674 (1996)
- (5) Yuan, H.M., Chen, J.S., Zhu, G.S., Li, J.Y., Yu, J.H., Yang, G.D. and Xu, R. *Inorg. Chem.*, **39**, 1476-1479 (2000)

**Gismondine****Type Material****GIS**

<b>Crystal chemical data:</b>	[Ca <sup>2+</sup> <sub>4</sub> (H <sub>2</sub> O) <sub>16</sub> ][Al <sub>8</sub> Si <sub>8</sub> O <sub>32</sub> ]-GIS monoclinic, P112 <sub>1</sub> /a a = 9.843Å, b = 10.023Å, c = 10.616Å, γ = 92.417° <sup>(1)</sup> (Relationship to unit cell of Framework Type: a' = a, b' = b, c' = c)
<b>Framework density:</b>	15.3 T/1000Å <sup>3</sup>
<b>Channels:</b>	{[100] 8 3.1 x 4.5 ↔ [010] 8 2.8 x 4.8}*** (variable due to considerable flexibility of the framework)



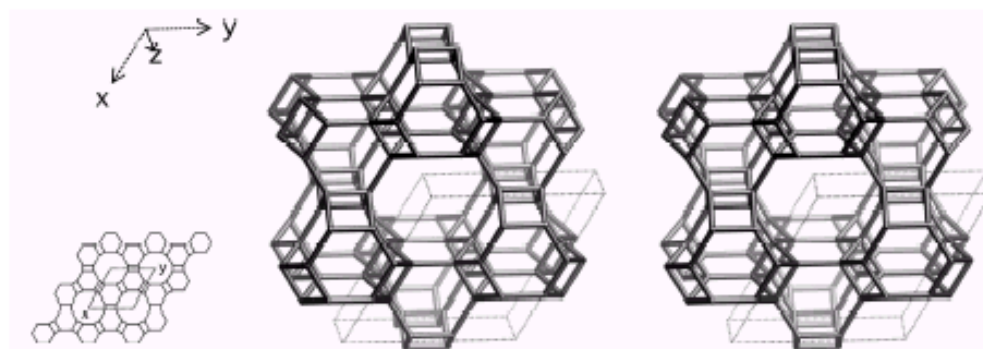
8-ring viewed along [100]

See Appendix A for 8-ring viewed along [010]

**References (cont.):**

- (6) Cho, H.H., Kim, S.H., Kim, Y.G., Kim, Y.C., Koller, H., Cambor, M.A. and Hong, S.B. *Chem. Mater.*, **12**, 2292-2300 (2000)
- (7) Chippindale, A.M., Cowley, A.R. and Peacock, K.J. *Microporous and Mesoporous Materials*, **24**, 133-141 (1998)
- (8) Kniep, R., Schäfer, G., Engelhardt, H. and Boy, I. *Angew. Chem. Int. Ed.*, **38**, 3642-3644 (1999)
- (9) Alberti, A. and Vezzalini, G. *Acta Crystallogr.*, **B35**, 2866-2869 (1979)
- (10) Artioli, G. *Am. Mineral.*, **77**, 189-196 (1992)
- (11) Artioli, G. and Marchi, M. *Powder Diffraction*, **14**, 190-194 (1999)
- (12) McCusker, L.B., Baerlocher, Ch. and Nawaz, R. *Z. Kristallogr.*, **171**, 281-289 (1985)
- (13) Håkansson, U., Fälth, L. and Hansen, S. *Acta Crystallogr.*, **C46**, 1363-1364 (1990)
- (14) Albert, B.R., Cheetham, A.K., Stuart, J.A. and Adams, C.J. *Microporous and Mesoporous Materials*, **21**, 133-142 (1998)
- (15) Pluth, J.J., Smith, J.V. and Bennett, J.M. *J. Am. Chem. Soc.*, **111**, 1692-1698 (1989)
- (16) Flanigen, E.M., Lok, B.M., Patton, R.L. and Wilson, S.T. *Pure Appl. Chem.*, **58**, 1351-1358 (1986)
- (17) Flanigen, E.M., Lok, B.M., Patton, R.L. and Wilson, S.T. In *Proc. 7th Int. Zeolite Conf.*, (eds. Y. Murakami, A. Iijima and J.W. Ward), pp. 103-112 (1986), Kodansha, Tokyo
- (18) Baerlocher, Ch. and Meier, W.M. *Z. Kristallogr.*, **135**, 339-354 (1972)
- (19) Hansen, S., Håkansson, U. and Fälth, L. *Acta Crystallogr.*, **C46**, 1361-1362 (1990)
- (20) Helliwell, M., Kaucic, V., Cheetham, G.M.T., Harding, M.M., Kariuki, B.M. and Rizkallah, P.J. *Acta Crystallogr.*, **B49**, 413-420 (1993)
- (21) Schropfer, L. and Joswig, W. *Eur. J. Mineral.*, **9**, 53-65 (1997)
- (22) Ghobarkar, H. and Schaefer, O. *Mater. Res. Bull.*, **34**, 517-525 (1999)
- (23) Baerlocher, Ch. and Meier, W.M. *Helv. Chim. Acta*, **53**, 1285-1293 (1970)

**CAN** **Framework Type** **P6<sub>3</sub>/mmc**



framework viewed along [001] (bottom left: projection down [001])

<b>Idealized cell constants:</b>	hexagonal, P6 <sub>3</sub> /mmc, a = 12.5Å, c = 5.3Å	
<b>Coordination sequences and vertex symbols:</b>	T <sub>1</sub> (12, m) 4 10 20 34 54 78 104 134 168 210	4-6-4-6-6-6
<b>Secondary building units:</b>	4-2 or 6 or 4	
<b>Loop configuration of T-Atoms:</b>		
<b>Framework description:</b>	AB sequence of 6-rings	
<b>Isotypic framework structures:</b>	*Cancrinite <sup>(1,2)</sup> [Al-Ge-O]-CAN <sup>(3)</sup> [Ga-Si-O]-CAN <sup>(4)</sup> [Zn-P-O]-CAN <sup>(5)</sup> Basic cancrinite <sup>(6,7)</sup> Cancrinite hydrate <sup>(8)</sup>	Davyne <sup>(9)</sup> ECR-5 <sup>(10)</sup> Microsommite <sup>(11)</sup> Synthetic cancrinite <sup>(12)</sup> Tiptopite <sup>(13)</sup> Vishnevite <sup>(14)</sup>

**References:**

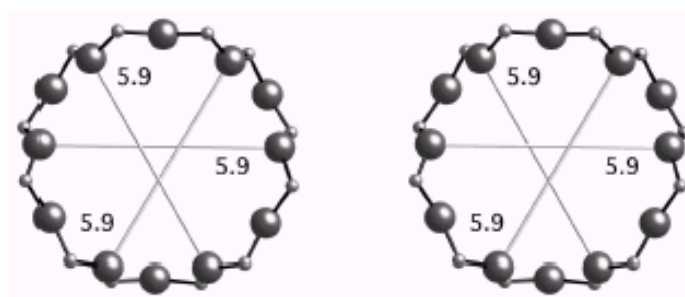
- (1) Pauling, L. *Proc. Natl. Acad. Sci.*, **16**, 453-459 (1930)
- (2) Jarchow, O. *Z. Kristallogr.*, **122**, 407-422 (1965)
- (3) Belokoneva, E.L., Uvarova, T.G. and Dem'yanets, L.N. *Sov. Phys. Crystallogr.*, **31**, 516-519 (1986)
- (4) Newsam, J.M. and Jorgensen, J.D. *Zeolites*, **7**, 569-573 (1987)
- (5) Yakubovich, O.V., Karimova, O.V. and Mel'nikov, O.K. *Crystallogr. Reports*, **39**, 564-568 (1994)
- (6) Barrer, R.M. and White, E.A.D. *J. Chem. Soc.*, 1561-1571 (1952)
- (7) Bresciana Pahor, N., Calligaris, M., Nardin, G. and Randaccio, L. *Acta Crystallogr.*, **B38**, 893-895 (1982)
- (8) Wyart, J. and Michel-Levy, M. *Compt. Rend.*, **229**, 131- (1949)
- (9) Hassan, I. and Grundy, H.D. *Can. Mineral.*, **28**, 341-349 (1990)
- (10) Vaughan, D.E.W. *E. Patent A-190,90* (1986)

**Cancrinite****Type Material****CAN**

**Crystal chemical data:**  $[\text{Na}^+_6 \text{Ca}^{2+} \text{CO}_3^{2-} (\text{H}_2\text{O})_2] [\text{Al}_6\text{Si}_6 \text{O}_{24}]$ -CAN  
hexagonal, P6<sub>3</sub>, a = 12.75Å, c = 5.14Å <sup>(2)</sup>

**Framework density:** 16.6 T/1000Å<sup>3</sup>

**Channels:** [001] 12 5.9 x 5.9\*



*12-ring viewed along [001]*

**References (cont.):**

- (11) Bonaccorsi, E., Comodi, P. and Merlino, S. *Phys. Chem. Mineral.*, **22**, 367-374 (1995)
- (12) Smolin, Y.I., Shepelev, Y.F., Butikova, I.K. and Kobaykov, I.B. *Kristallografiya*, **26**, 63-66 (1981)
- (13) Peacor, D.R., Rouse, R.C. and Ahn, J.-H. *Am. Mineral.*, **72**, 816-820 (1987)
- (14) Hassan, I. and Grundy, H.D. *Can. Mineral.*, **22**, 333-340 (1984)

## **Appendix C**

### **Simulated XRD powder patterns for zeolites**

(<http://www.iza-structure.org/databases/>)

## ANA

## Analcime

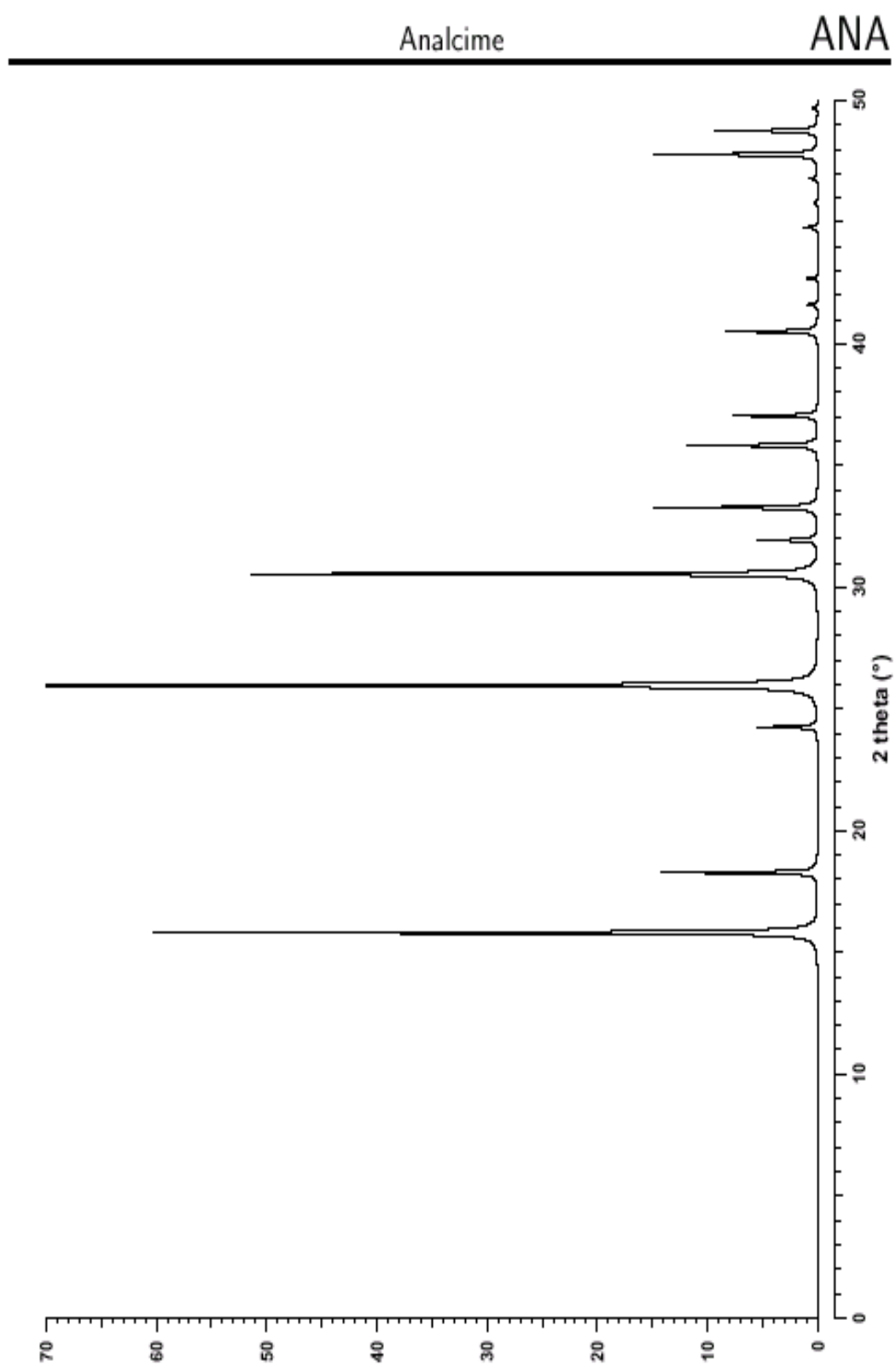
CHEMICAL COMPOSITION:  $[\text{Na}_{16}(\text{H}_2\text{O})_{16}] [\text{Si}_{32}\text{Al}_{16}\text{O}_{96}]$   
Cyclopean Islands, Greece

REFINED COMPOSITION:  $[\text{Na}_{16}(\text{H}_2\text{O})_{16}] [\text{Si}_{32}\text{Al}_{16}\text{O}_{96}]$

CRYSTAL DATA:  $Ia\bar{3}d$  (No. 230)  
 $a = 13.73 \text{ \AA}$      $b = 13.73 \text{ \AA}$      $c = 13.73 \text{ \AA}$   
 $\alpha = 90^\circ$      $\beta = 90^\circ$      $\gamma = 90^\circ$   
 X-ray single crystal refinement,  $R = 0.04$

REFERENCE: G. Ferraris, D. W. Jones and J. Yerkess,  
*Z. Kristallogr.* **135** 240-252 (1972).

<i>h</i>	<i>k</i>	<i>l</i>	$2\theta$	<i>d</i>	<i>M</i>	<i>I</i> <sub>rel</sub>	<i>h</i>	<i>k</i>	<i>l</i>	$2\theta$	<i>d</i>	<i>M</i>	<i>I</i> <sub>rel</sub>	<i>h</i>	<i>k</i>	<i>l</i>	$2\theta$	<i>d</i>	<i>M</i>	<i>I</i> <sub>rel</sub>
2	1	1	15.81	5.605	24	60.2	5	2	1	35.82	2.507	48	11.9	4	4	4	45.78	1.982	8	0.4
2	2	0	18.28	4.854	12	14.1	4	4	0	37.04	2.427	12	7.7	5	4	3	46.78	1.942	48	0.7
3	2	1	24.25	3.669	48	5.4	6	1	1	40.50	2.227	24	2.8	6	4	0	47.77	1.904	24	14.9
4	0	0	25.96	3.433	6	100.0	5	3	2	40.50	2.227	48	5.5	5	5	2	48.74	1.868	24	0.2
3	3	2	30.54	2.927	24	51.3	6	2	0	41.60	2.171	24	1.0	6	3	3	48.74	1.868	24	6.9
4	2	2	31.93	2.803	24	5.5	5	4	1	42.68	2.119	48	0.9	7	2	1	48.74	1.868	48	2.3
4	3	1	33.27	2.693	48	14.8	6	3	1	44.77	2.024	48	1.3	6	4	2	49.69	1.835	48	0.4



## GIS

## Na-P1

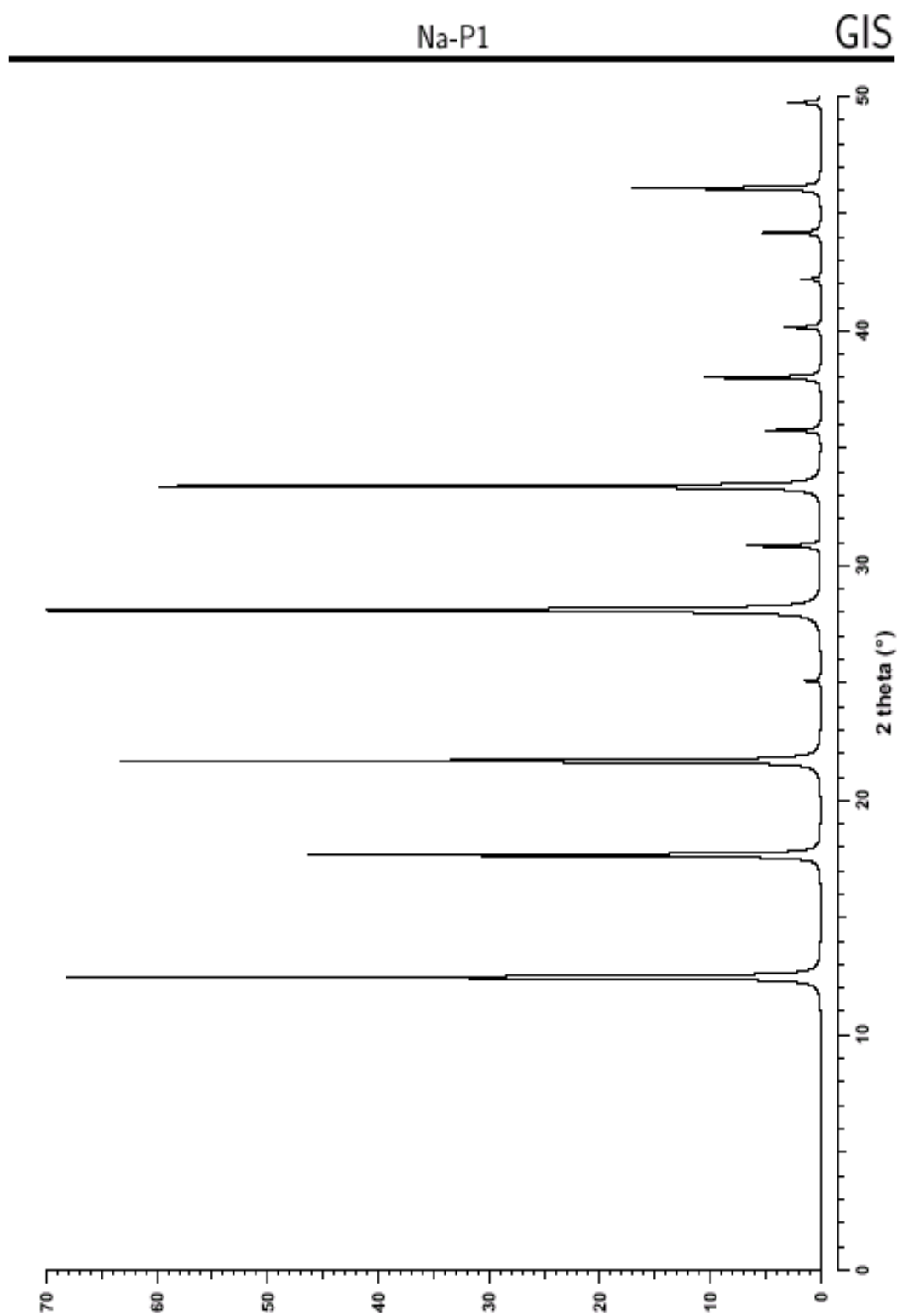
CHEMICAL COMPOSITION:  $[\text{Na}_6(\text{H}_2\text{O})_{12}] [\text{Si}_{10}\text{Al}_6\text{O}_{32}]$

REFINED COMPOSITION:  $[\text{Na}_{5.92}(\text{H}_2\text{O})_{11.28}] [\text{Si}_{9.92}\text{Al}_{6.08}\text{O}_{32}]$

CRYSTAL DATA:  $\bar{1}4$  (No. 82)  
 $a = 10.043 \text{ \AA}$     $b = 10.043 \text{ \AA}$     $c = 10.043 \text{ \AA}$   
 $\alpha = 90^\circ$     $\beta = 90^\circ$     $\gamma = 90^\circ$   
 X-ray twinned crystal refinement,  $R = 0.05$

REFERENCE: Ch. Baerlocher and W. M. Meier,  
*Z. Kristallogr.* **135** 339–354 (1972).

<i>h</i>	<i>k</i>	<i>l</i>	$2\theta$	<i>d</i>	<i>M</i>	<i>I</i> <sub>rel</sub>	<i>h</i>	<i>k</i>	<i>l</i>	$2\theta$	<i>d</i>	<i>M</i>	<i>I</i> <sub>rel</sub>	<i>h</i>	<i>k</i>	<i>l</i>	$2\theta$	<i>d</i>	<i>M</i>	<i>I</i> <sub>rel</sub>
1	0	1	12.46	7.101	8	92.1	2	3	1	33.38	2.684	8	11.5	2	4	2	44.18	2.050	8	0.5
1	1	0	12.46	7.101	4	1.0	1	3	2	33.38	2.684	8	12.7	2	2	4	44.18	2.050	8	0.4
2	0	0	17.66	5.022	4	60.6	1	2	3	33.38	2.684	8	7.5	1	4	3	46.08	1.970	8	0.2
0	0	2	17.66	5.022	2	2.7	0	0	4	35.76	2.511	2	6.8	3	1	4	46.08	1.970	8	0.1
2	1	1	21.67	4.100	8	13.3	3	0	3	38.01	2.367	8	0.4	5	0	1	46.08	1.970	8	3.3
1	1	2	21.67	4.100	8	66.1	4	1	1	38.01	2.367	8	0.6	5	1	0	46.08	1.970	4	2.2
1	2	1	21.67	4.100	8	7.0	1	1	4	38.01	2.367	8	1.0	1	3	4	46.08	1.970	8	11.1
2	0	2	25.08	3.551	8	0.8	3	3	0	38.01	2.367	4	0.3	4	3	1	46.08	1.970	8	0.9
2	2	0	25.08	3.551	4	1.1	1	4	1	38.01	2.367	8	12.0	1	0	5	46.08	1.970	8	1.6
3	1	0	28.10	3.176	4	1.6	4	0	2	40.15	2.246	8	1.4	4	1	3	46.08	1.970	8	2.0
3	0	1	28.10	3.176	8	100.0	2	0	4	40.15	2.246	8	0.9	3	4	1	46.08	1.970	8	1.8
1	0	3	28.10	3.176	8	34.9	4	2	0	40.15	2.246	4	2.3	2	5	1	49.72	1.834	8	0.2
2	2	2	30.84	2.899	8	9.0	3	2	3	42.20	2.141	8	1.0	5	1	2	49.72	1.834	8	2.9
2	1	3	33.38	2.684	8	3.5	2	3	3	42.20	2.141	8	0.3	2	1	5	49.72	1.834	8	0.7
3	1	2	33.38	2.684	8	45.0	3	3	2	42.20	2.141	8	1.0	1	5	2	49.72	1.834	8	0.3
3	2	1	33.38	2.684	8	1.2	4	2	2	44.18	2.050	8	6.5							



## CAN

## Cancrinite

CHEMICAL COMPOSITION:  $[\text{Na}_7\text{Ca}_{0.9}(\text{CO}_3)_{1.4}(\text{H}_2\text{O})_{2.1}] [\text{Si}_6\text{Al}_6\text{O}_{24}]$   
Synthetic crystal.

REFINED COMPOSITION:  $[\text{Na}_8(\text{CO}_3)_{1.2}(\text{H}_2\text{O})_2] [\text{Si}_6\text{Al}_6\text{O}_{24}]$

CRYSTAL DATA:  $P6_3$  (No. 173)

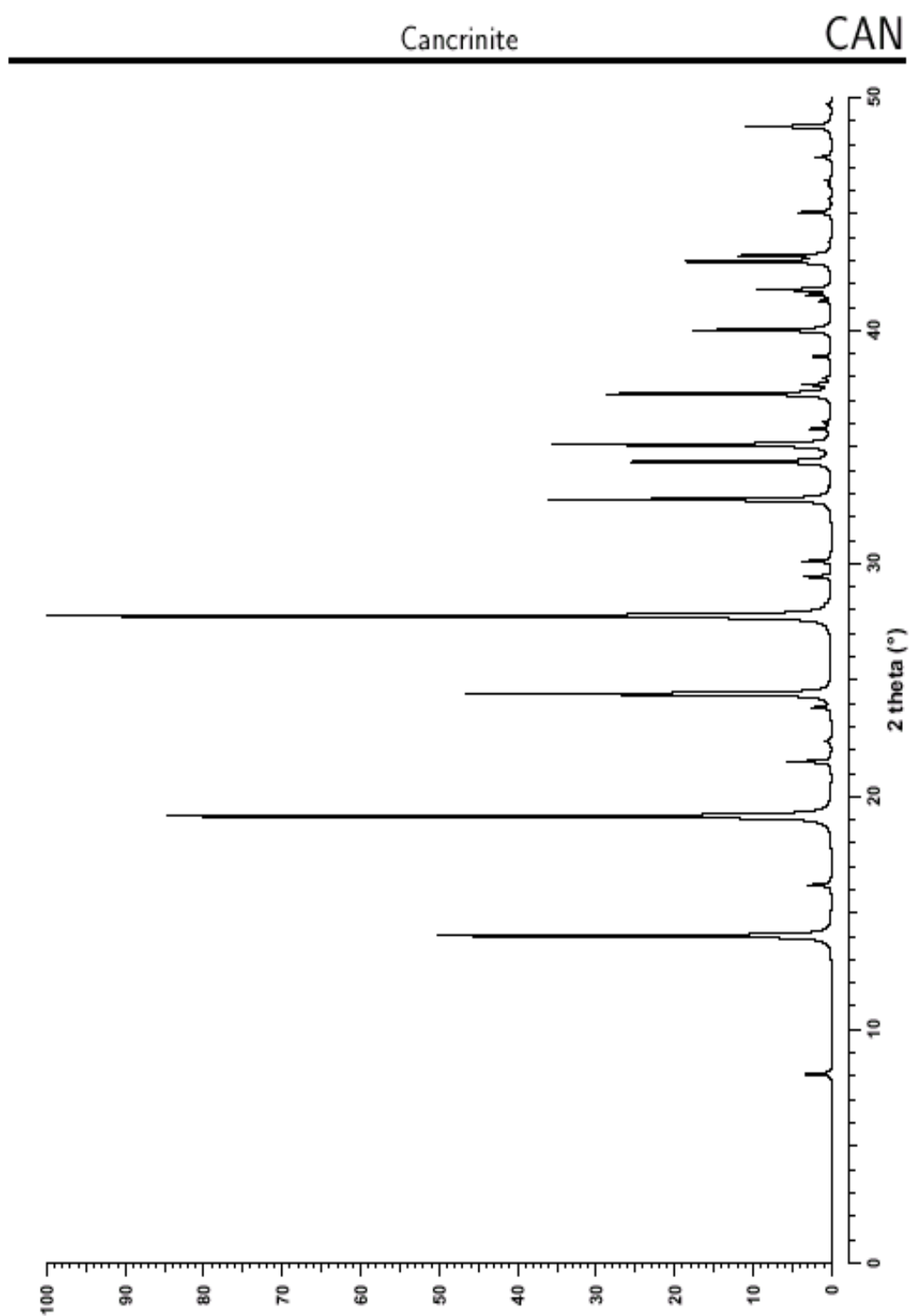
$a = 12.635 \text{ \AA}$     $b = 12.635 \text{ \AA}$     $c = 5.115 \text{ \AA}$

$\alpha = 90^\circ$     $\beta = 90^\circ$     $\gamma = 120^\circ$

X-ray single crystal refinement,  $R = 0.04$

REFERENCE: Y. I. Smolin, Y. F. Shepelev, I. K. Butikova and I. B. Kobayakov,  
*Kristallografiya* **26** 63–66 (1981).

$h$	$k$	$l$	$2\theta$	$d$	$M$	$I_{\text{rel}}$	$h$	$k$	$l$	$2\theta$	$d$	$M$	$I_{\text{rel}}$	$h$	$k$	$l$	$2\theta$	$d$	$M$	$I_{\text{rel}}$
1	0	0	8.08	10.942	6	3.9	2	2	1	33.34	2.688	12	0.1	2	1	2	41.51	2.175	12	1.9
1	1	0	14.02	6.317	6	59.5	3	1	1	34.36	2.610	12	10.2	1	4	1	41.75	2.164	12	6.7
2	0	0	16.20	5.471	6	3.7	1	3	1	34.36	2.610	12	19.8	4	1	1	41.75	2.164	12	4.4
1	0	1	19.15	4.634	12	100.0	0	0	2	35.09	2.557	2	42.0	3	3	0	42.95	2.106	6	21.6
1	2	0	21.49	4.136	6	0.6	3	2	0	35.77	2.510	6	1.3	3	0	2	43.20	2.094	12	13.6
2	1	0	21.49	4.136	6	6.1	2	3	0	35.77	2.510	6	1.7	2	4	0	43.78	2.068	6	0.2
1	1	1	22.36	3.975	12	1.0	1	0	2	36.06	2.490	12	1.2	5	0	1	45.06	2.012	12	4.9
2	0	1	23.81	3.736	12	2.7	4	0	1	37.27	2.412	12	34.0	2	2	2	45.64	1.988	12	0.5
3	0	0	24.40	3.647	6	55.1	1	4	0	37.67	2.388	6	3.4	5	1	0	46.19	1.965	6	0.5
1	2	1	27.74	3.216	12	56.9	4	1	0	37.67	2.388	6	0.7	3	1	2	46.43	1.956	12	0.4
2	1	1	27.74	3.216	12	61.4	1	1	2	37.95	2.371	12	1.1	1	3	2	46.43	1.956	12	0.5
2	2	0	28.25	3.159	6	0.3	2	0	2	38.87	2.317	12	2.6	2	4	1	47.42	1.917	12	1.3
3	1	0	29.43	3.035	6	0.9	2	3	1	40.01	2.254	12	10.4	4	2	1	47.42	1.917	12	1.1
1	3	0	29.43	3.035	6	3.2	3	2	1	40.01	2.254	12	10.4	4	0	2	48.74	1.868	12	13.1
3	0	1	30.09	2.970	12	4.3	5	0	0	41.25	2.188	6	1.7	1	5	1	49.70	1.835	12	0.5
4	0	0	32.74	2.736	6	42.6	1	2	2	41.51	2.175	12	1.5	5	1	1	49.70	1.835	12	0.3



# CURRICULUM VITAE

**NAME: MS. SUDAPORN TANGKAWANIT**

**DATE OF BIRTH:** 14 January 1973

**CITIZENSHIP:** Thailand

**PLACE OF BIRTH:** Ubon Ratchathani, Thailand

**INSTITUTIONS ATTENDED:**

Ubon Ratchathani Rajabhat University, Ubon Ratchathani, Thailand, 1991-1995, Bachelor of Science (Chemistry)

Srinakarinwirot University (Phasanmit), Bangkok, Thailand, 1996-1997, Master of Science Education (Chemistry)

Suranaree University of Technology, Nakhon Ratchasima, Thailand, 2000-2004, Doctor of Philosophy (Chemistry)

**Experience:**

Lecturer in Chemistry, School of Chemistry, Institute of Science and Technology, Ubon Ratchathani Rajabhat University, Ubon Ratchathani, Thailand, 1998–Present

**Publications:**

Dyer, A., Tangkawanit, S. and Rangsiwatananon, K. (2004). Exchange diffusion of  $\text{Cu}^{2+}$ ,  $\text{Ni}^{2+}$ ,  $\text{Pb}^{2+}$  and  $\text{Zn}^{2+}$  into analcime synthesized from perlite. Microporous and Mesoporous Materials (accepted: July 09 2004).

**Study Visit:**

Institute of Materials Science, University of Salford, Manchester, United Kingdom, 31 January 2003-30 April 2003.